Directional relay co-ordination in ungrounded medium voltage radial distribution networks using a Real-Time Digital Simulator

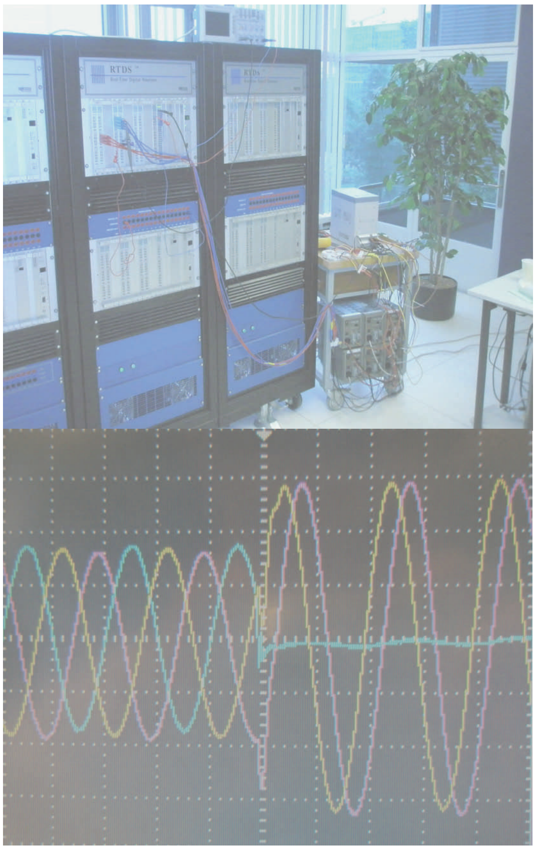

Arjen van der Meer

August 2008

Delft University of Technology

Faculty of Electrical Engineering, Mathematics and Computer Science

Electrical Power Systems

TU Delft

Delft University of Technology

Directional relay co-ordination in ungrounded medium voltage radial distribution networks using a Real-Time Digital Simulator

Arjen van der Meer

August 2008

Delft University of Technology

Faculty of Electrical Engineering, Mathematics and Computer Science

Electrical Power Systems

Msc Thesis Committee

Prof. ir. L.van der Sluis
Dr. ir. M. Popov
Dr. ir. P. Bauer

Table of contents

Introduction

The electricity market liberalisation process has forced the Dutch utility companies to develop a sustainable, clear asset management strategy. To fulfil electricity supply duty, the amount of downtime should be reduced while resulting costs should be minimised. Within this entire process, protection equipment plays an important part because it encloses the erroneous part from the healthy part of the network and hence reduces the cumulative consumers' down-time.

This work presents a technical study of protection relay co-ordination during single phase-to-ground faults in ungrounded medium voltage (MV) networks. The results can contribute to a general grounding and protection philosophy for MV networks. Ungrounded networks are still applied in some parts of The Netherlands and fault currents continue to increase as these networks continue to expand. Single phase-to-ground faults were not switched off before since sheath-currents and overvoltages are within the cables' design limits. However, a short-circuit is an unwanted situation and fast circuit interruption could prevent further cable damage.

During this work, which is a part of the author's final thesis, Real-Time Digital Simulator (RTDS) is extensively applied. The proposed circuit is modelled in RSCAD and a Siemens 7SJ62 directional relay was connected in closed loop with the RTDS system. Quad 50E audio amplifiers have been applied to convert RTDS output signals to rated secondary voltages and currents. The amplifiers play an important role within interfacing between the RTDS and the relay and have therefore been tested thoroughly. The amplifiers' application has been verified at KEMA T&D in Arnhem, The Netherlands. Frequency characteristics have been determined for each amplifier at the Electrical Power Processing (EPP) laboratory of Delft University of Technology.

First, a general introduction to the Dutch MV distribution network is given. Several circuit topologies are discussed. The network model is introduced to the reader and an introduction is given to several overcurrent protection methods. In Chapter 2 the relay co-ordination problem is being discussed. The MV network is being aggregated and then modelled using the Z_{bus} building algorithm. The fault current injection method is used to determine fault currents and hence relay operation. A method is proposed for correct relay co-ordination during single phase-to-ground faults in feeder cables. Furthermore, the network parameters for which this method is applicable are calculated. The simulation results are verified by modelling the same network in Simulink as well.

In Chapter 3, the application of RTDS using the given network will be discussed. The amplifier interface between the RTDS and the 7SJ62 is being described step-by-step for future reproduction by the faculty. Frequency characteristics and KEMA verification results are also discussed. Furthermore, three particular cases are studied: a fault at which the directional relay reacts first, a fault at which the overcurrent relay reacts first and a fault at which no relay reacts at all.

As a result, an interface between the RTDS and the 7SJ62 relay has been established and a correct single phase-to-ground fault relay co-ordination method has been developed.

1 Distribution network: Topology and Protection

The current electrical power system has been formed over a period of about 120 years. Small isolated grids have been combined to larger grids over the past 50 years in order to obtain better economical efficiency and a more reliable electricity supply [1]. Electric power is mainly generated in a centralised way, as can be seen in Figure 1-1. A power plant transforms energy from fossil fuels to electrical energy by use of a synchronous generator. This electricity is generated at a certain voltage, typically MV, and will be transformed to a higher voltage level in a nearby substation. From the power station, the electric energy is transported to the distribution substation, mostly a substation in the neighbourhood of a city. From here, the electric energy will be further distributed at MV and be delivered to the low voltage (LV) network, at which most consumers are connected.

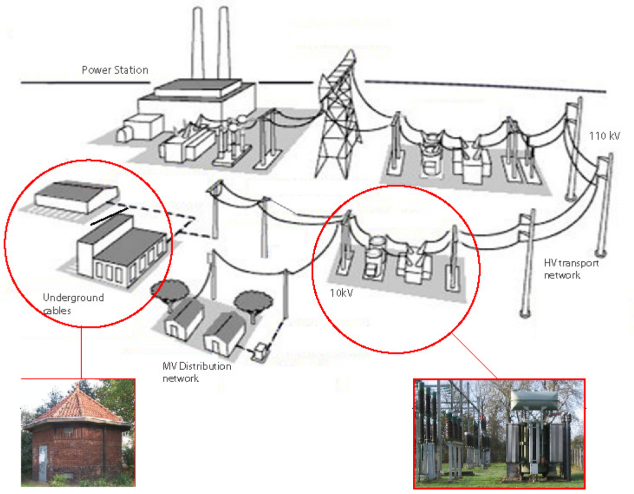

Figure 1-1: Electricity is mainly generated in a centralised way

1.1 Distribution network topology

At MV, the power is being distributed to consumers and industries. The exact voltage level varies from country to country and strongly depends on geological and geographical circumstances. In The Netherlands the MV network ranges from 10kV to 50kV and consists mainly of underground cables.

The MV distribution network can be built up in several ways, which seriously depend on the historical background of the area and on the way how the local government is foreseeing the future expansion of urbanised and industrialised areas. Normally, the power flow is directed from the feeding substation towards MV/LV distribution transformers. Since the MV distribution network is powered centrally by the HV/MV substation, the most of the MV distribution networks are radially built up. In many urbanised areas ring-shaped distribution networks are used in order to increase the reliability.

Radial Distribution network: Agricultural areas and areas with low population density are often equipped with radial distribution networks. Typically only one node is fed from the HV side and hence the power will flow *top-bottom.* A radial network can be very extensive, especially in agricultural areas. A typical radial distribution network is depicted in Figure 1-2. The MV network is connected to the HV network at the HV/MV substation (*p)* by at least 2 power transformers. From here, *feeder cables* supply 10kV distribution substations (*q*), at which the power is supplied further on to the LV side by distribution cables and distribution transformers (*r*). Some *distribution strings* have been laid in a circular way in order to be manually interconnected in the case of an emergency (*s*). Feeder cables have been laid in parallel in order to comply with the *n-1* criterion.

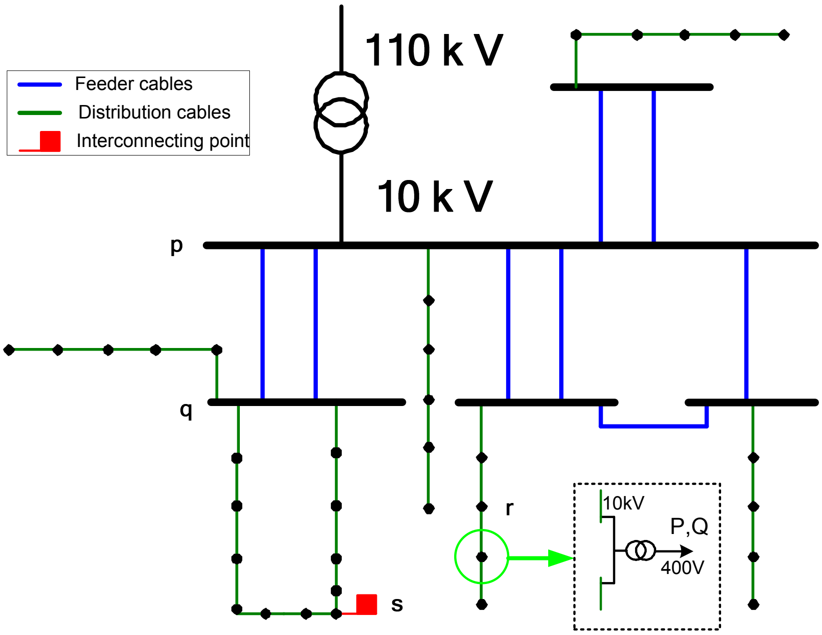

Figure 1-2: a typical radial MV network.

Ring-shaped distribution network: In densely populated urban areas with many industry units, it is insufficient to rely on a radial structure. The whole city would be fed by only a couple of feeders which badly decreases the reliability of the electricity supply. More than one interconnecting point with the HV network is possible in a ring-shaped MV network which increases reliability even more. A typical ring-shaped MV network is depicted in Figure 1-3. The transport feeders are connected in a circular way while distribution strings still exist. Circular networks are more difficult to be protected from short circuits however, and short-circuit power is dramatically increased by the presence of multiple supply points.

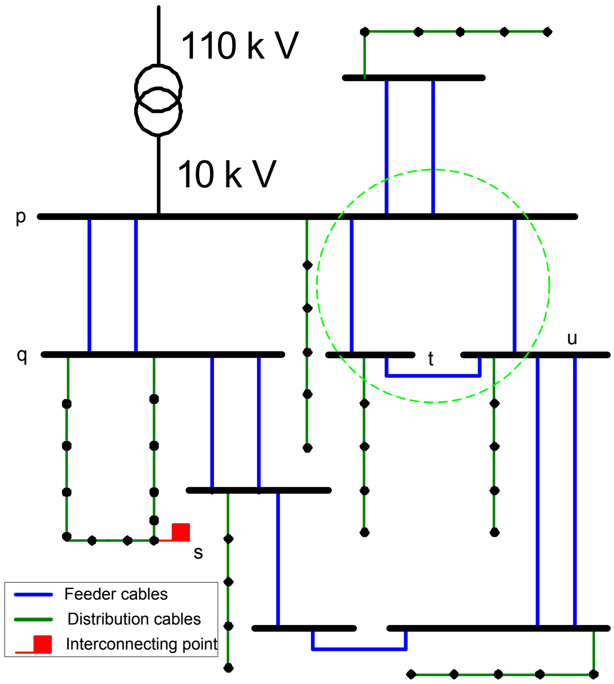

Figure 1-3: Ring shaped MV network with meshed elements.

Meshed MV network: In many areas a MV network will be expanded with ring shaped structures in order to create a partly meshed network, which is even more reliable. This is indicated in Figure 1-3 by a dotted circle between *p*, *t* and *u.*

1.2 Cable modelling

The Dutch distribution network mainly consists of underground power cables and only a few MV overhead lines are utilised. The Dutch soil is suitable for the appliance of electrical power cables and overhead lines fit less well in the Dutch landscape according to general consensus. Underground cables are more expensive to lay on however and the production costs are higher in comparison with overhead lines. Electrically, the power cable differs from an overhead line in several ways:

Insulation level: A cable needs to be as small as possible in order to keep the production and the installation costs low. Commonly used insulating materials in MV cables are Oil-impregnated paper (GPLK[1]/PILC) and Polyethylene (XLPE), while overhead lines use air as insulating medium.

Capacitance to ground: The compact structure of cables has consequences for the capacitance to ground. For circular conductors yields [2]:

$$C = \frac{2\pi\varepsilon}{\ln\frac{R}{r}} \tag{2.1 }$$

where C is the capacitance between the conductor and earthscreen in [F/m], ε is the dielectric constant of the insulation medium in [F/m], r is the radius of the conductor in [m] and R is the inner radius of the earth screen in [m]. Although cable conductors are not exactly circular, are often bundled in 3 phases and the ground potential is not circular around an overhead line, it can be concluded that the capacitance to earth will be much higher for cables and hence cannot be neglected during short circuit studies.

X/R ratio: Series impedance of cables and overhead lines differ in a way which is important for short circuit studies. Overhead lines have a higher reactance/resistance (X/R) ratio then cables do, which plays a significant role in short circuit studies. Especially directional feeder protection and distance protection have to be adjusted to the X/R ratio accurately.

1.2.1 The electrical power cable

Mainly two kinds of MV distribution cables are being used nowadays. *Paper insulated lead covered cables* (PILC) are being used for nearly 120 years now and are still being installed today. Oil impregnated paper is being used as insulating medium and PIL cables can be bundled or single phase. Figure 1-4a gives an example of a bundled 15 kV PIL cable. The first *Cross-linked Polyethylene* (XLPE) cables have been laid during the 1940's and are commonly being installed today. Installed MV XLPE cables can be single phase or three phase and Figure 1-4b gives an example of a MV single phase XLPE cable.

The copper- or lead-*sheath* should be grounded at both ends of the cable in order to avoid dangerously high touch voltages [3]. The *conductor* can be made of copper or aluminium. Copper has better electrical properties but it is more expensive than aluminium.

[1] In Dutch: Gewikkelde Papier Lood Kabel

Although some physical differences exist, PIL cables and XLPE cables can be described to a certain extent with the same electrical model. Cables are represented by their lumped parameters forming a *pi-section*, which is allowed for relative short cables/lines [4]. Series impedance can be modelled by a single resistance and a single reactance for both the sheath (R_m,X_m) and the conductor (R,X). The conductors of three single phase cables have only capacitances to ground (C_G) whereas for a bundled cable, capacitances between conductors (C_k) also exist and have to be modelled as well (Figure 1-5). In order to simulate short-circuits correctly, the method of symmetrical components is used, which is briefly described in Appendix A.

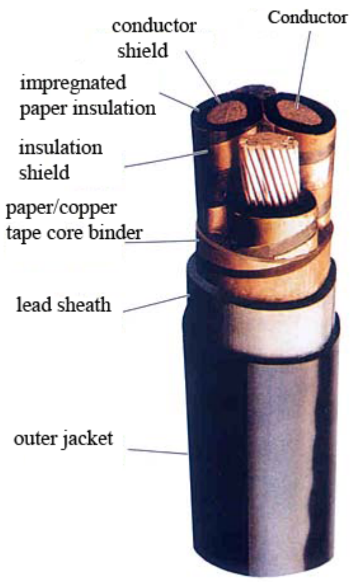

Figure 1-4a: PILC cable

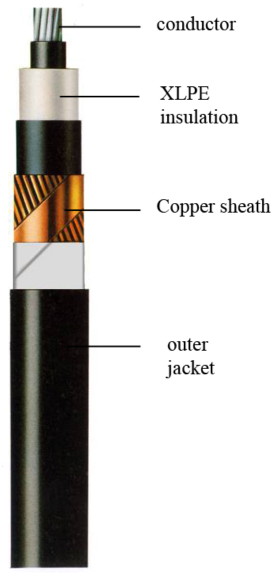

Figure 1-4b: XLPE cable

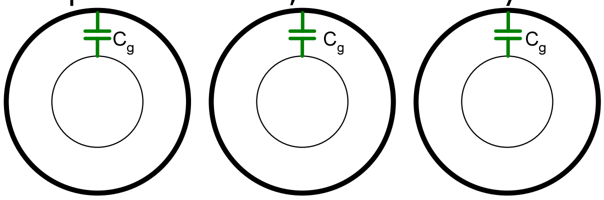

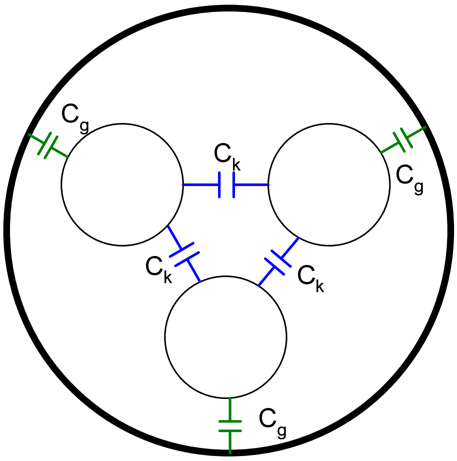

Figure 1-5: Cable capacitances for both bundled cable (right) and single phase cables (above). Distributed capacitances are represented as lumped parameters.

Cable parameters are usually given in sequence components form by the manufacturer in order to simulate both steady state situations and faulted situations. As depicted in Figure 1-6, two pi-sections describe the cable in the RTDS: a *positive-sequence* pi-section and a *zero-sequence* section. Both circuits are used for fault calculations, whereas the normal pi-section will be used for balanced situations as well. Sequence parameters of cables have been derived from lumped physical parameters in Appendix B and are summarised in Table 1-1.

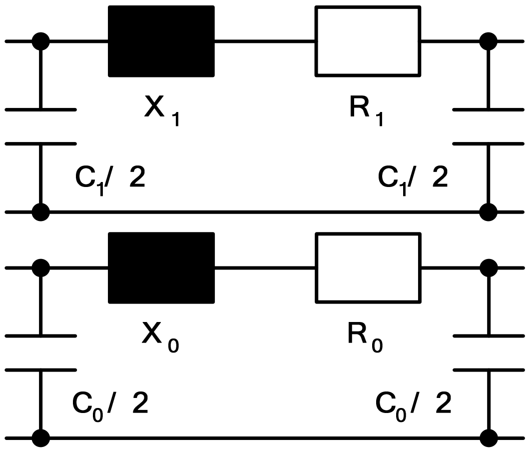

Figure 1-6: Pi-section model for both positive / negative sequence and zero-sequence

Single pi-section networks can be connected in order to obtain a distribution network. At the fault point the pi-section will be divided into two smaller parts with k in per unit cable length, as shown in Figure 1-7.

For normal conditions and short-circuits, it is imperative to take thermal aspects of the power cable into account. Due to resistive losses the cable will heat up. The heat radiates from the cable through the insulation into the soil. Although thermal properties of the soil vary from region to region, three parameters generally describe the thermal behaviour of the cable [5].

Sequence network element	Bundled three phase cable	3 single phase cables
R_1 [Ω/km]	R	R
X_1 [Ω/km]	$j\omega L - j\omega M$	$j\omega L$
C_1 [F/km]	$C_g + 3C_k$	C_g
R_0 [Ω/km]	$R + 3R_m$	$R + R_m$
X_0 [Ω/km]	$j\omega\left(L + 3L_m + 2M - 6M_s\right)$	$j\omega\left(L + L_m - 2M_s\right)$
C_0 [F/km]	C_g	C_g

Table 1-1: Sequence parameters derived from physical cable parameters for bundled and single phase cables.

Maximum current rating: This is the maximum current that may flow through the cable conductor for a maximum of 1 day cycle. Cables may be temporary overloaded with this current and electrical protection may not *pickup* on this current.

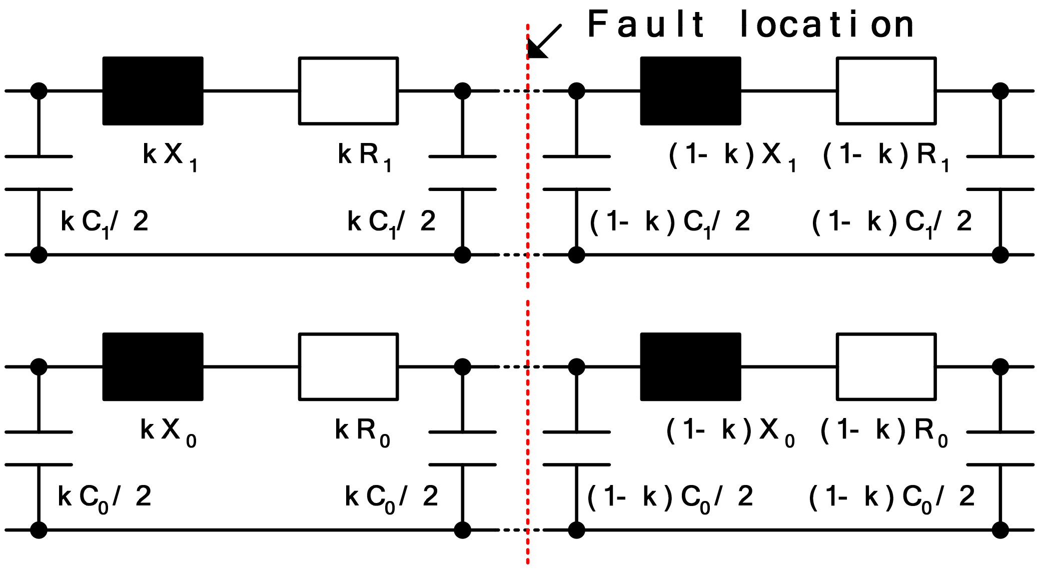

Figure 1-7: Pi-section model at fault location with k in per unit

1s. Maximum conductor current rating: During a short-circuit, high currents flow through the conductor and the insulation heats up by $P_{heat}=I^2R$. This heat cannot flow away and the amount of thermal energy, $E_{thermal}=P_{heat}*t \sim I^2t$, is an important factor during a short-circuit. *I_k-1sec* is an indicator for the maximum current that can flow through the conductor for 1 sec. without damaging the cable.

1s. Maximum sheath current rating: Dependent on the transformer grounding and the fault type, high currents can also flow through the cable sheath. *$I_{k,sheath}$-1sec* is an indicator for the maximum current that can flow through the cable sheath for 1 sec. without damaging the cable.

1.3 On the MV network neutral grounding

Neutral grounding is an important factor in MV distribution network design. Systems in which service continuity was of primary concern were initially left ungrounded[6]. Expansion of the MV network however yields higher fault currents through the cable sheaths during phase to ground faults. In order to provide correct relay coordination and lower overvoltages, network grounding is applied more often. Neutral grounding can be realised by grounding the transformer's neutral or through a *zigzag transformer* in case of a Delta-connected secondary winding. Common grounding types will be discussed briefly.

Ungrounded network: The neutral's coupling is realised by the distributed capacitance of the cables, as is shown in Figure 1-8. For symmetrically distributed phases, the charging currents provide the neutral voltage to be equal to the ground potential[7]. Neutral displacement takes place during single-phase-to-ground faults. Depending on whether the short-circuit is bolted or not, the voltage triangle will shift "downwards", as depicted in Figure 1-8, causing overvoltages of $\sqrt{3}V_{phase}$ in healthy phases.

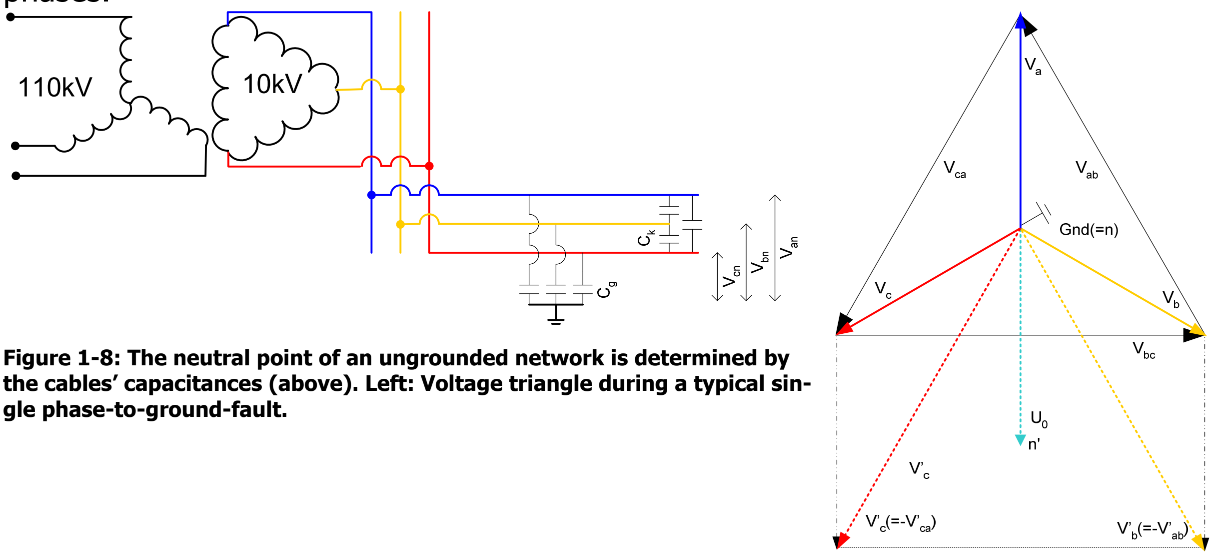

Figure 1-8: The neutral point of an ungrounded network is determined by the cables' capacitances (above). Left: Voltage triangle during a typical single phase-to-ground-fault.

Effectively grounded network: Impedance grounded networks are extensively used nowadays. Protective relaying is easier and voltage stresses are lower comparing to a floating neutral point. A network grounded through a low impedance (or no impedance at all) whereby Coefficient of Grounding (COG) does not exceed 80% *at every point in the network* is effectively grounded[8]. This condition is fulfilled in case of $0 < X_0/X_1 < 3$ **and** $0 < R_0/X_0 < 1$, where X_0, X_1 and R_0 are the sequence impedances of the whole network as "seen" from the fault point.

Compensated network: A special case of impedance grounded networks in which the (zigzag) transformer's neutral is grounded with a *Petersen coil* as depicted in Figure 1-9. The impedance of the compensating coil is matched with the sum of the distributed capacitances of the cable network:

$$j\omega L_n = -j\omega\sum_{1}^{n} C_{0G,n} = -j\omega C_{0,network} \Rightarrow X_n = X_{c0,network} \qquad (2.2)$$

Where L_n the inductance of the Peterson coil, $C_{0G,n}$ the nth zero sequence capacitance, $C_{0,network}$ the sum of the zero-sequence capacitance of *all* the cables, X_n the reactance of the Peterson coil and $X_{c0,network}$ the sum of the zero sequence reactance of all the cables. Capacitive fault-currents are *compensated* by the 180° lagging inductive current of the coil [8]. Seen from the fault location, the zero-sequence reactance is very high since the zero-sequence network is parallel resonant and hence the phase to ground fault current *at the fault location* will be significantly limited.

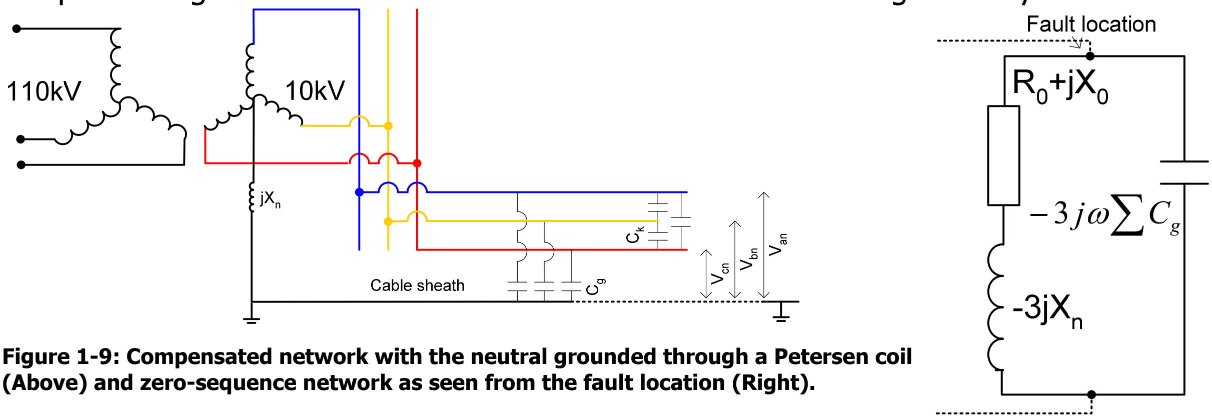

Figure 1-9: Compensated network with the neutral grounded through a Petersen coil (Above) and zero-sequence network as seen from the fault location (Right).

1.4 Protection of MV distribution networks

An electrical network can be protected from electrical hazards in several ways. Overvoltage protection is realised by surge arresters in order to control the flashover location in case of lightning overvoltages [9]. Overcurrent protection is extensively applied in MV cable networks and can be realised by fuses and protective relaying. Although fast and reliable, the utilisation of fuses in MV networks is expensive and subjected to long repair times. Hence it is rarely used in the modern Dutch MV cable network nowadays.

Protective relaying needs measuring transformers and a *secondary circuit* in order to provide adequate acquisition for *primary values* of voltages and currents. Figure 1-10 gives an outlined secondary circuit scheme as modelled in the RTDS. Despite the ungrounded cable network, the secondary circuit has got a connection to ground. During short-circuits, considerable high currents may flow through the secondary circuit as well and therefore, it has to be tested for these conditions. Although voltage transformers as well as current transformers can be saturated during energising and short-circuits respectively, the saturation of current transformers is more critical and it will seriously affect accurate protective relaying[10]. However, during single phase-to-ground-faults, no considerable high currents flow, so the saturation is not included in the model.

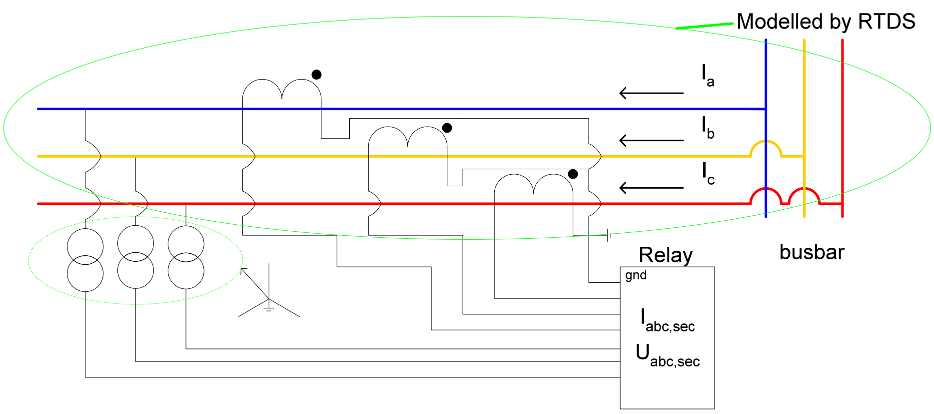

Figure 1-10: Secondary circuit as it appears in the proposed MV network

1.4.1 Overcurrent protection

Overcurrent protection relays were are introduced during the first decades of the 20th century. Nowadays, protection against excess current is indispensable and though technically inferior to other relaying methods, overcurrent relays are still installed in the MV distribution grid. Especially in radial MV networks with relative small short-circuit power, overcurrent relays are still extensively used. Co-ordination can be roughly distinguished in two protection modes which can preferably not be utilised in the same network:

Maximum definite-time overcurrent protection (OMT[1]): widely used in the Netherlands and co-ordination is generally realised through *discrimination by time*. Time grading is usually applied with grading times of 0.2 to 0.3 s, rising from load to source as depicted in Figure 1-11a. Mostly, 2 or more discrimination points can be set in the OMT. {$\mathbf{I_{>}},\mathbf{t_{>}}$} is used for (short-circuit) currents higher than the maximum current rating of the cable and as a backup protection for overcurrents not being interrupted by other OMT's further down the distribution network. {$\mathbf{I_{>>}},\mathbf{t_{>>}}$} is used for very high short circuit currents, which may reach the 1s. maximum conductor current rating. $t_{>>}$ is preferably set to 0 or 20ms. Relay characteristics for the distribution string of the depicted network are given in Figure 1-11b.

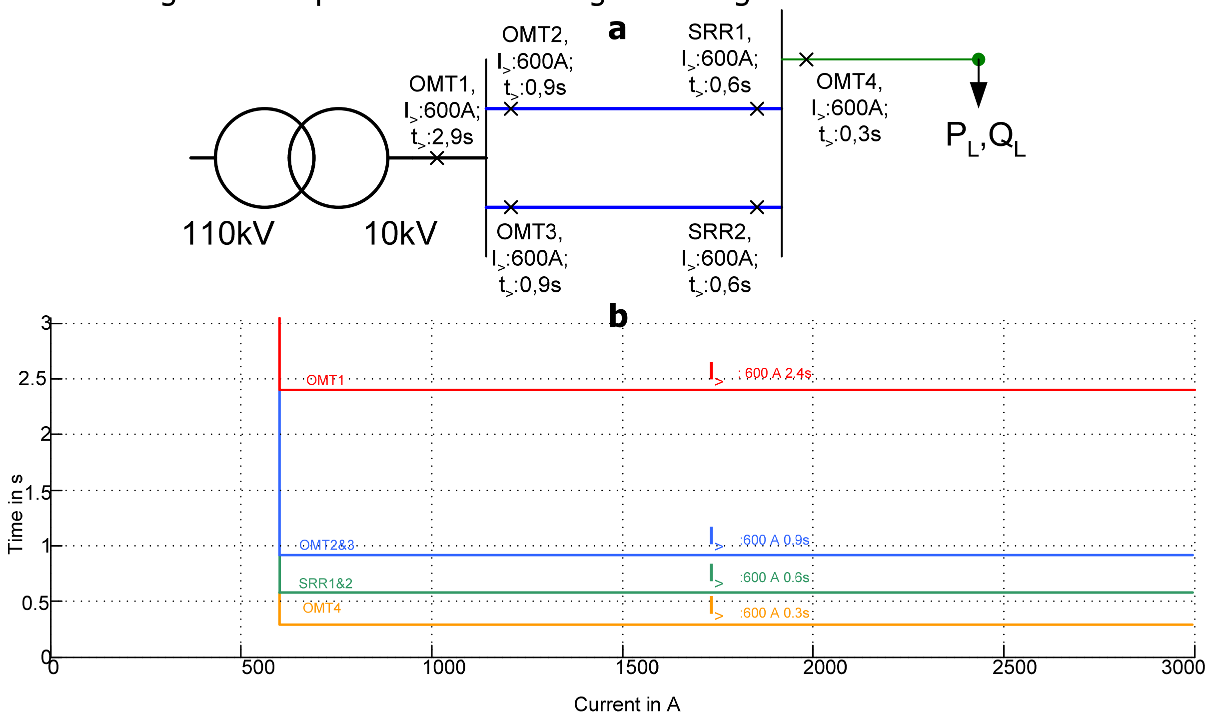

Figure 1-11: Relays' phasor element settings (a) and relay diagram (b) for the proposed system protection setup

Inverse definite minimum-time relays (IDMT): Co-ordination is generally realised through both discrimination by time and discrimination by current, making trip times dependent on short-circuit current. IDMT relay co-ordination is comparable to fuse co-ordination and can be realised by several curves which are standardised in IEC60255 [11]. Figure 1-12 gives the same network as Figure 1-11a , now utilised with IDMT relays. Directional relays are replaced by IDMT's as well, which is uncommon in practice.

[1] In Dutch: Maximum OverstroomTijd relais

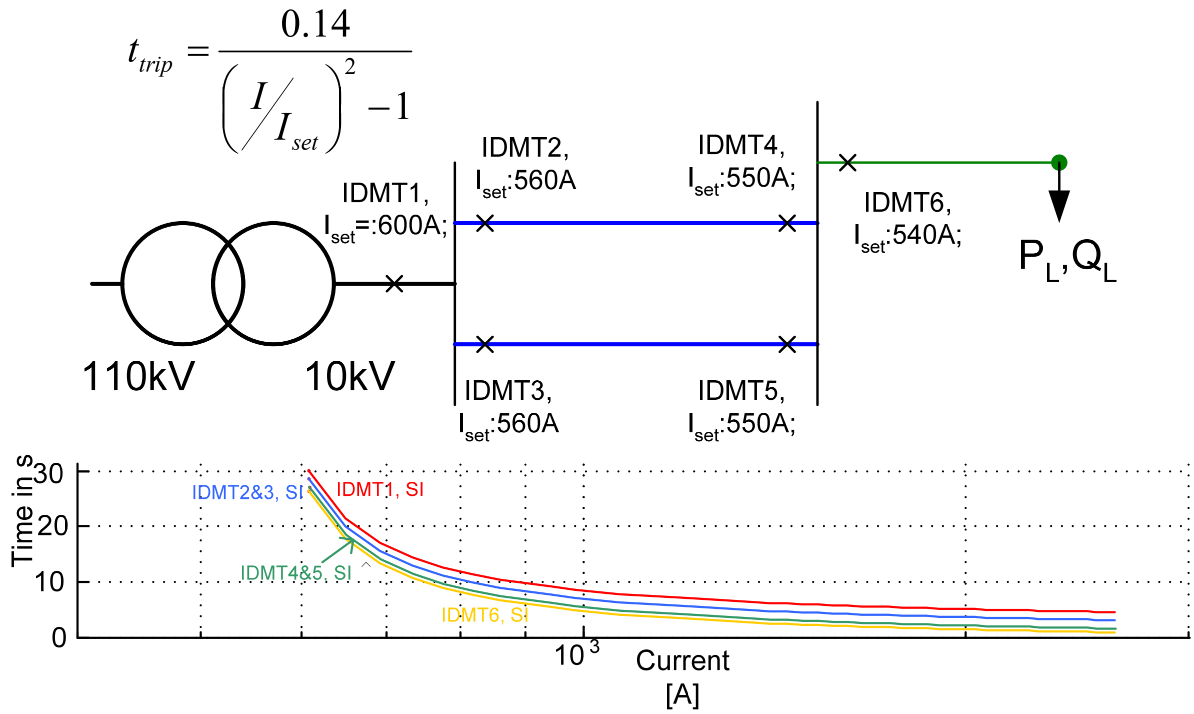

Figure 1-12: Relay settings and relay diagram when applying IDMT relays.

In general, instantaneous values of secondary currents are measured by sampling in case of an electronic relay and by magnetic forces in case of (older) mechanical relays. RMS values are calculated which are thereupon compared to set values {**I>,t>**} and the relay can eventually trip after a pick-up/drop-off hysteresis loop. Figure 1-13 gives the block diagram of a typical overcurrent relay as modelled in RSCAD.

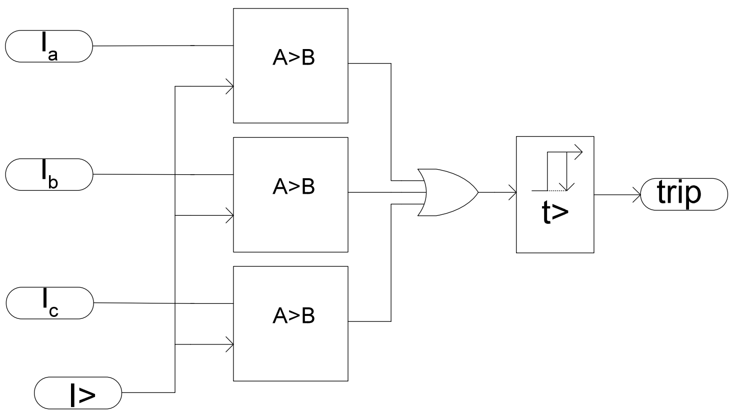

Figure 1-13: Simplified phasor element logical block diagram of an overcurrent relay.

1.4.2 Directional overcurrent relays

Feeder protection can be realised in several ways and it is traditionally done bywith a combination of directional overcurrent relays (SRR) and overcurrent relays. In order to provide correct relay co-ordination the directional relay has to determine the direction *of the fault*. Several methods exist which are mainly relying on the direction of active power flow which is briefly discussed below.

Consider the parallel feeder cables of Figure 1-11a with the secondary circuit of Figure 1-10 connected to SRR2. At the primary side, primary current $\underline{I}_{prim}$ *lags* the primary voltage $\underline{U}_{prim}$ by the power angle φ. Current transformers are grounded *towards busbar*, which is very important regarding the sign of the secondary currents ($\underline{I}_{sec}=I_{ph,sec}\angle\delta$) and hence the direction of primary phase currents. Secondary voltages ($\underline{U}_{sec}=U_{ph,sec}\angle\Psi$) with a typical nominal value of 100V are being measured as well and the phase angle Ψ is being compared with the phase angle of $\underline{I}_{sec}$, δ. Under normal conditions, $\underline{I}_{sec}$ leads $\underline{U}_{sec}$ by an angle 180°+φ (= δ- Ψ) and lags $\underline{U}_{line}$, whose stored values can also be used for direction determination, by an angle 90°- φ, as depicted in Figure 1-14. Seen from the position of the relay, the active power is flowing towards the load. For the measured three phase power holds:

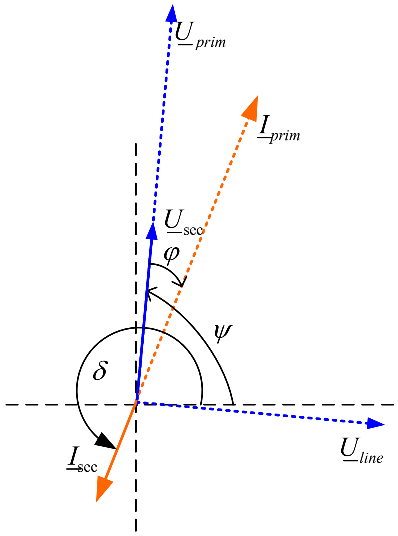

Figure 1-14: Phasor diagram of measured secondary voltages and currents during normal operation.

$$\begin{aligned} P &= \mathrm{Re}\left(3\underline{U}_{\sec}\underline{I}_{\sec}^{*}\right) = \mathrm{Re}\left(3U_{ph,\sec}e^{j\psi}I_{ph,\sec}e^{-j\delta}\right) \\ &= 3U_{ph,\sec}I_{ph,\sec}\cos\left(\psi-\delta\right) = 3U_{ph,\sec}I_{ph,\sec}\cos\left(180+\varphi\right) \end{aligned} \tag{2.3}$$

During a symmetrical three phase short-circuit, the current will flow towards the fault and hence the power is directed into the cable (*P*>0) with a phase angle which is dependent on the *X/R* ratio of the cable. For cables with a sufficient large conductor diameter this yields for the impedance towards the fault:

$$\frac{X_1}{R_1}\approx 1 \Rightarrow Z_{cable,1} = (1-k)\sqrt{X_1^2+R_1^2}\,e^{j\arctan\left(\frac{X_1}{R_1}\right)} \tag{2.4}$$

And hence the phase fault current will lag the faulted phase voltage by

$$\varphi_{sc} = -\arctan\left(\frac{X_1}{R_1}\right) \approx -45^{\circ} \tag{2.5}$$

In practice however, the faulted phase voltage is too small to be measured and the healthy, *opposing* line-to-line voltages should be used. Figure 1-15 gives the phase diagram for a three-phase short-circuit in the feeder cable picked-up *by phase element A*. Cross-polarising voltage $\underline{V}_{bc}$ is used as reference voltage ($\underline{V}_{ref}$) and is rotated counter clockwise by an angle RCA° (Relay Characteristic Angle), also known as the Maximum Torque Angle(MTA)[12]. For cables, a RCA of 45° is commonly used. Three-phase faults and phase-to-phase faults in the protected feeder cable should be detected correctly.

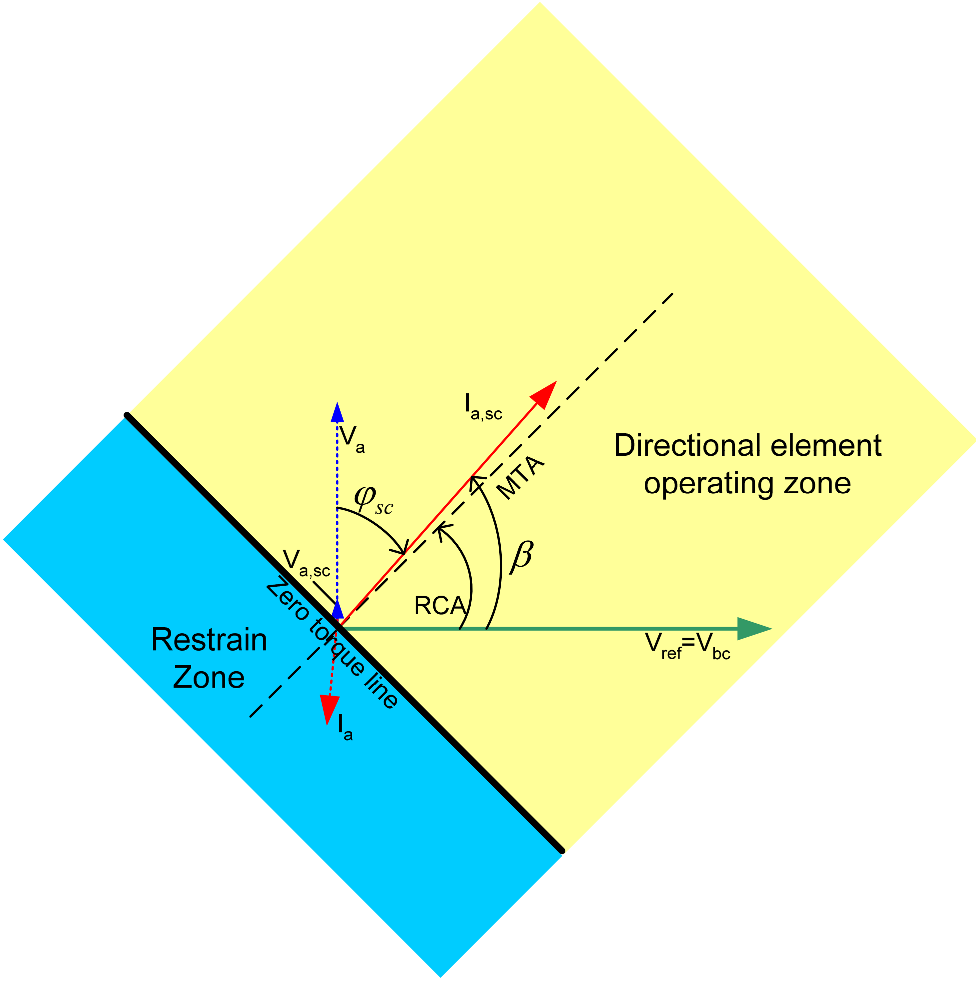

Figure 1-15: Phasor diagram of a typical directional overcurrent phase-element. Dashed arrows are prefault phasors. The 90° rotated cross-polarising line-voltage is used as reference phasor. A RCA of 45° is applied. A short-circuit current phasor located in the operating zone will cause the relay to pick up. V_a and I_a are the pre-fault phase-voltage and current phasors.

For the measured *phase* power holds, to operate in directional mode

$$\begin{aligned} P &= \mathrm{Re}\left(\underline{V}_{bc} e^{jRCA} \underline{I}^{*}_{a,sc}\right) = \mathrm{Re}\left(V_{bc} e^{j\gamma} e^{jRCA} \underline{I}^{*}_{a,sc}\right) \\ &= V_{bc} I_a \cos\left(\gamma - \delta + RCA\right) = V_{bc} I_a \cos\left(\delta - \gamma - RCA\right) \\ &= V_{bc} I_a \cos\left(\beta - RCA\right) > 0 \end{aligned} \qquad (2.6)$$

In which $\beta = \frac{\pi}{2} - \varphi_{sc}$ the angle between the cross-polarising voltage $\underline{V}_{bc}$ and the short-circuit current phasor $\underline{I}_{a,sc}$., γ the phase angle of the cross-polarising line-voltage $\underline{V}_{bc}$ and δ the phase angle of $\underline{I}_{a,sc}$ Figure 1-16 gives a brief block diagram of the directional element of the 7SJ62 relay. Detailed scheme is described in[13].

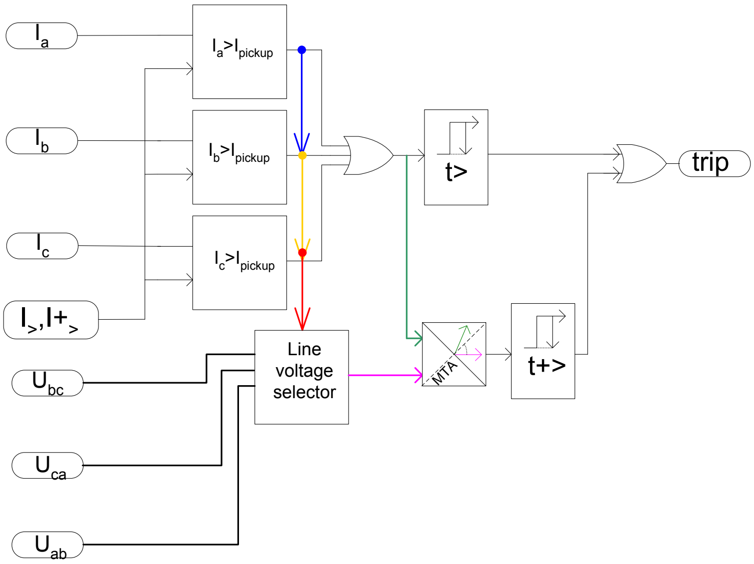

Figure 1-16: Simplified directional phasor element logical block diagram of a directional overcurrent relay.

Directional earth-fault element

It is especially for ungrounded systems not convenient to detect single-phase-to-ground faults with the directional phasor element. During ground-faults, a combination of load current and capacitive fault current is measured. Generally, the direction will be determined wrong if the load current component, $\underline{I}_1+\underline{I}_2$, is higher than the fault current component, $\underline{I}_0$. Direction of ground faults should therefore be determined with an earth-fault element, which uses zero-sequence components $\underline{U}_0$ and $\underline{I}_{e,7SJ62}=-3\underline{I}_0$ as phasor quantities.

Consider again the network of Figure 1-11a with a phase A-to-ground-fault in the "bottom" cable (cable 3). The voltage triangle will be shifted as shown in Figure 1-8. The residual voltage $3\underline{U}_0$ can be calculated or either be measured by an open delta connection. Generally, the direction of $\underline{U}_0$ is determined by the healthy phase voltages. The contribution of $\underline{V}_a$ is assumed sufficiently small in comparison with $\underline{V}_b$ and $\underline{V}_c$ to neglect. The component $\underline{I}_0$ can be extracted from the three phase currents and is mainly formed by the distributed capacitive charging currents of the sound phases[7]. It should be noted that the phase angle of $\underline{I}_0$ depends on whether the fault is bolted or not and is typically 90° *lagging* $\underline{U}_0$.

In order to use wattmetric measurements during ground-faults as well, $\underline{U}_0$ has to be rotated counter clockwise by an angle RCA_0. It must be noted that in practice, the value of RCA_0 should be chosen with the predicted arc-resistance taken into consideration. Therefore, a RCA_0 between 30° and 60° is commonly used for underground cables. In Figure 1-17 it can be seen that for the zero-sequence real power, to locate the ground-fault inside the protected cable holds:

$$\begin{aligned} P_0 &= \mathrm{Re}\left(\underline{U}_0 e^{jRCA_0} \underline{I}_{e,7sj62}^{\ *}\right) = \mathrm{Re}\left(U_0 e^{j\psi_0} e^{jRCA_0} I_{e,7sj62} e^{-j\delta_0}\right) \\ &= U_0 I_{e,7sj62}\cos\left(\psi_0 + RCA_0 - \delta_0\right) = U_0 I_{e,7sj62}\cos\left(-\left(\psi_0 + RCA_0 - \delta_0\right)\right) \\ &= U_0 I_{e,7sj62}\cos\left(\varphi_{sc,0} - RCA_0\right) > 0 \end{aligned} \tag{2.7}$$

Where $\varphi_{sc,0}$ the angle between $\underline{U}_0$ and $\underline{I}_{e,7SJ62}$. Note that the relay determines direction with $\underline{I}_{e,7SJ62}=-3\underline{I}_0$, which is *leading* $\underline{U}_0$ during a forward single phase-to-ground-fault.

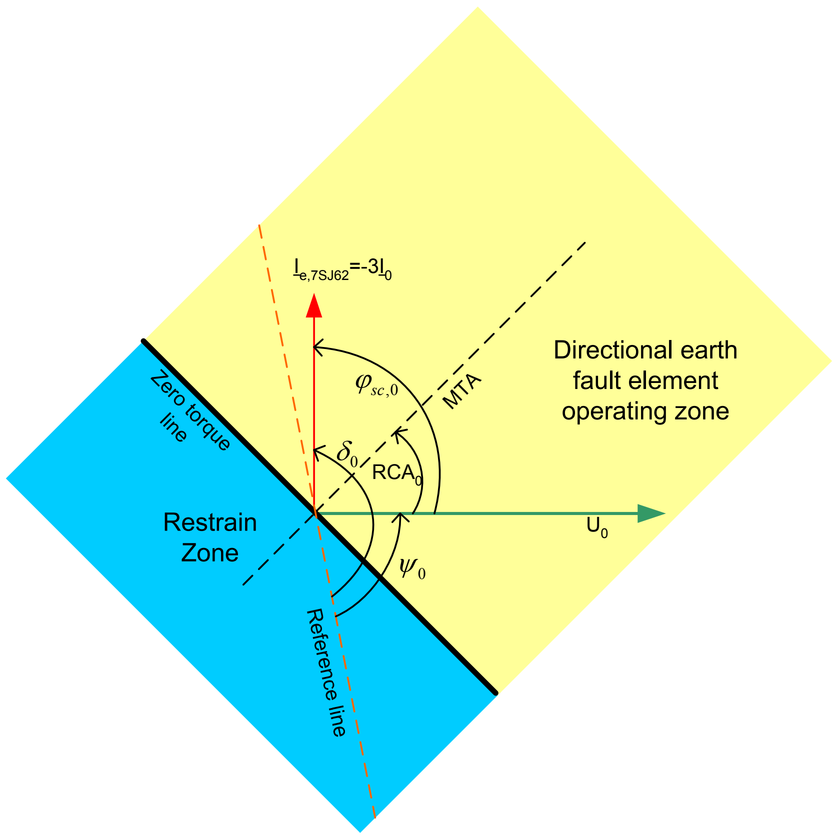

Figure 1-17: Phasor diagram of a typical directional overcurrent earth-fault element. Zero-sequence voltage $\underline{U}_0$ is used as a reference phasors for direction determination. A RCA_0 of 45° is applied.

1.4.3 Other protection methods

As already mentioned, overcurrent protection is a traditional method to protect the network from short-circuits. The relatively slow fault clearance times have led over-current relaying to perform a backup function for more sophisticated protection methods. Although these methods are beyond the scope of this thesis, some of them are discussed below briefly.

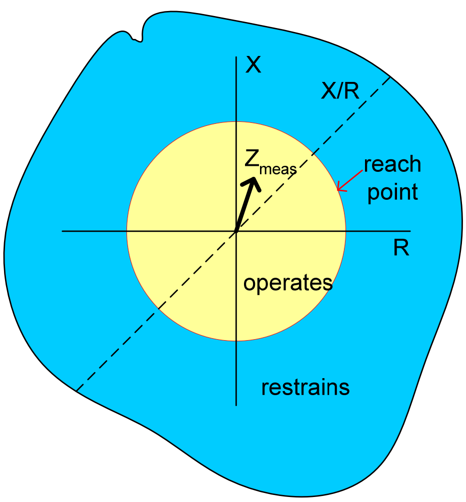

Figure 1-18a: Unidirectional Distance relay. Relay picks-up faults 'behind' the relay as well

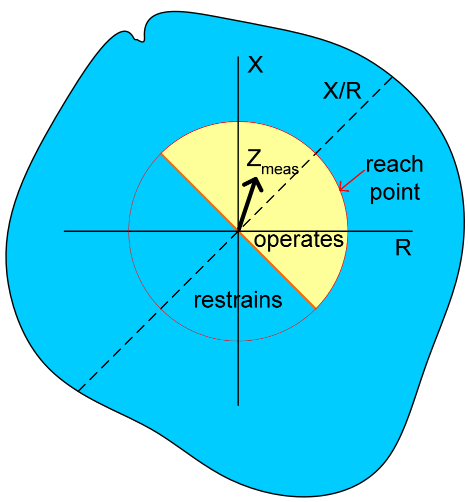

Figure 1-18b: Distance relay with directional functionality.

Distance Protection (D): Widely used as main protection in HV en MV networks. Operation of distance relays is based on the measured impedance at the position of the relay in the grid. Comparing this impedance, which is known at every time instant, with the impedance of the cable up to the *reach point*, short-circuits within *zone 1* (~85% of the cable) can be switched off quickly. The majority of modern distance relays have several zones, each with its own delay time to maintain proper relay co-ordination. Distance relay characteristics are normally given in a R/X diagram. Electronic distance relays can be almost adjusted to any impedance area implying directional functionality as well. Figure 1-18 a and b give typical impedance setting areas of a distance relay.

Differential feeder protection (DIFF): Extensively applied in new cable paths and as a part of transformer protection. At both sides of the cable the protection determines the difference between incoming and outgoing phase-currents by making use of *pilot-wires*. Switching times are very fast and every type of fault inside the cable should be able to be interrupted. Secondary circuits have to be fully symmetric however and current transformer saturation can lead to incorrect disconnection of the cable. Overcurrent protection should be used as a backup protection since differential protection can only be used as main protection[11].

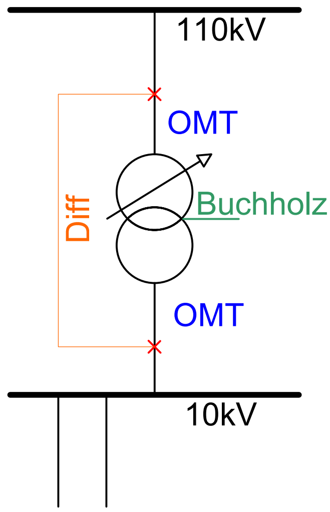

Figure 1-19: Typical transformer protection.

Transformer protection: Transformers are the most expensive objects in the distribution network and are therefore very well protected against electrical and mechanical hazards. As can be seen in Figure 1-19, protection against overcurrents is realised with DIFF as main protection and OMT as backup protection at both HV-side and MV-side. Buchholz protection is the main protection for faults inside the transformer core in which gas or flowing oil is being formed and is therefore a backup protection for over-currents through the transformer[14].

Busbar protection: MV installations are generally enclosed switchgear units in the Netherlands and therefore the fault-arc can be detected by use of optical-detection or pressure-detection. Differential protection is generally being used as main protection while optical protection is used as a backup protection. Relay co-ordination is realised by communication between the relays connected to the busbar. Sectionalisation of the busbar is applied in order to reduce the number of circuits that have to be switched off during a fault [10].

Sophisticated methods: Although commonly used protection devices can detect most kinds of short circuits, not every fault can be switched off selectively. Rarely occurring faults like *cross-country* faults are difficult to interrupt selectively. Wavelet methods and neural network methods have therefore been developed and are still being improved [15][16][17]. A major drawback of the proposed methods is however the need for a certain kind of *system automation*, which requires investments.

2 Single phase-to-ground-fault in ungrounded MV networks

About 86% of all short-circuits originate from a single-phase to ground fault [18]. A lot of single-phase short-circuits will eventually develop into polyphase faults. For cables, three main causes can be classified:

Insulation failure due to ageing: Degradation of cable insulation can be a serious cause of failures. During breakdown an immense amount of heat is produced at the fault point, which can easily make the fault-arc to strike over to healthy phases as well. Mostly, insulation failures have an *intermitting* nature, which should be taken into account using protective relaying. Partial Discharges (PD) occur naturally in PILC cables and is only affecting the insulation strength above a certain level[2]. Therefore, PD is an important indicator using condition assessment[19].

Breakdown due to overheating: Cables and cable joints can overheat while overloaded or by ageing. In joints, this can lead to degradation of the conductor connections which leads to overheating even more, to insulation degradation and eventually to flashover.

Failure due to excavation work: A major cause for cable faults is breakdown due to excavation work. Lack of cable position knowledge can be destructive during construction activities. Almost needless to say, the insulation will be partly destructed and breakdown is inevitable. Depending on the type of cable, the short circuit will be single-phase or three-phase immediately.

2.1 Case study: feeder protection co-ordination problem

2.1.1 Problem definition

Network definition

Consider the radial network of Figure 1-2, which is a simplification of typical ungrounded 10kV networks as extensively being utilised in the province of Overijssel, the Netherlands. In fact, the network model can be aggregated even more when only single-phase to ground faults are involved since cables' capacitances define the fault current. The network of Figure 2-1 represents for instance the feeder cables between p and q of Figure 1-2.

Distribution cables between q and s are being represented by their capacitance to ground at node q by

$$C_{dist,0} = \sum_{n=q}^{distribution\ string} C_{G,n} \tag{3.1}$$

Where $C_{G,n}$ the capacitance to ground of every cable section of the distribution strings on the right-hand side of q. This is allowed for single-phase to ground faults since the fault current is mainly produced by the charging currents of the cable's distributed capacitances.

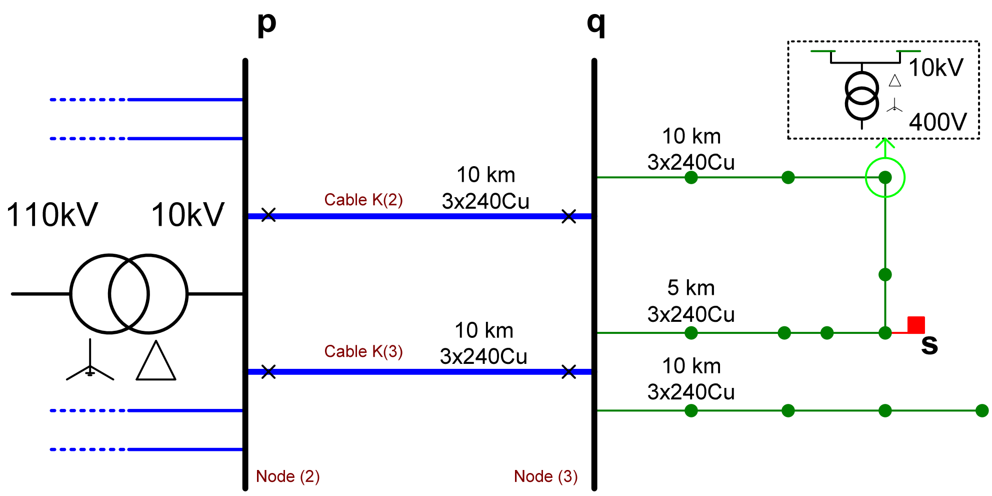

Figure 2-1: Simplified MV network with two feeder cables between p and q

It will be shown later that the load has negligible influence on the zero-sequence fault current and will hence be aggregated to one load at both node p and q. The major part of the MV network is however the network *not* fed by feeder cables K(2) and K(3). This load has been neglected since it has little influence on the fault current amplitude and direction at node q. The influence of the cables is represented by their aggregated capacitance to ground at node p by

$$C_{grid,0} = \sum_{n=p}^{10kV\ grid} C_{G,n} \tag{3.2}$$

Where $C_{G,n}$ the capacitance to ground of every cable section of the transport and distribution network on the left-hand side of p. The aggregated network model of Figure 2-1 is given in Figure 2-2.

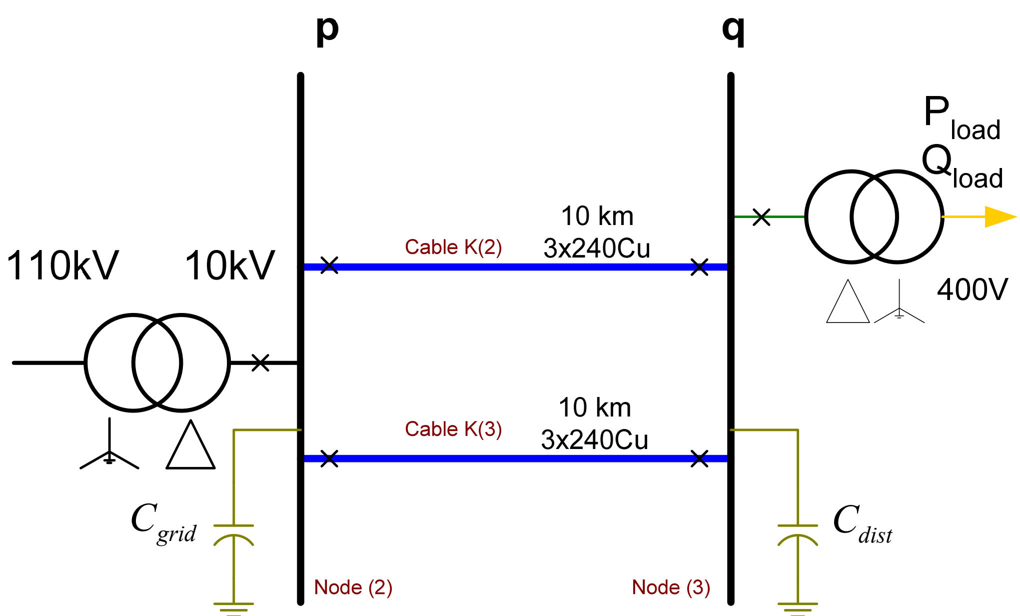

Figure 2-2: Aggregated network suitable for single phase-to-ground fault calculation.

Ground fault: co-ordination problem

During a single-phase to ground fault, the voltage triangle is being shifted as depicted in Figure 1-8. Owing to the unbalance in the circuit, charging currents will flow through the distributed capacitance of the network towards the fault point. As can be seen in Figure 2-3, both the distribution strings and the rest of the MV network contribute to the fault current. The amplitude of the cable's fault current contribution, $\underline{I}_0$, depends on the total distributed capacitance of the cable sections involved. Direction of $\underline{I}_0$ *in* the faulted cable itself, cable K(3), is always determined correctly by directional relays equipped with an earth-fault element[20]. The direction of $\underline{I}_0$ in the parallel feeder cable, cable K(2), is dependent on the network topology and the fault location in cable K(3).

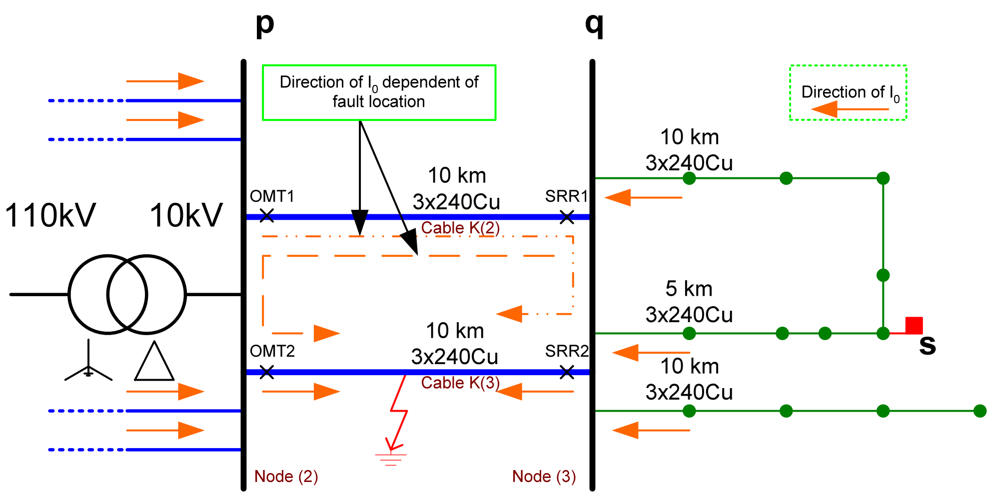

Figure 2-3: Zero-sequence fault current direction relative to zero-sequence voltage during a single phase-to-ground fault in cable K(3).

The reader should notice that the direction is being determined by making use of the zero-sequence components of currents and voltages and not by phase quantities since these contain both the fault and load-component.

For phase-to-phase and three-phase faults, the fault current will flow from the three-phase source to the fault location. In radial MV networks this source is predominantly the HV/MV transformer. Relay co-ordination is easily satisfied by setting the directional relay to a shorter pick up period than the opposing overcurrent relay. Overcurrent pick up set value should be sufficiently high in order to prevent the relay's phasor-element picking up on ground faults. Figure 2-4a depicts a three-phase short-circuit at 0.5 per unit in cable K(3) of Figure 2-3 being switched off correctly. However, for single-phase to ground faults, the fault current will flow from multiple directions. Using the same co-ordination strategy will result in unselectively interrupted cables. Figure 2-4b depicts a single-phase to ground fault being switched off incorrectly. The $\underline{I}_e$ pickup value of the directional relays is 40 A. The healthy cable has to carry the capacitive charging current of the distribution string and, as will be shown, the directional earth-fault element may not pick up on this current. This charging current is, according to [21], approximately equal to the rms value of

$$\underline{I}_{e,dist} = 3\underline{I}_{dist,0} \overset{Z_0 << 1/\omega C_{dist,0}}{\approx} 3\underline{U}_{q,0}\omega C_{dist,0} = \left(\underline{U}'_a + \underline{U}'_b + \underline{U}'_c\right)\omega C_{dist,0} \overset{U'_a << U'_b}{\approx} \left(\underline{U}'_{ca} + \underline{U}'_{ab}\right)\omega C_{dist,0} = \frac{3\underline{U}_{line}\omega C_{dist,0}}{\sqrt{3}} \tag{3.3}$$

where Z_0 the zero-sequence impedance of the distribution string, which is much smaller than capacitive shunt-impedance for relative short cables. For this example the charging current is approximately equal to

$$\underline{I}_{e,dist} = \frac{3U_{line}\omega C_{dist,0}}{\sqrt{3}} = \frac{3\cdot 10400\cdot 2\cdot\pi\cdot 50\cdot 0.28\times 10^{-6}\, F/km \cdot 25km}{\sqrt{3}} \approx 40A \tag{3.4}$$

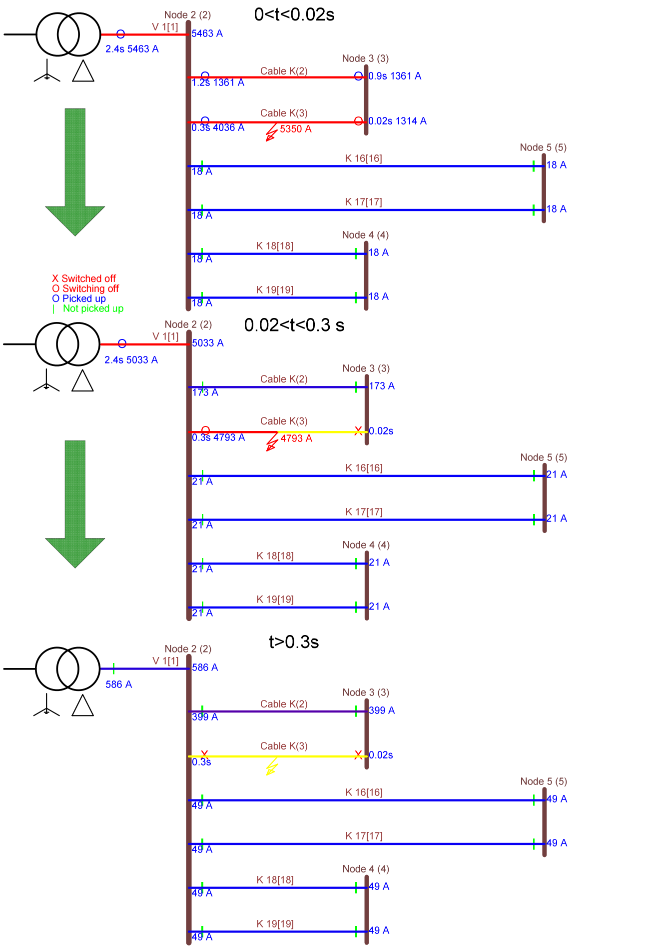

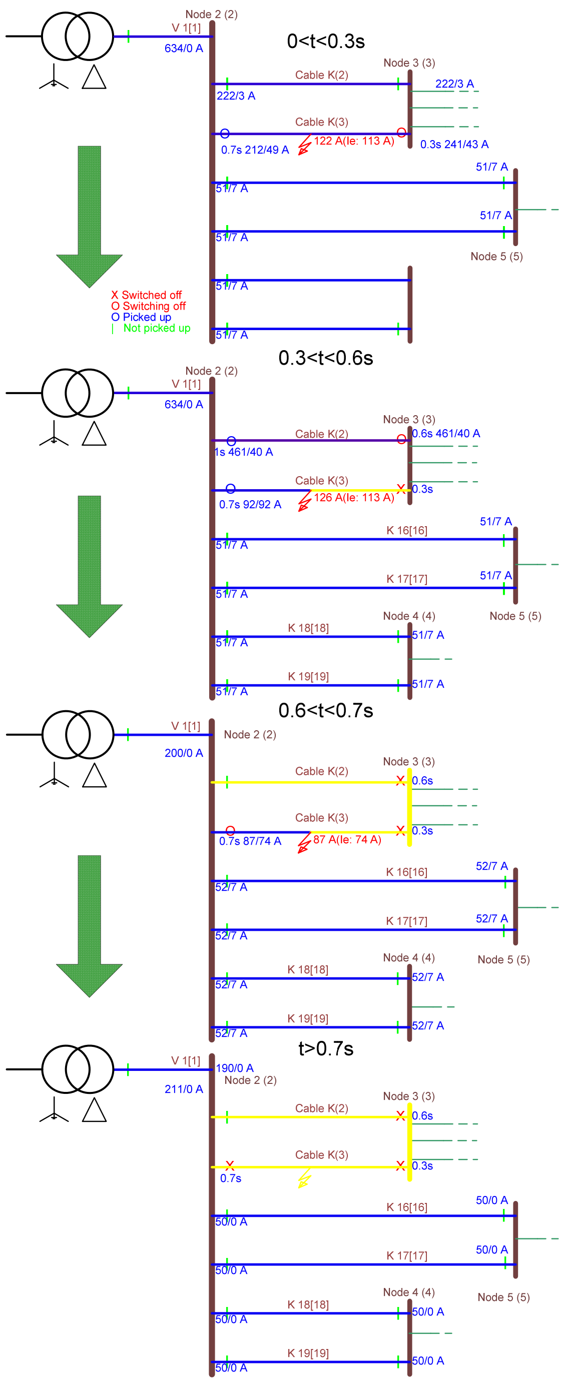

Figure 2-4: (above) three phase-to-ground-fault in cable (3) interrupted correctly. Visualisation has been done using the "Instelpan" Matlab environment. (right) Single phase-to-ground-fault interrupted incorrectly. Both feeder cables have been interrupted while correct fault-isolation is required.

For 0<t<0.3 sec. the fault is being detected by both the directional relay in cable K(3) at node 3 and the overcurrent relay in cable K(2) at node 2. The reader should notice that in this case, the parallel feeder cable carries a negligible fault current. After 0.3s the directional earth-fault element trips and one line end will be switched off. For 0.3<t<0.6s $I_{e,dist}$ flows through the healthy parallel feeder cable towards the fault and is hence detected by the directional earth-fault element, which trips after 0.3 s. as well. Now, the distribution string fed by the parallel cables has been disconnected which is not allowed. After t=0.6 s the fault will be interrupted.

From this can be concluded that, for two parallel feeder cables, the directional earth-fault element may not pick up on fault currents lower than or equal to $I_{e,dist}$. This can also be satisfied by calculating the fault current $3I_0$ during a single phase-to-ground-fault at the substation busbar with only one feeder cable in operation. This current is the very minimum pick up value setting and a certain margin should be taken.

Operation of the overcurrent relays at the substation side of the feeder cables rely on the fault current caused by the sum of the capacitive charging currents of the remaining MV network. The RMS value of this charging current approximately equals

$$I_{e,grid} = 3I_{grid,0} \approx \frac{3U_{line}\omega C_{grid,0}}{\sqrt{3}} \tag{3.5}$$

The earth-fault element should pick up on this value in order to realise correct relay co-ordination. However, $I_{e,grid}$ is not the minimum pick up current setting since the earth-fault element may preferably *not* pick up on single phase-to-ground faults outside the relay's primary- and backup protection zone (i.e. cables 'beyond' the directional overcurrent relay). This holds for n-1 situations as well. Moreover, the overcurrent relay measures a higher current than the directional overcurrent relay due to the distributed capacitive charging current of the protected cable:

$$I_{e,OMT} = I_{e,dist} + \frac{3U_{line}\omega C_{cable}}{\sqrt{3}} = I_{e,dist} + I_{e,cable} \tag{3.6}$$

As can be seen in Figure 2-5, the overcurrent relay and the directional overcurrent relay measure different fault currents. Therefore $I_{e,dist}+I_{e,cable}$ should be chosen as a minimum setting for the earth-fault overcurrent element pick up value.

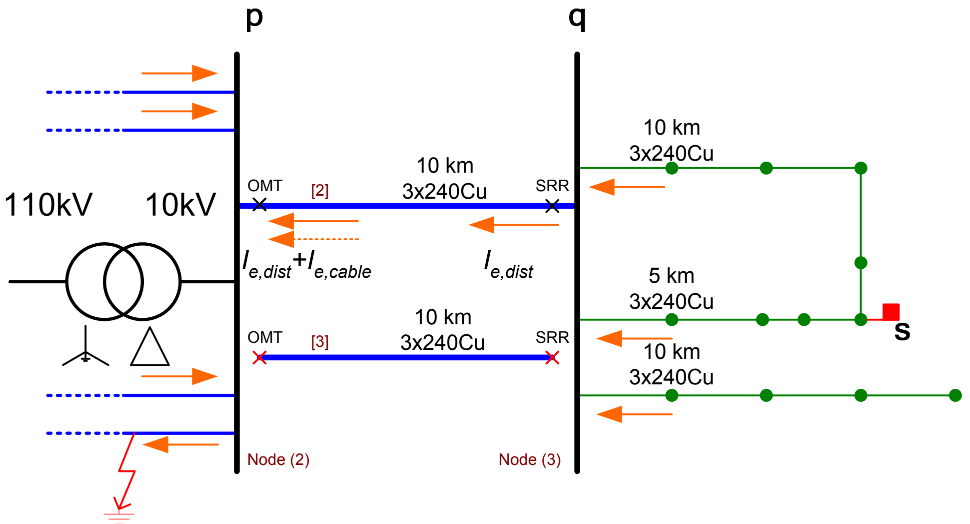

Figure 2-5: Zero-sequence current through a single feeder cable during a remote ground-fault outside the discussed feeder cable

The overcurrent function of the directional relay can be used as a backup protection for ground-faults in the distribution string, but this is *not* recommended since it may certainly not affect the relay co-ordination for faults inside the feeder cables. A pick up value of $\frac{1}{2} I_{e,grid}$ should be set for that purpose. On the other hand, a single-phase to ground fault *inside* the distribution string will cause the capacitive charging current of the cable to flow in opposite direction, making the current measured by the directional relay higher than the current measured by the overcurrent lay. Table 2-1 summarises the minimum pick up current settings for the earth-fault elements of the (directional) overcurrent relays protecting the feeders.

Current Setting	Application	Overcurrent	Directional overcurrent
$+I_e, +t_e$	Dir. earth-fault element pick up current and time	n/a	$I_{e,dist}, 0.3s$
I_e, t_e	Unidirectional earth-fault element pick up current and time	$I_{e,dist} + I_{e,cab}$	$\frac{1}{2} I_{e,grid}, 0.9s$
$+I_>, +t_>$	Dir. Phase element pick up current and time	n/a	600 A, 0.3 s
$+I_{>>}, +t_{>>}$	Dir. Phase element pick up current and time (High setting)	n/a	1500, 20ms.
$I_>, t_>$	Phase element pick up current and time	600 A, 0.9 s	600 A
$I_{>>}, t_{>>}$	Phase element pick up current and time (High setting)	1500 A, 0.1 s	not set

Table 2-1: Minimum (directional) overcurrent relay settings for correct relay co-ordination.

Usually, for large MV networks with a lot of feeders and distribution strings, $I_{e,grid}$ is higher than $I_{e,dist}$ and correct relay co-ordination is satisfied. For a large distribution string however, $I_{e,dist}$ and hence $C_{dist,0}$, reaches a value for which the single phase-to-ground-fault cannot be isolated selectively. The $+I_e$ setting of the directional over-current setting becomes too high to detect ground-faults over the whole protection zone. Since the I_e setting of the overcurrent relay should be at least the $+I_e$ setting of the opposite directional overcurrent relay plus the capacitive charging current of the protected cable ($I_{e,dist}+I_{e,cable}$), ground-faults will not be detected over the whole cable by the overcurrent relay as well. A certain *death-zone* will arise in which ground-faults will not be detected and interrupted by *any* relay in the MV network. Figure 2-6 illustrates the presence of a death zone in both parallel feeder cables of the network of Figure 2-1.

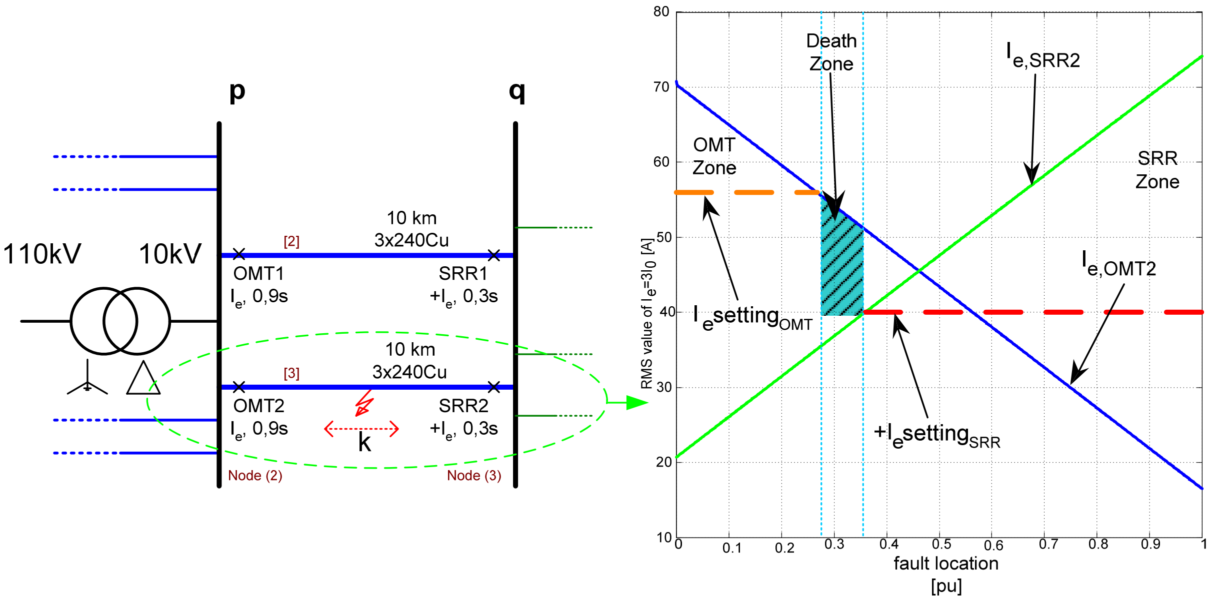

Figure 2-6: The presence of a death zone in the encircled part of the network. Within a certain range of the fault location k, the fault currents from both sides are too small for the relays to pick up. Orange dashed line represents the $I_{e,OMT}$ setting while the red dashed line represents the $+I_{e,SRR}$ setting. k can be varied from 0 (node p) to 1 (node q).

Apparently, the death zone is affected by the position of the $+I_e$ setting line, the I_e setting line of the overcurrent relay, $I_{e,OMT}$ and $I_{e,SRR}$. Since the $+I_e$ setting line depends on $I_{e,dist}$, the presence of the death-zone depends on $C_{dist,0}$. The overcurrent relay and the directional overcurrent relay measure $I_{e,OMT}$ and $I_{e,SRR}$ respectively, which depend on $C_{cable,0}$, $C_{Grid,0}$ and $C_{dist,0}$.

By making use of the aggregated network model as depicted in Figure 2-2, a method will be proposed for relay co-ordination in ungrounded MV distribution networks. It will be examined if the presence of a death-zone depends on the ratio μ:

$$\mu = \frac{C_{dist,0}}{C_{grid,0}} \qquad (3.7)$$

Moreover, the influence of $C_{cable,0}$ on the minimum value of μ, μ_{lim} will be examined as well. For that, the theoretical background of single phase-to-ground-fault calculation will be revised briefly.

2.1.2 Theoretical background

A single-phase short-circuit is generally made up of three periods: the initiating period, the fault itself and the post-fault period. Detection methods are based on the faulted period. Steady-state voltages and currents will be calculated using the sequence components method. Short-circuit calculation is already extensively being applied in (commercial) relay testing software. By means of the block diagram of Figure 2-7, which depicts the basic operation and hence the fault calculation method of this software, the fault calculation method will be explained.

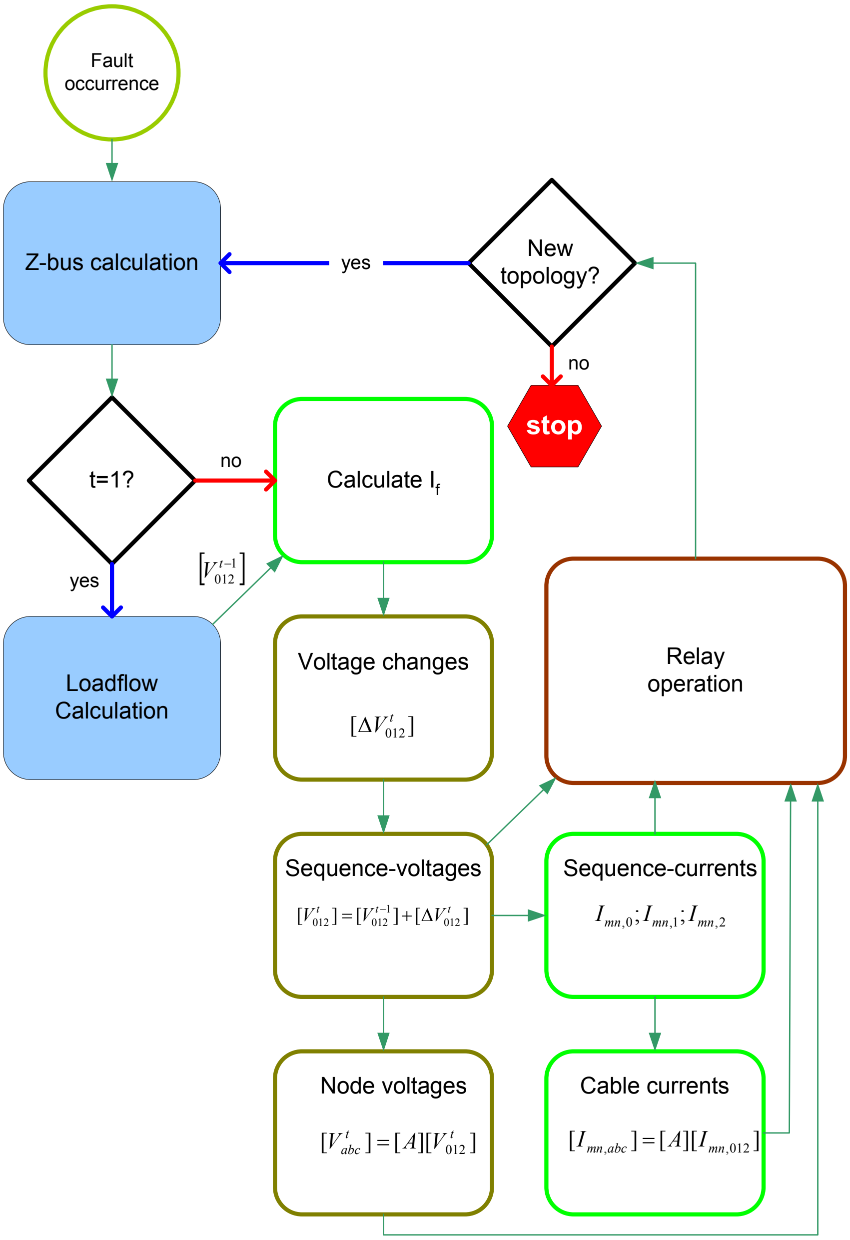

Figure 2-7: Block diagram of the used fault calculation method. Z_{bus} determination and Loadflow calculation are indispensable elements regarding fault calculation. After correct voltage and current calculation, it will be examined if any relay/switchgear operates. A new topology implies another fault calculation step.

Z_{bus} calculation

Usage of Z_{bus} (or Y_{bus}) is indispensable for the discussed fault-calculation method. From the network topology, sequence networks should be constructed which represent the real cable network. Therefore, the construction of sequence-networks is being repeated briefly. From the network of Figure 2-2, a feasible Z_{bus} will be built using the Z_{bus} building algorithm.

Sequence networks: For every sequence-component, a different model represents the network. Normal and negative-sequence network construction is left as a reference [18][22]. The zero-sequence network bears a more sophisticated structure:

- Transformer connections should be taken into account
- Source and load neutral connections should be modelled properly

Transformer connections strongly depend on the neutral grounding method applied to the MV network. As can be seen in Figure 2-8, ungrounded networks are defined by whether a zero-sequence connection between primary and secondary is present or not. Delta connections always yield an interrupted zero-sequence network and could possibly lead to ungrounded parts of the MV network.

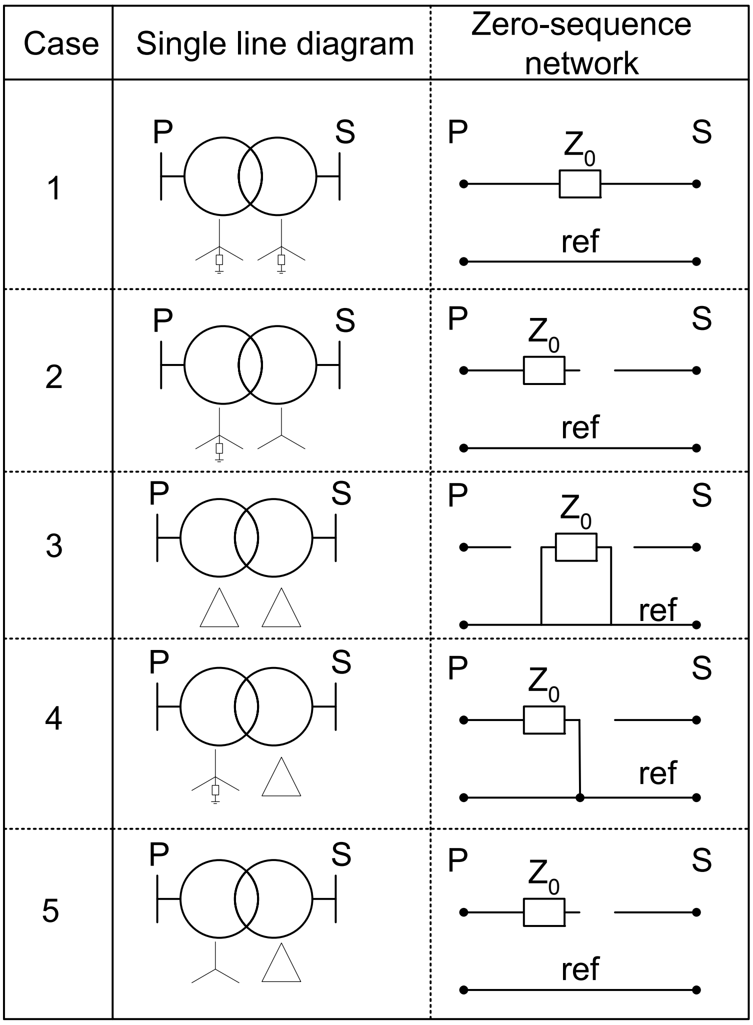

Figure 2-8: Zero-sequence network connection for several transformer winding topologies[18].

The aggregated network is constructed with "type 4" transformers comprising an ungrounded MV network. HV and LV neutral impedances are assumed to be very small (Z_n=0Ω) and of negligible influence on the short-circuit behaviour of in the MV part of the network. Source and load neutral impedances have been chosen very small as well for the same reason.

The aggregated network is decomposed in its sequence networks in Figure 2-9. The healthy cable has been modelled according to Figure 1-6 while the faulted cable has been modelled according to Figure 1-7. The reader should notice that each cable has been split into several parts in order to prevent modelling the capacitance of the cables on the busbars of the MV substations. Current will be measured correctly in this way through a shunt resistance R_{shunt}. Network parameters are given in Appendix C.

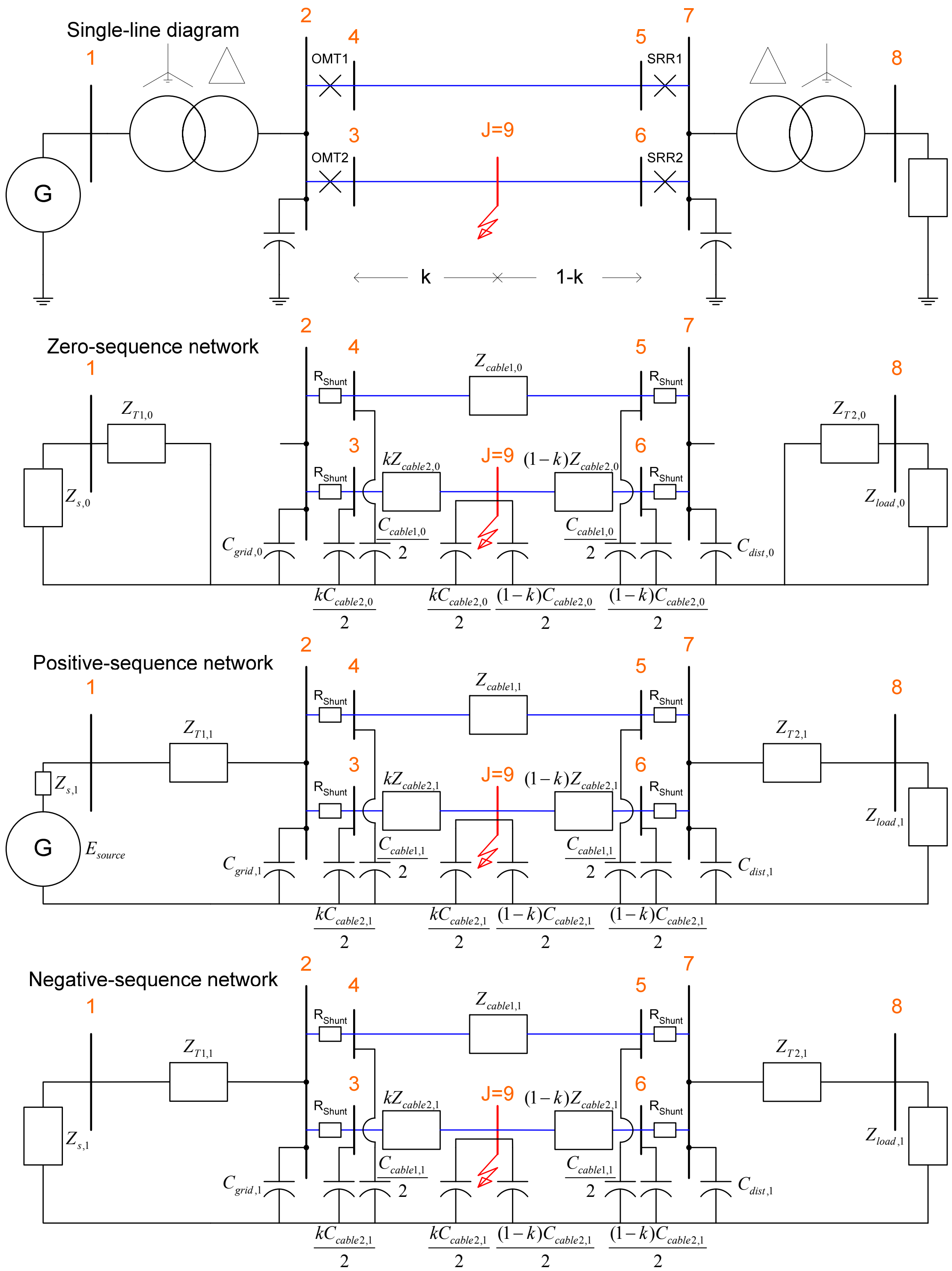

Figure 2-9: Sequence networks for the proposed aggregated MV network. Cable parameters depend on fault location.

Z_{bus} calculation: In order to make short-circuit calculations, a Z_{bus} has to be built for every sequence network. For that, the Z_{bus} building algorithm has been used which has been extensively described in [18] and [23]. Not every step of the building algorithm has been used however and a brief revision of the steps being taken is given now.

Suppose the cable network of Figure 2-1 for which the aggregated sequence-network model of Figure 2-9 is being used for building the Z_{bus}. For all sequence-networks, the same algorithm is used which is principally relying on two basic steps:
Adding a branch from the reference to a new node: Suppose an empty Z_{bus}, for which a new bus (node) is being connected to the reference node. In cable networks, every node has a connection to the reference node by a lumped capacitance, which is representing the distributed capacitance of the cables. For every *new* node, which is connected to the reference by an impedance Z_b, $Z_{bus,new}$ is given by:

$$Z_{new}^{bus} = \left[\begin{array}{c|c} Z_{old}^{bus} & \begin{matrix} 0 \\ \vdots \\ 0 \end{matrix} \\ \hline 0 \;\cdots\; 0 & Z_b \end{array}\right] \tag{3.8}$$

For no connection to ground, $Z_b = 0$ should be taken[23]. For the first node holds:

$$Z^{bus} = [Z_b] \tag{3.9}$$

Adding a branch between two existing nodes: Connections between nodes are being addicted to the Z_{bus} by using the *current injection* method as well. For adding an impedance Z_b between node m and n holds:

$$Z_{temp}^{bus} = \left[\begin{array}{c|c} Z_{orig}^{bus} & \begin{matrix} (col.\, n - col.\, m) \\ of\ Z_{orig}^{bus} \end{matrix} \\ \hline (row\ n - row\ m)\ of\ Z_{orig}^{bus} & Z_{bb} \end{array}\right] \tag{3.10}$$

In which for Z_{bb} holds:

$$Z_{bb} = Z_{mm} + Z_{nn} - 2Z_{mn} + Z_b \tag{3.11}$$

However, Kron-reduction is necessary to remove newly added rows and columns: the total number of nodes should be the same as the total number of rows and columns of the Z_{bus}. Therefore, (3.10) is being rewritten as

$$Z_{temp}^{bus} = \left[\begin{array}{c|c} Z_{orig}^{bus} & \boldsymbol{a} \\ \hline \boldsymbol{b} & Z_{bb} \end{array}\right] \tag{3.12}$$

Now, according to the Kron-reduction algorithm [23]:

$$Z_{new}^{bus} = Z_{orig}^{bus} + \frac{\boldsymbol{ab}}{Z_{bb}} \tag{3.13}$$

The Z_{bus} building algorithm holds for both the zero-sequence network as well as for the positive-sequence network. The negative-sequence Z_{bus} is assumed to be equal to the positive-sequence Z_{bus} since the effects of rotating devices are being neglected[1]. Now, two bus-impedance matrices have been composed which will be used for short-circuit calculations:

$$Z^{bus,0} \text{ and } Z^{bus,1} = Z^{bus,2} \tag{3.14}$$

Loadflow calculation

A loadflow determines the steady-state voltages and currents. Since the system is in balance, only positive-sequence values are present before the fault. For short-circuit calculations, pre-fault voltages should be known in order to model the influence of the load current correctly. In most short-circuit studies, load current is being neglected as a simplification due to the high-amplitude of the fault-currents by taking the pre-fault voltage on every node equal to E_{source}[18]. In ungrounded networks

[1] Generators and motors are assumed to have equal impedances for a clockwise and counter clockwise set of balanced three phase voltages.

however, the load current is of great importance for phase-element operation of protection relays and it should be taken into account by the described assumption.

For single phase-to-ground-faults in ungrounded networks, only the zero-sequence component of currents and voltages should be used for direction determination. As will be shown later on, the positive-sequence network has a negligible influence on the zero-sequence fault current since

$$Z_{jj}^{bus,0} \gg Z_{jj}^{bus,1} \tag{3.15}$$

Where Z_{jj} is the Thévenin impedance of the sequence network at the faulted node j. *Therefore, when only taking zero-sequence currents into account, pre-fault voltages are of minor importance.*

The reader should notice that although the error made in the zero-sequence component is negligible, the error made in the positive-sequence component is certainly not. *The fault-calculation is therefore only adequate for the zero-sequence and negative sequence component*. In order to reduce the error made, the aggregated network is modelled in SIMULINK as well and consequently steady state RMS node voltages are used as input for the fault calculation. A time consuming loadflow calculation, which is of minor importance for zero-sequence quantities, can be avoided in this way.

Fault current calculation

The single phase-to-ground-fault current is defined as the fault current flowing *out* of the faulted bus. Figure 2-10 depicts the faulted situation in the abc-domain. As is shown, the fault current is flowing through fault impedance Z_f which represents the fault arc.

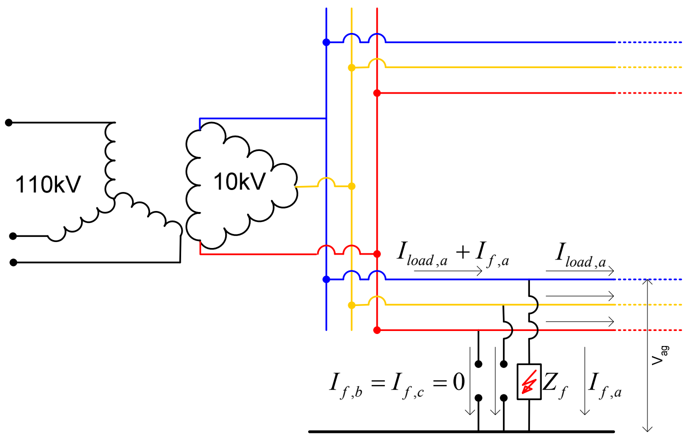

Figure 2-10: Current of phase a flows partly into the fault

For the current *into the fault* holds

$$\underline{I}_{f,a} = \frac{\underline{V}_{f,ag}}{\underline{Z}_f};\ \underline{I}_{f,b} = \underline{I}_{f,c} = 0 \tag{3.16}$$

For the sequence currents into the fault this yields

$$\begin{aligned}
\underline{I}_{f,0} &= \frac{1}{3}\left[\underline{I}_{f,a} + \underline{I}_{f,b} + \underline{I}_{f,c}\right] = \frac{1}{3}\underline{I}_{f,a} \\
\underline{I}_{f,1} &= \frac{1}{3}\left[\underline{I}_{f,a} + a^{-2}\underline{I}_{f,b} + a^{-1}\underline{I}_{f,c}\right] = \frac{1}{3}\underline{I}_{f,a} \\
\underline{I}_{f,2} &= \frac{1}{3}\left[\underline{I}_{f,a} + a^{-1}\underline{I}_{f,b} + a^{-2}\underline{I}_{f,c}\right] = \frac{1}{3}\underline{I}_{f,a}
\end{aligned} \tag{3.17}$$

Because $\underline{I}_{f,0}=\underline{I}_{f,1}=\underline{I}_{f,2}$, the currents flowing out of the sequence networks at the fault bus are equal, yielding a series connection which is shown in Figure 2-11. Knowing the bus impedance matrices, the approximation of the fault arc impedance Z_f and the source voltage $\underline{E}_{source}$, the fault current $\underline{I}_{f,a}$ can be calculated by

$$\underline{I}_{f,a}=\frac{\underline{V}_{f,ag}}{Z_f}=\frac{\underline{E}_{source}}{Z_{jj}^{bus,1}+Z_{jj}^{bus,1}+Z_{jj}^{bus,0}+3Z_f} \tag{3.18}$$

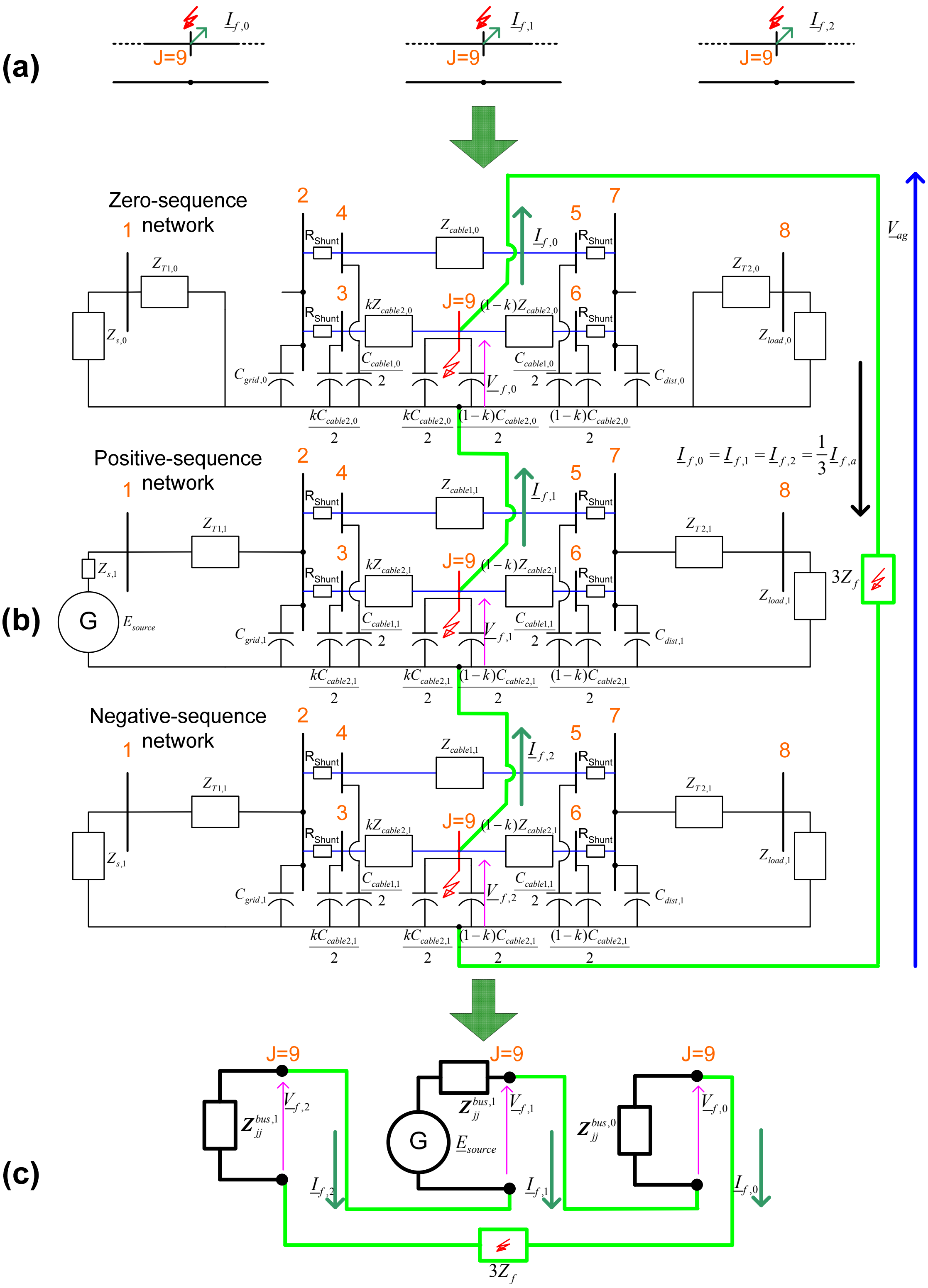

Figure 2-11: Sequence network connection during single phase-to-ground-fault

Voltage calculation

Sequence voltage changes calculation: The fault current flowing out of the faulted bus causes a voltage change in the sequence networks comparing to the pre-fault voltages. This change is defined as the sequence voltage change on every node caused by the *injection* of only the fault current *into* the fault bus[18]. Thus, the zero sequence voltage changes of a network with *N* nodes and one fault bus *j* are given by

$$\begin{bmatrix} \Delta\underline{V}^{1}_{f,0} \\ \vdots \\ \Delta\underline{V}^{N}_{f,0} \\ \Delta\underline{V}^{j}_{f,0} \end{bmatrix} = \begin{bmatrix} Z^{bus,0}_{1,1} & \cdots & Z^{bus,0}_{1,N} & Z^{bus,0}_{1,j} \\ \vdots & \ddots & \vdots & \vdots \\ Z^{bus,0}_{N,1} & \cdots & Z^{bus,0}_{N,N} & Z^{bus,0}_{N,j} \\ Z^{bus,0}_{j,1} & \cdots & Z^{bus,0}_{j,N} & Z^{bus,0}_{j,j} \end{bmatrix} \begin{bmatrix} 0 \\ 0 \\ 0 \\ -\underline{I}_{f,0} \end{bmatrix} = \begin{bmatrix} -Z^{bus,0}_{1,j}\,\underline{I}_{f,0} \\ \vdots \\ -Z^{bus,0}_{N,j}\,\underline{I}_{f,0} \\ -Z^{bus,0}_{j,j}\,\underline{I}_{f,0} \end{bmatrix} \tag{3.19}$$

The reader should notice that the fault bus is located at the last element of $Z_{bus,0}$. Changes in the network topology can be made faster in this way. For fault calculation itself it should not make a difference. For voltage changes in the positive-sequence network holds

$$\begin{bmatrix} \Delta\underline{V}^{1}_{f,1} \\ \vdots \\ \Delta\underline{V}^{N}_{f,1} \\ \Delta\underline{V}^{j}_{f,1} \end{bmatrix} = \begin{bmatrix} Z^{bus,1}_{1,1} & \cdots & Z^{bus,1}_{1,N} & Z^{bus,1}_{1,j} \\ \vdots & \ddots & \vdots & \vdots \\ Z^{bus,1}_{N,1} & \cdots & Z^{bus,1}_{N,N} & Z^{bus,1}_{N,j} \\ Z^{bus,1}_{j,1} & \cdots & Z^{bus,1}_{j,N} & Z^{bus,1}_{j,j} \end{bmatrix} \begin{bmatrix} 0 \\ 0 \\ 0 \\ -\underline{I}_{f,1} \end{bmatrix} = \begin{bmatrix} -Z^{bus,1}_{1,j}\,\underline{I}_{f,1} \\ \vdots \\ -Z^{bus,1}_{N,j}\,\underline{I}_{f,1} \\ -Z^{bus,1}_{j,j}\,\underline{I}_{f,1} \end{bmatrix} \tag{3.20}$$

And consequently for the voltage changes in the positive-sequence network

$$\begin{bmatrix} \Delta\underline{V}^{1}_{f,2} \\ \vdots \\ \Delta\underline{V}^{N}_{f,2} \\ \Delta\underline{V}^{j}_{f,2} \end{bmatrix} = \begin{bmatrix} Z^{bus,1}_{1,1} & \cdots & Z^{bus,1}_{1,N} & Z^{bus,1}_{1,j} \\ \vdots & \ddots & \vdots & \vdots \\ Z^{bus,1}_{N,1} & \cdots & Z^{bus,1}_{N,N} & Z^{bus,1}_{N,j} \\ Z^{bus,1}_{j,1} & \cdots & Z^{bus,1}_{j,N} & Z^{bus,1}_{j,j} \end{bmatrix} \begin{bmatrix} 0 \\ 0 \\ 0 \\ -\underline{I}_{f,2} \end{bmatrix} = \begin{bmatrix} -Z^{bus,1}_{1,j}\,\underline{I}_{f,2} \\ \vdots \\ -Z^{bus,1}_{N,j}\,\underline{I}_{f,2} \\ -Z^{bus,1}_{j,j}\,\underline{I}_{f,2} \end{bmatrix} \tag{3.21}$$

Since $\underline{I}_{f,1}=\underline{I}_{f,2}$ and $Z_{bus,2}=Z_{bus,1}$ in case of a single-phase to ground fault in the described MV network, (3.20) and (3.21) imply the same calculation in this case.

Sequence voltages calculation: After calculating the sequence-voltage changes due to a fault at node j, these voltages should be superposed to the pre-fault voltages according to

$$\begin{bmatrix} \underline{V}^{1}_{f,0} \\ \vdots \\ \underline{V}^{N}_{f,0} \\ \underline{V}^{j}_{f,0} \end{bmatrix} = \begin{bmatrix} \Delta\underline{V}^{1}_{f,0} \\ \vdots \\ \Delta\underline{V}^{N}_{f,0} \\ \Delta\underline{V}^{j}_{f,0} \end{bmatrix} = \begin{bmatrix} -Z^{bus,0}_{1,j}\,\underline{I}_{f,0} \\ \vdots \\ -Z^{bus,0}_{N,j}\,\underline{I}_{f,0} \\ -Z^{bus,0}_{j,j}\,\underline{I}_{f,0} \end{bmatrix} \quad \text{and} \quad \begin{bmatrix} \underline{V}^{1}_{f,2} \\ \vdots \\ \underline{V}^{N}_{f,2} \\ \underline{V}^{j}_{f,2} \end{bmatrix} = \begin{bmatrix} \Delta\underline{V}^{1}_{f,2} \\ \vdots \\ \Delta\underline{V}^{N}_{f,2} \\ \Delta\underline{V}^{j}_{f,2} \end{bmatrix} = \begin{bmatrix} -Z^{bus,1}_{1,j}\,\underline{I}_{f,2} \\ \vdots \\ -Z^{bus,1}_{N,j}\,\underline{I}_{f,2} \\ -Z^{bus,1}_{j,j}\,\underline{I}_{f,2} \end{bmatrix} \tag{3.22}$$

For zero-sequence and negative-sequence component and yielding for the positive-sequence component

$$\begin{bmatrix} \underline{V}^{1}_{f,1} \\ \vdots \\ \underline{V}^{N}_{f,1} \\ \underline{V}^{j}_{f,1} \end{bmatrix} = \begin{bmatrix} \underline{V}^{1}_{prefault,1} \\ \vdots \\ \underline{V}^{N}_{prefault,1} \\ \underline{V}^{j}_{prefault,1} \end{bmatrix} + \begin{bmatrix} \Delta\underline{V}^{1}_{f,1} \\ \vdots \\ \Delta\underline{V}^{N}_{f,1} \\ \Delta\underline{V}^{j}_{f,1} \end{bmatrix} = \begin{bmatrix} \underline{V}^{1}_{prefault,1} \\ \vdots \\ \underline{V}^{N}_{prefault,1} \\ \underline{V}^{j}_{prefault,1} \end{bmatrix} + \begin{bmatrix} -Z^{bus,1}_{1,j}\,\underline{I}_{f,1} \\ \vdots \\ -Z^{bus,1}_{N,j}\,\underline{I}_{f,1} \\ -Z^{bus,1}_{j,j}\,\underline{I}_{f,1} \end{bmatrix} \tag{3.23}$$

Phase voltages calculation: Now, sequence voltages on every node in the network have been calculated. Phase voltages can be calculated by the inverse symmetrical component transformation yielding

$$\begin{bmatrix} \underline{V}^1_{f,a} \\ \underline{V}^1_{f,b} \\ \underline{V}^1_{f,c} \\ \vdots \\ \vdots \\ \vdots \\ \underline{V}^j_{f,a} \\ \underline{V}^j_{f,b} \\ \underline{V}^j_{f,c} \end{bmatrix} = \frac{1}{3} \left[\begin{array}{ccc|ccc|ccc} 1 & 1 & 1 & \cdot & \cdot & \cdot & \cdot & \cdot & \cdot \\ 1 & a^{-2} & a^{-1} & \cdot & \cdot & \cdot & \cdot & \cdot & \cdot \\ 1 & a^{-1} & a^{-2} & \cdot & \cdot & \cdot & \cdot & \cdot & \cdot \\ \hline \cdot & \cdot & \cdot & \ddots & \ddots & \ddots & \cdot & \cdot & \cdot \\ \cdot & \cdot & \cdot & \ddots & \ddots & \ddots & \cdot & \cdot & \cdot \\ \cdot & \cdot & \cdot & \ddots & \ddots & \ddots & \cdot & \cdot & \cdot \\ \hline \cdot & \cdot & \cdot & \cdot & \cdot & \cdot & 1 & 1 & 1 \\ \cdot & \cdot & \cdot & \cdot & \cdot & \cdot & 1 & a^{-2} & a^{-1} \\ \cdot & \cdot & \cdot & \cdot & \cdot & \cdot & 1 & a^{-1} & a^{-2} \end{array} \right] \begin{bmatrix} \underline{V}^1_{f,0} \\ \underline{V}^1_{f,1} \\ \underline{V}^1_{f,2} \\ \vdots \\ \vdots \\ \vdots \\ \underline{V}^j_{f,0} \\ \underline{V}^j_{f,1} \\ \underline{V}^j_{f,2} \end{bmatrix} = \left[\begin{array}{c|c|c} A^{-1} & \cdot & \cdot \\ \hline \cdot & \ddots & \cdot \\ \hline \cdot & \cdot & A^{-1} \end{array} \right] \begin{bmatrix} \underline{V}^1_{f,0} \\ \underline{V}^1_{f,1} \\ \underline{V}^1_{f,2} \\ \vdots \\ \vdots \\ \vdots \\ \underline{V}^j_{f,0} \\ \underline{V}^j_{f,1} \\ \underline{V}^j_{f,2} \end{bmatrix} \tag{3.24}$$

Where A^{-1} is the inverse symmetrical component transformation matrix. The most essential part of the fault calculation has now been established forming a foundation for fault-current calculations.

Cable currents calculation

Sequence currents calculation: Since the sequence voltages on every node are known, the phase currents through the cable conductors can be calculated. For a cable *between* node *m* and *n*, the sequence currents are given by

$$\begin{bmatrix} \underline{I}^0_{m\to n,(v)} \\ \underline{I}^1_{m\to n,(v)} \\ \underline{I}^2_{m\to n,(v)} \end{bmatrix} = \begin{bmatrix} \frac{1}{Z^0_{mn,v}} & \cdot & \cdot \\ \cdot & \frac{1}{Z^1_{mn,v}} & \cdot \\ \cdot & \cdot & \frac{1}{Z^1_{mn,v}} \end{bmatrix} \begin{bmatrix} \underline{V}^m_{f,0} - \underline{V}^n_{f,0} \\ \underline{V}^m_{f,1} - \underline{V}^n_{f,1} \\ \underline{V}^m_{f,2} - \underline{V}^n_{f,2} \end{bmatrix} \tag{3.25}$$

Note that subscript v implies the possibility of more than one connection between node m and n. Moreover, it should be stated expressly that

$$Z^0_{mn,v} \neq Z^{bus,0}_{mn} \neq Z^0_{mn,Thévenin} \quad \text{and} \quad Z^1_{mn,v} \neq Z^{bus,1}_{mn} \neq Z^1_{mn,Thévenin} \tag{3.26}$$

Large networks will generally be calculated using the Y_{bus} calculation method for the currents between nodes. For the parallel admittance of the cables between nodes m and n can be written

$$Y^0_{mn} = Y^0_{mn,1} + \cdots + Y^0_{mn,v} = -Y^{bus,0}_{mn} \quad \text{and} \quad Y^1_{mn} = Y^1_{mn,1} + \cdots + Y^1_{mn,v} = -Y^{bus,1}_{mn} \tag{3.27}$$

Both calculation methods can be used and should lead to the same results. Here, the first method is being used since the network is relatively small.

Phase currents calculation: Now, the sequence currents through every cable are known. In order to finish the fault calculation, phase currents will be calculated by

$$\begin{bmatrix} \underline{I}^a_{m\to n,(v)} \\ \underline{I}^b_{m\to n,(v)} \\ \underline{I}^c_{m\to n,(v)} \end{bmatrix} = \frac{1}{3} \begin{bmatrix} 1 & 1 & 1 \\ 1 & a^{-2} & a^{-1} \\ 1 & a^{-1} & a^{-2} \end{bmatrix} \begin{bmatrix} \underline{I}^0_{m\to n,(v)} \\ \underline{I}^1_{m\to n,(v)} \\ \underline{I}^2_{m\to n,(v)} \end{bmatrix} \tag{3.28}$$

For every node N and for every cable *v* between node *m* and *n*.

The complete fault current calculation has now been established. Again it is emphasized to the reader that calculated voltages and currents strongly depend on the pre-fault voltages, which have not been acquired by a loadflow but by simulation with Simulink. This can lead to differences between calculated and real currents and voltages. However, for the zero-sequence values of voltages and currents this error is negligible and thus the directional earth-fault element will be simulated correctly.

2.1.3 Simulation

The short-circuit calculations are realised with Matlab. The bus impedance matrices of the sequence networks of Figure 2-9 are given in Appendix C. First, $C_{Grid,0}$ and $C_{Grid,1}$ will be assumed fixed and both $C_{dist,0}$ and $C_{dist,1}$ will be varied from 0 to $2C_{Grid,0}$ and $2C_{Grid,1}$ respectively. From k=0 to k=1 a ground-fault will be simulated. Second, $C_{Grid,0}$ and $C_{Grid,1}$ are varied as well and again, a ground-fault will be simulated from k=0 to k=1. Thereafter, the influence of μ on the relay co-ordination will be examined.

The minimum setting of the overcurrent en directional overcurrent relays given in Table 2-1 will be applied during the relay co-ordination simulation. In practice however, the relay overcurrent settings should be higher than the minimum setting for two reasons.

First, the proposed minimum overcurrent settings are the lowest minimum setting and leave little margin for any expansion of the distribution network. More cables inevitably lead to higher capacitances to ground and thus to higher zero-sequence fault currents. Correct relay co-ordination is no longer satisfied and therefore the $+I_e$ and I_e setting of all the relays in the affected part of the network should be adjusted. Second, the reader should notice that fault-current calculations always depend on the model used. Although the described model is widely used in general, it is still a simplification of the actual network behaviour. Therefore, a margin of αx100% has been introduced to the $+I_e$ and I_e settings of both overcurrent and directional overcurrent relays, yielding the settings of Table 2-2. The value of α cannot be determined scientifically and strongly depends on expected expansions by the operational management in the near future. α=0, α=25, α=40 and α=50 will be examined in the relay co-ordination study.

Current Setting	Overcurrent	Directional overcurrent
$+I_e,+t_e$	n/a	$>\left(1+\frac{\alpha}{100}\right)\cdot I_{e,dist}, 0.3s$
I_e, t_e	$\left(1+\frac{\alpha}{100}\right)\cdot I_{e,dist}+I_{e,cable}, 0.9s$	$>\left(\frac{1}{2}+\frac{\alpha}{50}\right)I_{e,grid}, 0.9s$
$+I_>,+t_>$	n/a	600 A, 0.3 s
$+I_{>>},+t_{>>}$	n/a	1500A, 20ms.
$I_>,t_>$	600 A, 0.9 s	600 A
$I_{>>},t_{>>}$	1500 A, 0.1 s	not set

Table 2-2: Recommended minimum overcurrent settings

Results

For the aggregated network depicted in Figure 2-9, of which the parameters are given in Appendix C, the fault location k is being varied from 0 to 1 per unit. The directional relays and overcurrent relays have been set according to Table 2-2. Figure 2-12 gives zero-sequence fault current distribution measured by both relays for α=0, 25, 40 and 50. Correct relay co-ordination is only satisfied if

$$I_{e,SRR2} > I_{e,dist} \cup I_{e,OMT2} > I_{e,dist} + I_{e,Cable} \quad \forall \quad k \in \{0..1\} \tag{3.29}$$

The reader should notice that only for α=0 relay co-ordination will be satisfied: for every value of k, SRR2 or OMT2 (or both) will pick up. For α=25, a death-zone is present in which the fault current is too small for the relays to pick up on.

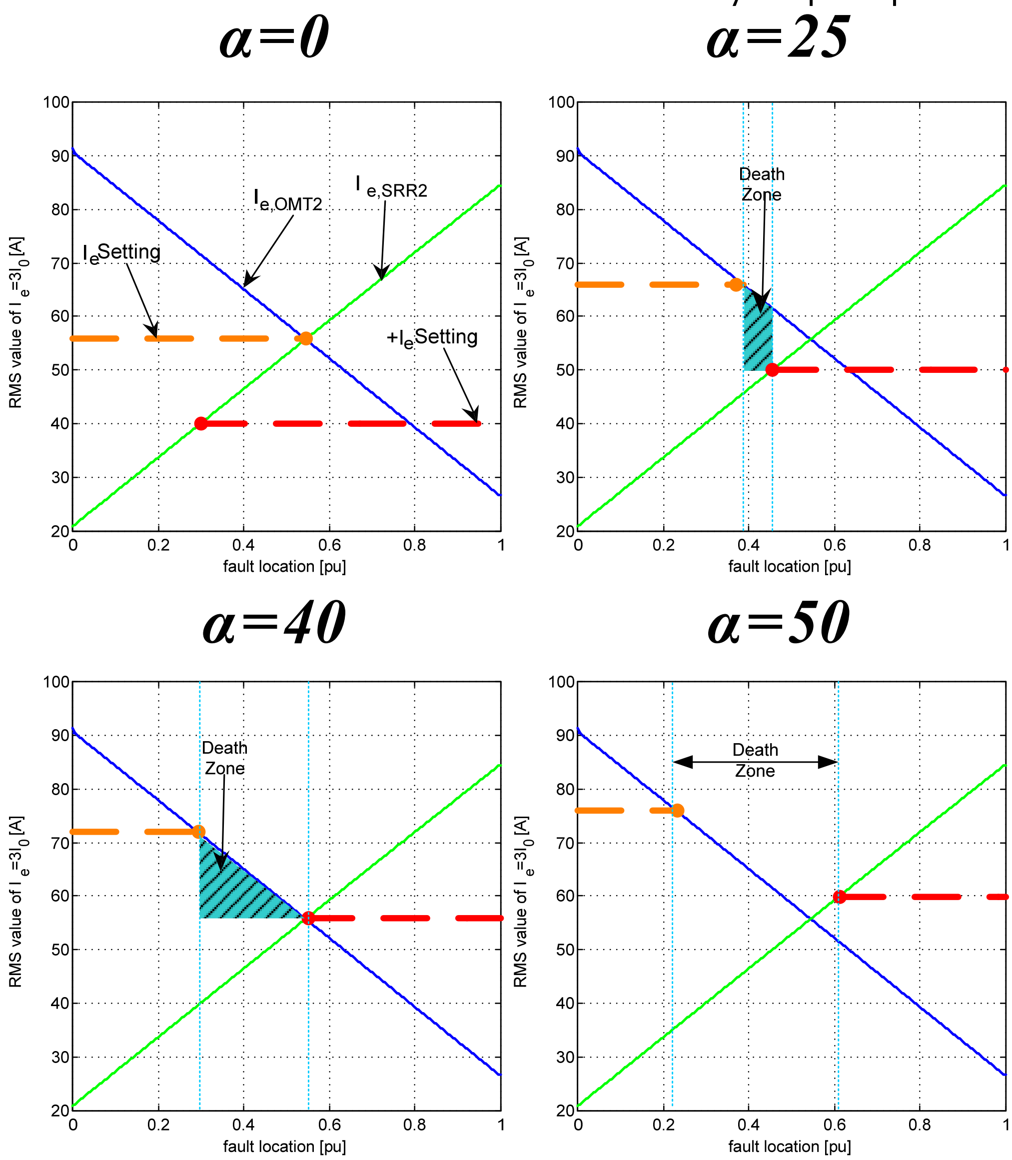

Figure 2-12: Earth-fault current distribution as a function of fault location. For α=25,40 & 50, a death-zone is present.

α=0 is the very minimum setting of the relay's pickup current to satisfy relay co-ordination. For 0<k<0.3, only the overcurrent relay's earth-fault element picks up. For 0.3<k<0.55 both SRR2 and OMT2 will pick up and SRR2 will trip first. For k>0.55, only the directional overcurrent relay picks up.

The above-mentioned fault-current calculation only relies on one value of $C_{dist,0}$ and hence on only one value of μ. No conclusions can be drawn about the dependency of μ on the relay co-ordination. Therefore, $C_{dist,0}$ and $C_{dist,1}$ are being varied as $C_{cable,0}$, $C_{cable,1}$, $C_{Grid,0}$ and $C_{Grid,1}$ are being held constant. This results in the three-dimensional fault-current plots of Figure 2-13 to Figure 2-16, in which the fault currents $I_{e,OMT2}$ and $I_{e,SRR2}$ have been plotted as a function of the factor μ and the fault location k for several values of α. Since the relays pickup settings depend mainly on $I_{e,dist}$ and hence on μ, these settings form a surface with pickup values proportional to μ.

For $\mu \approx 1.2 = \mu_{lim}$ in Figure 2-13, the pickup setting of the relays becomes too high to switch off a ground-fault at any place in the cable. For $\mu > 1.2$, a death-zone is present and single phase-to-ground-faults cannot be switched off selectively.

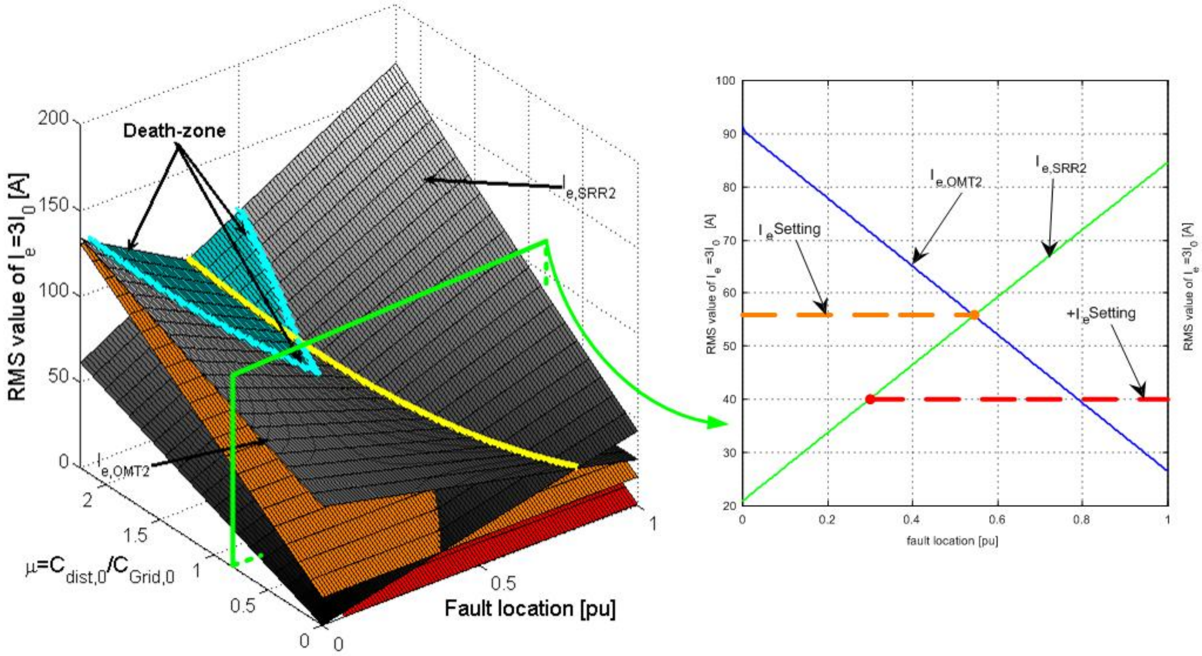

Figure 2-13: Overcurrent and directional overcurrent relay's earth-fault current as a function of the network capacitance ratio μ and the fault location k for α=0. The three dimensional plot is constructed by calculation fault-current distribution of Figure 2-12 for several values of μ. The development of a death-zone is indicated with arrows.

As already mentioned, $\alpha=0$ is the very minimum current setting. For $\alpha>0$, the death-zone will be more extended and hence $\mu_{lim,\alpha=0} \approx 1.2$. For $\alpha=25$ the permitted capacitance, and hence cable length has been more reduced, as can be seen in Figure 2-14. The X-Y view gives a better insight in the death-zone distribution. This zone is located approximately in the upper left corner of the X-Y plane, stretching out nearly 75% of the cable length. While μ is high and so is the earth-fault overcurrent setting, single-phase to ground faults will not be switched off. *It should be stated that only the lowest value of μ for which a death-zone exists,* ***μ_{lim},*** *is important for relay co-ordination studies* and for $\alpha=25$ holds $\mu_{lim,\alpha=25} \approx$ **0.7**. Figure 2-15 and Figure 2-16 depict the death-zone distribution for $\alpha=40$ and $\alpha=50$, leading to even smaller values of μ_{lim}. For $\alpha=40$ holds $\mu_{lim,\alpha=40} \approx$ **0.65** and for $\alpha=50$ holds $\mu_{lim,\alpha=50} \approx$ **0.6**, implying a permissible distribution string capacitance of only

$$C_{dist,0} = \sum_{n=q}^{\text{distribution string}} C_{G,n} = \mu_{lim,\alpha=50} C_{Grid,0} = 0.65 * 8.96\mu F = 5.82\mu F \qquad (3.30)$$

corresponding to approximately 21 km of 3x240 Cu PIL cable.

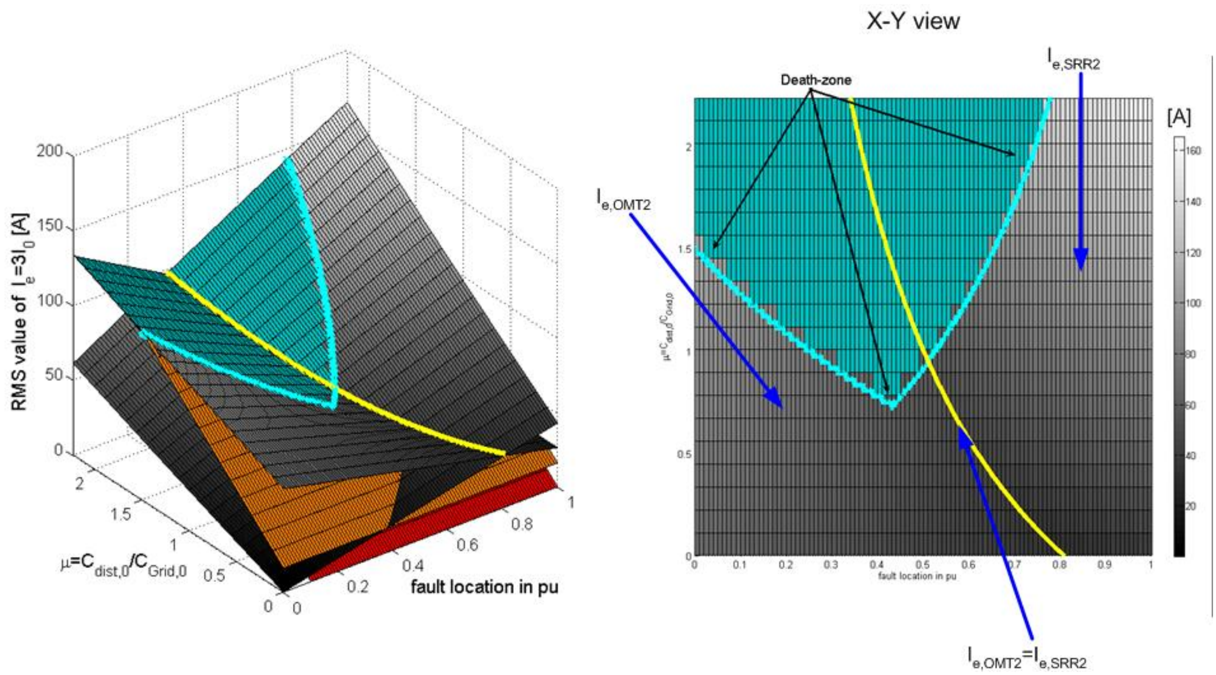

Figure 2-14: Overcurrent and directional overcurrent relay's earth-fault current as a function of the network capacitance ratio μ and the fault location k for α=25 (left). The death-zone presence is illustrated by the X-Y view (right)

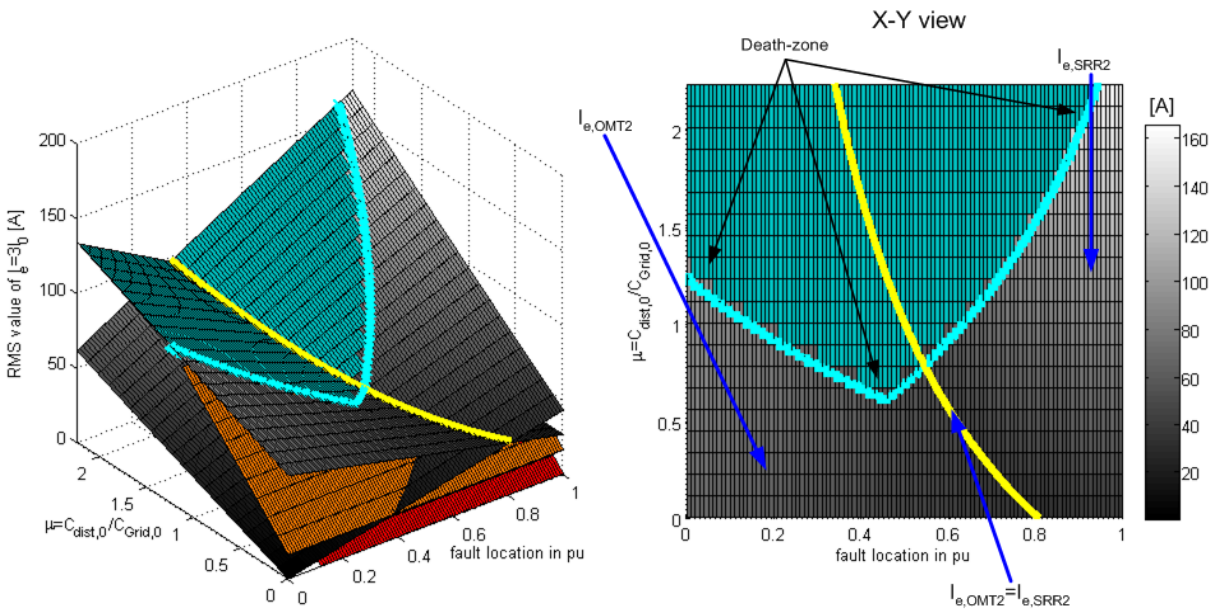

Figure 2-15: Overcurrent and directional overcurrent relay's earth-fault current as a function of the network capacitance ratio μ and the fault location k for α=40 (left). The death-zone presence is illustrated by the X-Y view (right)

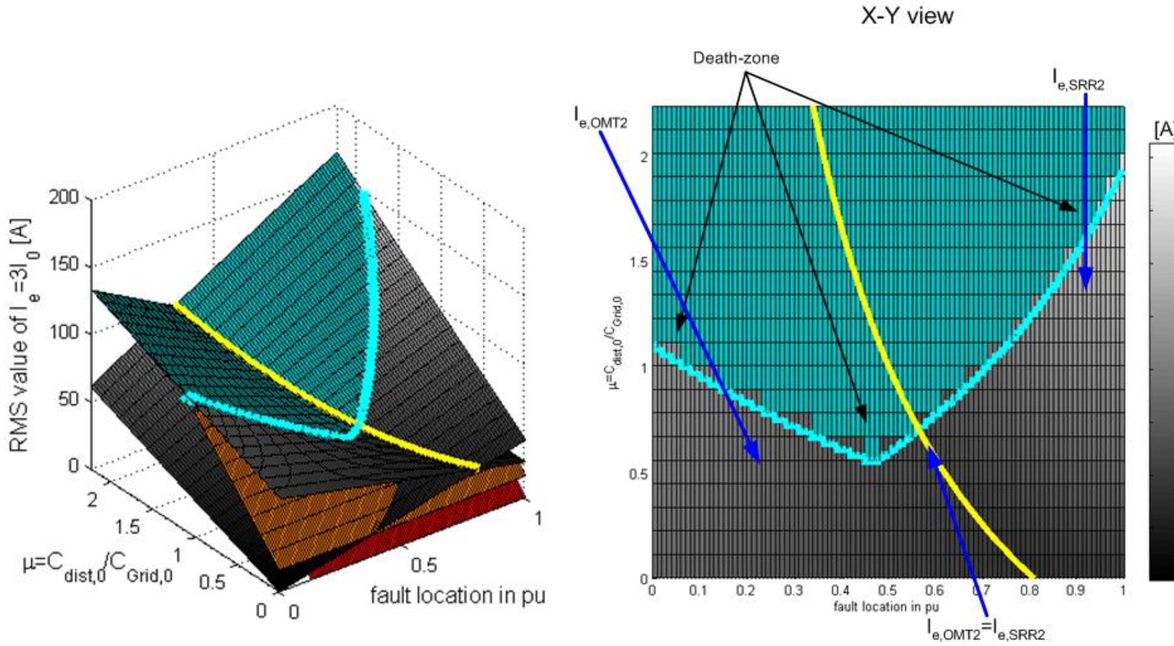

Figure 2-16: Overcurrent and directional overcurrent relay's earth-fault current as a function of the network capacitance ratio μ and the fault location k for α=50 (left). The extensive death-zone presence is illustrated by the X-Y view (right)

The discussed short-circuit study corresponds to the circuit parameters given in Appendix C. Although the variation of the length of the distribution string's cables , and so the values of $C_{dist,0}$ and $C_{dist,1}$ are realistic, the cable's length of the remaining part of the MV network is underestimated (32 km 3x240 Cu PILC). A more realistic length would be 60 km. Therefore, the relay co-ordination study is repeated with $C_{Grid,0}$=16.8μF and $C_{Grid,1}$=30.6μF for α=0 and α=25, as can be seen in Figure 2-17 and Figure 2-18.

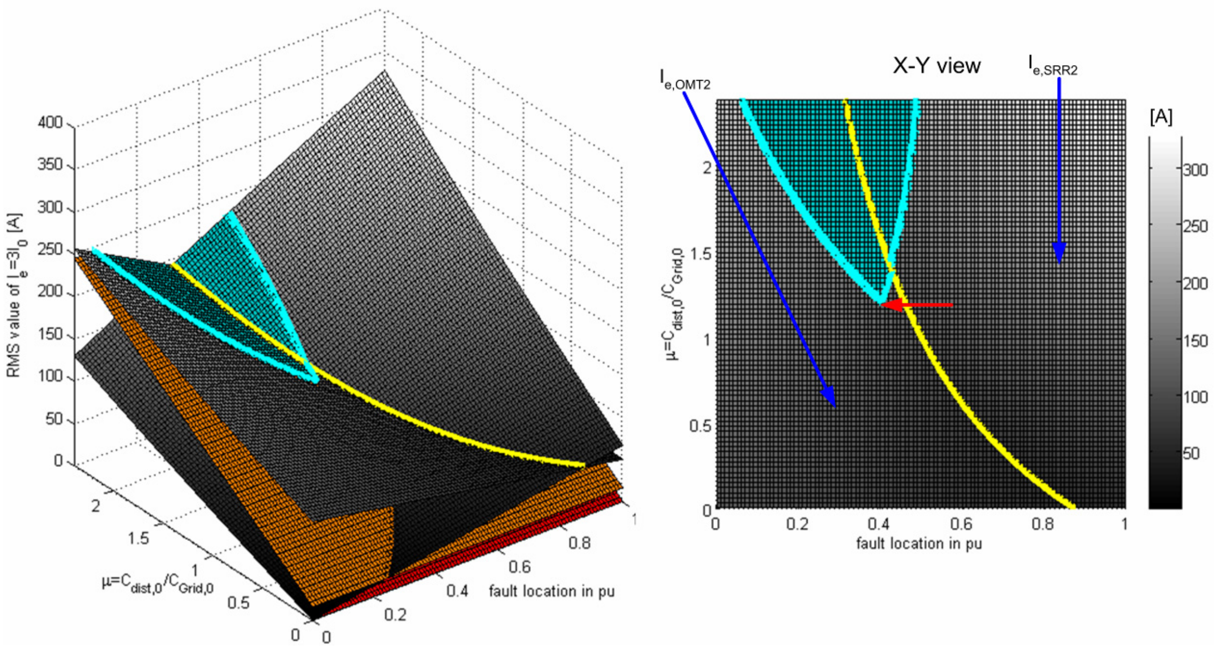

Figure 2-17: Overcurrent and directional overcurrent relay's earth-fault current as a function of the network capacitance ratio μ and the fault location k for α=0 (left) and $C_{Grid,0}$=16.8μF. The death-zone presence is illustrated by the X-Y view (right)

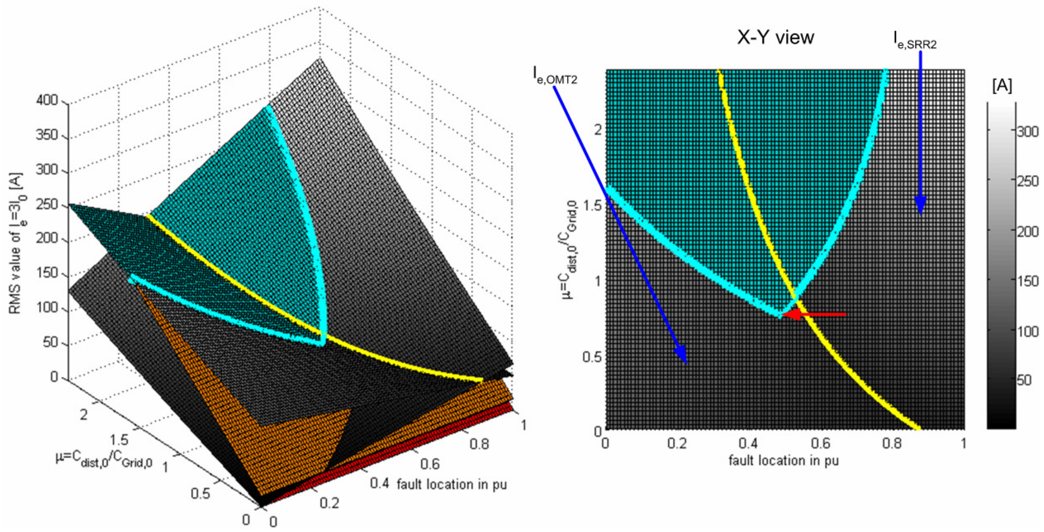

Figure 2-18: Overcurrent and directional overcurrent relay's earth-fault current as a function of the network capacitance ratio μ and the fault location k for α=25 (left) and $C_{Grid,0}$=16.8μF. The death-zone presence is illustrated by the X-Y view (right)

For this value of $C_{Grid,0}$, a few changes regarding the previous value of $C_{Grid,0}$ can be observed. First, the values of μ_{lim} (indicated by the red arrows in the X-Y view) differ slightly from the previous values. Since the length of the MV network cables has been increased and the distribution string length has been kept fixed, the influence of $I_{e,dist}$ has been decreased comprising a higher value of μ_{lim}. Second, the area of the death-zone is smaller compared to the previous size of the network-side cables.

Both observations indicate a rebuttal of the previously stated influence of μ on correct relay co-ordination. Since μ_{lim} varies with $C_{Grid,0}$ as well, the influence of $C_{Grid,0}$ on μ_{lim} should be examined by calculating μ_{lim} (and hence $C_{dist,0,lim}$) for several values of $C_{Grid,0}$. Figure 2-19 depicts both the values of μ_{lim} and the *limit* values of $C_{dist,0}$ (=$C_{dist,0,lim}$) as a function of $C_{Grid,0}$ for α=0, α=25, α=40 and α=50. Capacitances have been varied with steps of 1 μF and the fault location has been varied from 0 to 1 per unit with steps of 1/100 of the feeder cable length. Note that every data point in Figure 2-19a is a value of μ_{lim}, the first appearance of a death-zone as indicated by a red arrow for only one calculation like Figure 2-18.

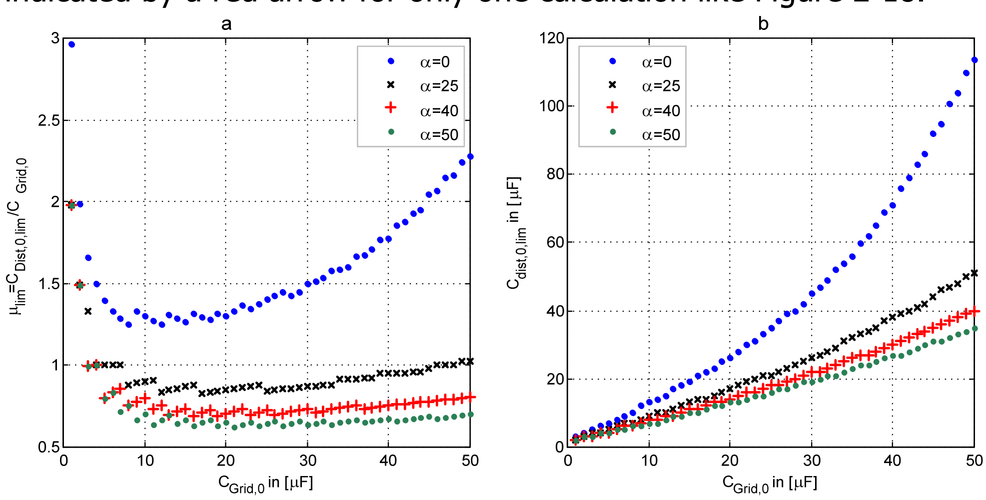

Figure 2-19(a) μ_{lim} as a function of $C_{Grid,0}$ for a feeder cable length of 10km and α=0, 25, 40 and 50; (b) $C_{dist,0,lim}$ as a function of $C_{Grid,0}$ for a feeder cable length of 10km and α=0, 25, 40 and 50.

For α=25, α=40 and α=50 the relation between $C_{Grid,0}$ and $C_{dist,0,lim}$ (and hence μ_{lim}) is relatively linear from $C_{Grid,0}$=5 µF. However, for α=0 the relation is only relatively linear between $C_{Grid,0}$=5 µF and $C_{Grid,0}\approx$30 µF. It should be noted that the majority of the MV networks has a total capacitance smaller than 30 to 35 µF (approximately the linear region). Above $C_{Grid,0}$=30 µF, the value of μ_{lim} increases with $C_{Grid,0}$, allowing a comparatively higher value of $C_{dist,0,lim}$ and thus a more extensive distribution network beyond the feeder cables. Again, it can be doubted as to whether α=0 should be applied while this is the very minimum setting of the protection system.

Above calculations comprise a feeder cable length of 10 km. Although present in extensive agricultural areas, feeder cables in urban areas are a lot shorter, leading to different current settings for the overcurrent relays. Therefore, previous calculations are repeated with feeder cable lengths of 5, 2 and 1 km, as can be seen in Figure 2-20 to Figure 2-22.

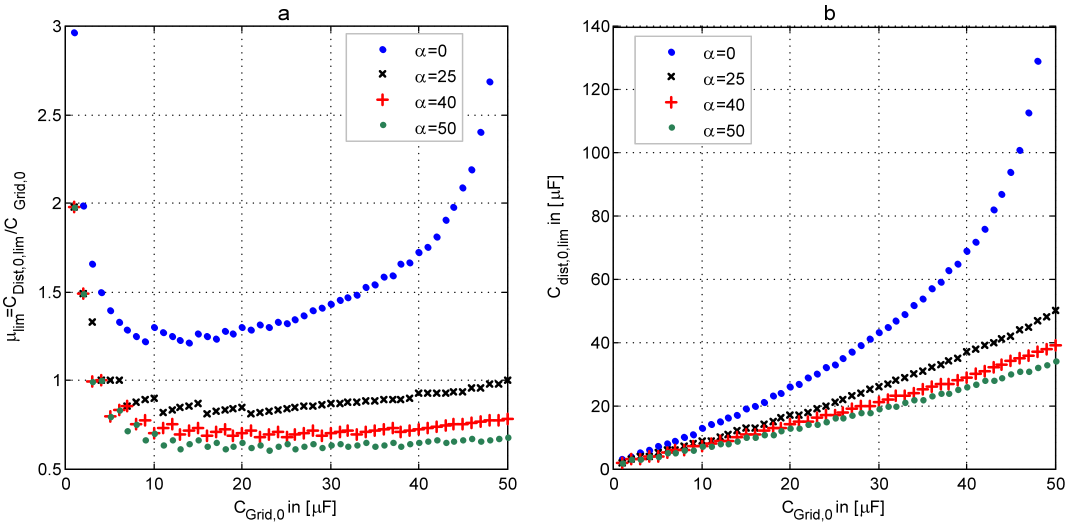

Figure 2-20(a) μ_{lim} as a function of $C_{Grid,0}$ for a feeder cable length of 5km. and α=0, 25, 40 and 50; (b) $C_{dist,0}$ as a function of $C_{Grid,0,lim}$ for a feeder cable length of 5km and α=0, 25, 40 and 50.

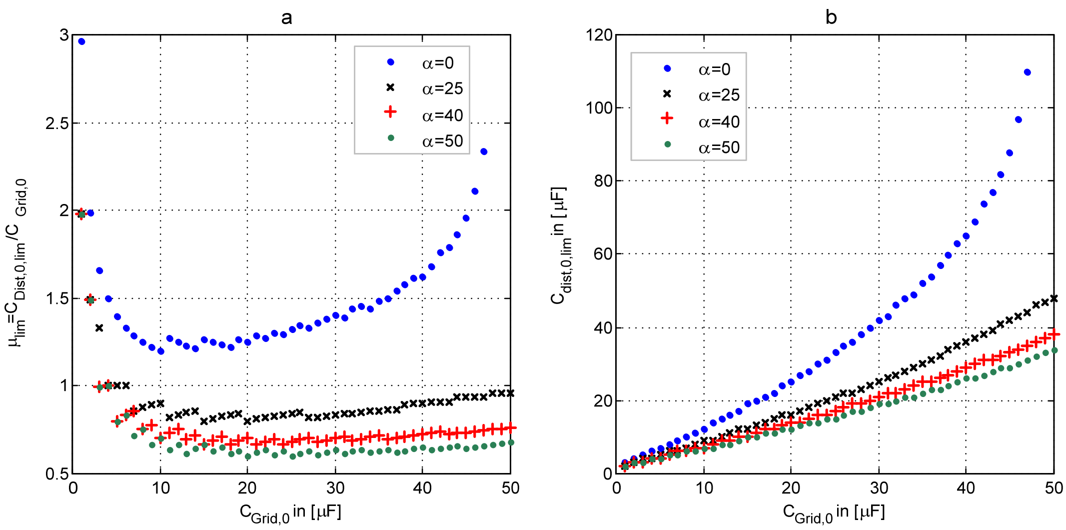

Figure 2-21(a) μ_{lim} as a function of $C_{Grid,0}$ for a feeder cable length of 2km and α=0, 25, 40 and 50; (b) $C_{dist,0}$ as a function of $C_{Grid,0,lim}$ for a feeder cable length of 2km and α=0, 25, 40 and 50.

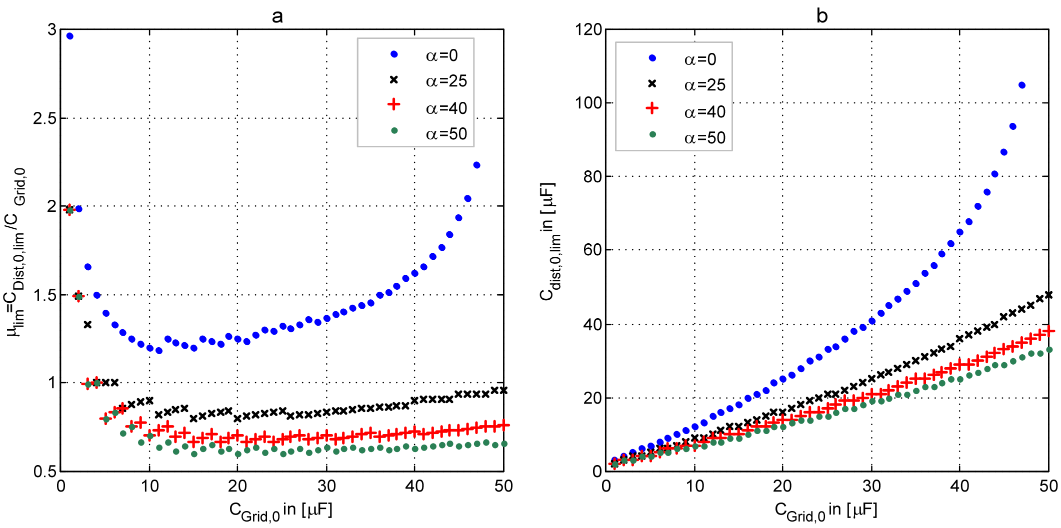

Figure 2-22(a) μ_{lim} as a function of $C_{Grid,0}$ for a feeder cable length of 1km and α=0, 25, 40 and 50; (b) $C_{dist,0}$ as a function of $C_{Grid,0,lim}$ for a feeder cable length of 1km and α=0, 25, 40 and 50.

It can be concluded that the variation of cable length has little influence on the values of μ_{lim}. Although the minimum current setting of the overcurrent relays varies with the cable length, the *position* of μ_{lim} in the cable displaces and its value does not change. The statement that μ_{lim} is independent of $C_{Grid,0}$ is only true for approximately 5 μF≤$C_{Grid,0}$≤35 μF. Most MV networks comply to this criterion and therefore, Table 2-3 gives the values of μ_{lim} for the applied settings of α(averaged over 5 μF≤$C_{Grid,0}$≤35 μF for feeder cables of 5km.).

α	$\mu_{lim}=\dfrac{C_{dist,0,lim}}{C_{Grid,0}}$
0	1.33
25	0.86
40	0.72
50	0.65

Table 2-3: Average μ_{lim} for 5 μF≤$C_{Grid,0}$≤35 μF

2.2 *Application with Simulink*

The sequence components method is applicable for time-domain analysis and steady state-fault analysis [22][31]. The discussed fault calculations only rely on the steady-state fault analysis method. In order to simulate the (dynamic) behaviour of the network depicted in Figure 2-2 in the time-domain, the network has been modelled in Simulink. The network parameters mainly rely on the values given in Appendix C. However, some different, additional settings considering the protection relays are given in Table 2-4.

Setting	Value
SRR;+I_e,+t_e	$65A, 0.3s$
OMT;I_e, t_e	$82A, 0.9s$
$C_{Grid,0}$	20 μF
$C_{dist,0}$	10 μF

Table 2-4: Relay settings and network capacitances for Simulation with Simulink

At t=0.2s, a ground fault is initiated at k=0.5 pu as depicted in the single line diagram of Figure 2-9. The ground fault will be detected by the (directional) overcurrent relays and eventually be isolated, as depicted in Figure 2-23 for both abc-domain zero-sequence components. During the fault, four periods can be distinguished:

I. Pre-fault period;
II. fault initiating period (SRR2 trips at t=0.54);
III. OMT2 pickup period (OMT2 trips at t=1.1);
IV. Post-fault period;

During the **pre-fault** period, the system is in steady state and therefore only load currents flow through the feeder cables, as can be seen in Figure 2-24. The relatively small load currents are well below the maximum current rating of 3x240 Cu PIL cables and the overcurrent relays should not pickup. In practice, load currents will be higher since the aggregated network is being studied here. No zero-sequence currents flow in the network as the single phase-to-ground-fault has not yet been initiated. It should be noted that the cable's charging current is approximately 5 A, which can be derived from the current difference between the feeder cables' ends.

After **fault initiation**, which is in this case in phase a at t=0.2, the system is unbalanced and zero-sequence currents and voltages will be present. Figure 2-25 shows the period between fault initiation (t=0.2) and directional overcurrent relay trip (SRR2 at t≈0.54). The reader should notice that in practice, ground-faults will generally not initiate at once and the fault will have an intermittent nature. Modern (electronic) relays will detect these faults very well using their pick-up/drop-off timer however and therefore the simulations are satisfactory for practical situations as well. Only SRR2 will pickup since $\underline{I}_{e,SRR2}$ *lags* $\underline{U}_0$ by 90° in cable K3 and $\underline{I}_{e,SRR1}$ *leads* $\underline{U}_0$ by 90° in cable K2. The relay will not pick up immediately as it needs at least one period for correct direction determination and RMS-measurement. The voltage triangle will shift as is shown in Figure 1-8. However, due to the relatively long feeder cable $\underline{U}_a$ is not negligibly small at node 3. A phase voltage of $\underline{U}_a$≈180V is present meaning a higher $\underline{U}_0$ and thus a higher $\underline{I}_{e,dist}$ according to (3.3). Although the error is small, it is recommended to use a slightly higher minimum pickup current setting for compensation.

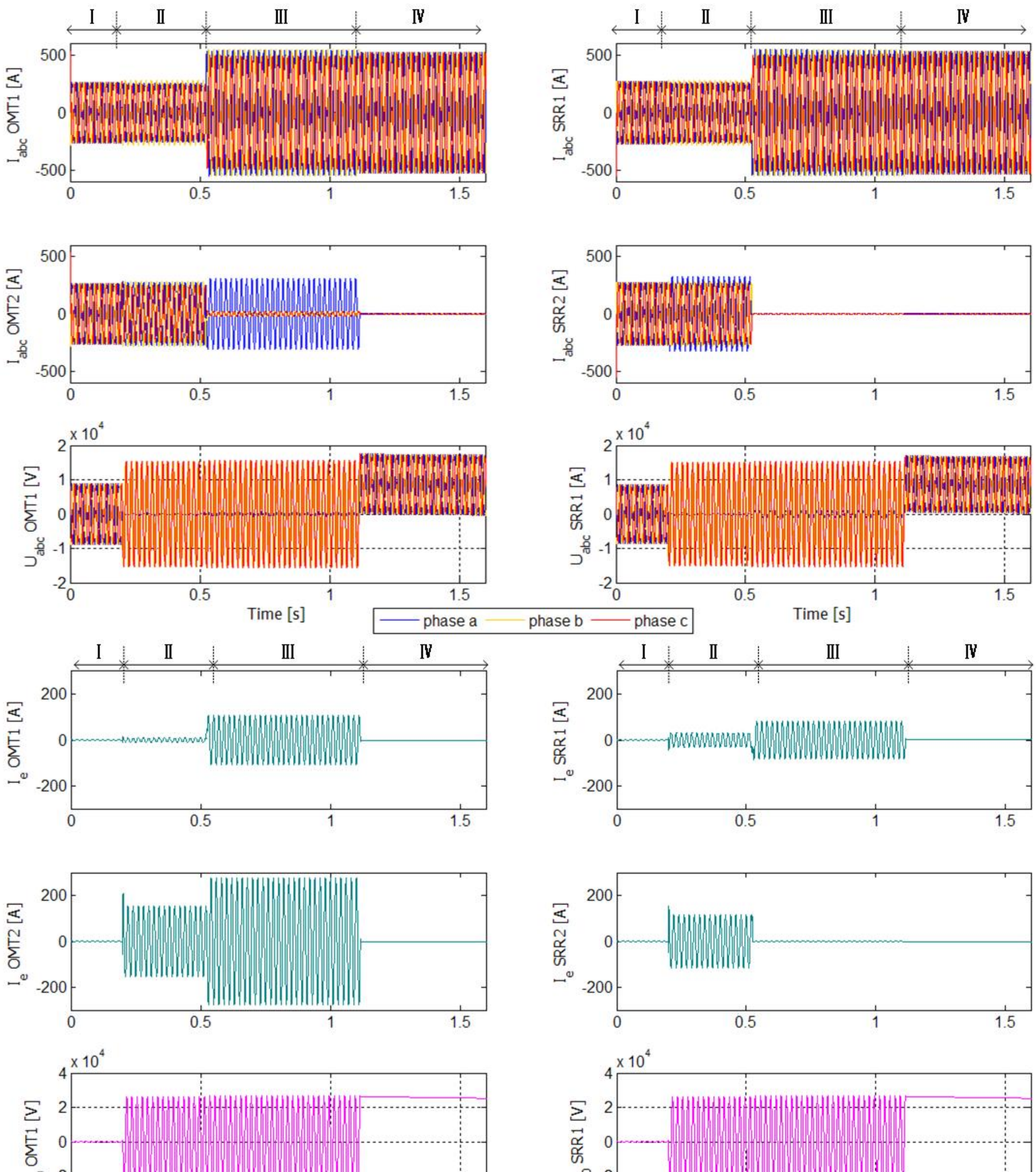

Figure 2-23: Phase and zero-sequence currents and voltages during a correct interruption of a single phase to ground fault in cable K3. The fault is detected by both OMT2 and SRR2. Four periods can be distinguished. Note that after the load current through cable K2 doubles after the first interruption.

Now, only one circuit breaker has been switched open and the substation side circuit breaker is still closed. Therefore, the fault current flows through the healthy feeder cable (cable K2) towards the fault. This current, together with the capacitive fault current by $C_{Grid,0}$, makes the **overcurrent relay** to trip at t=1.14. SRR1 and OMT1 must not pick up on $I_{e,dist}$, the zero-sequence fault current caused by $C_{dist,0}$. Figure 2-26 depicts the currents during the pick up period of OMT2, which lasts for 0.9 s after fault initiation before tripping. At t=0.54 SRR2 trips and therefore the capacitive fault current will change direction i.e. the phase angle of $\underline{I}_{e,SRR2}$ will shift from *lagging* $\underline{U}_0$ 90° to *leading* $\underline{U}_0$ 90°.

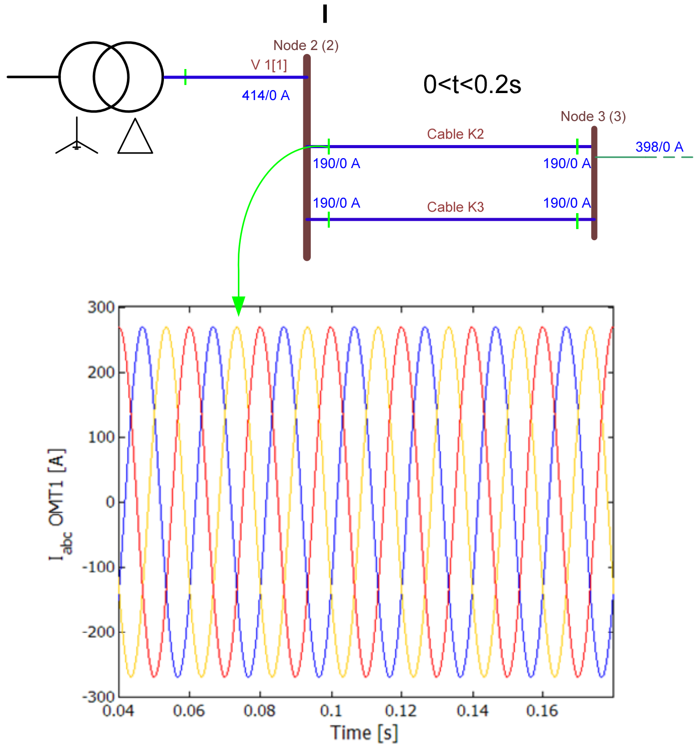

Figure 2-24. Phase 1: Rated load current flows through both feeder cables.

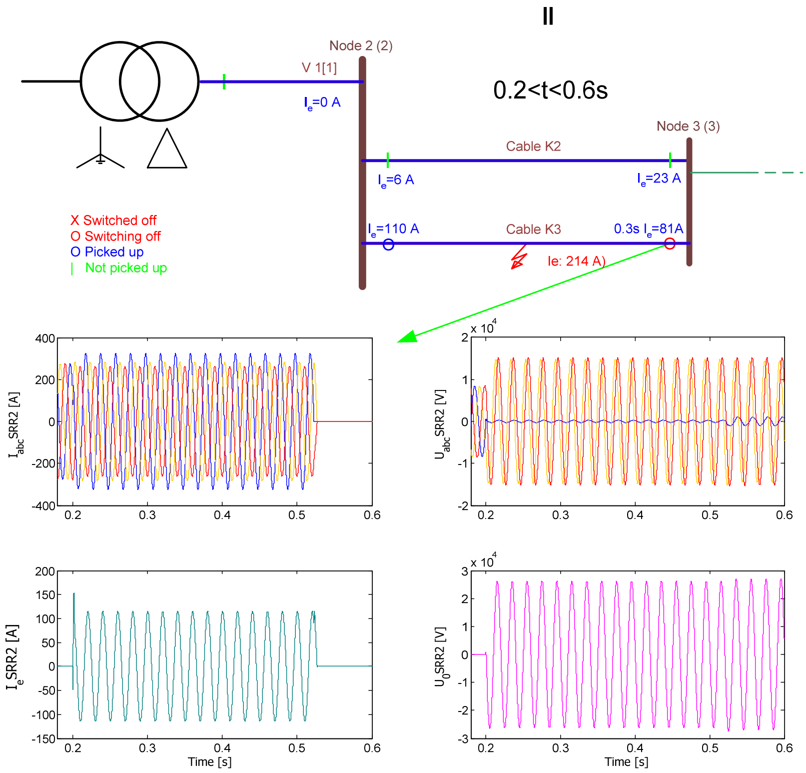

Figure 2-25. Phase 2: Current and voltage waveforms after single phase-to-ground fault initiation at t=0.2 s. The directional overcurrent relay picks-up and trips at t=0.52s.

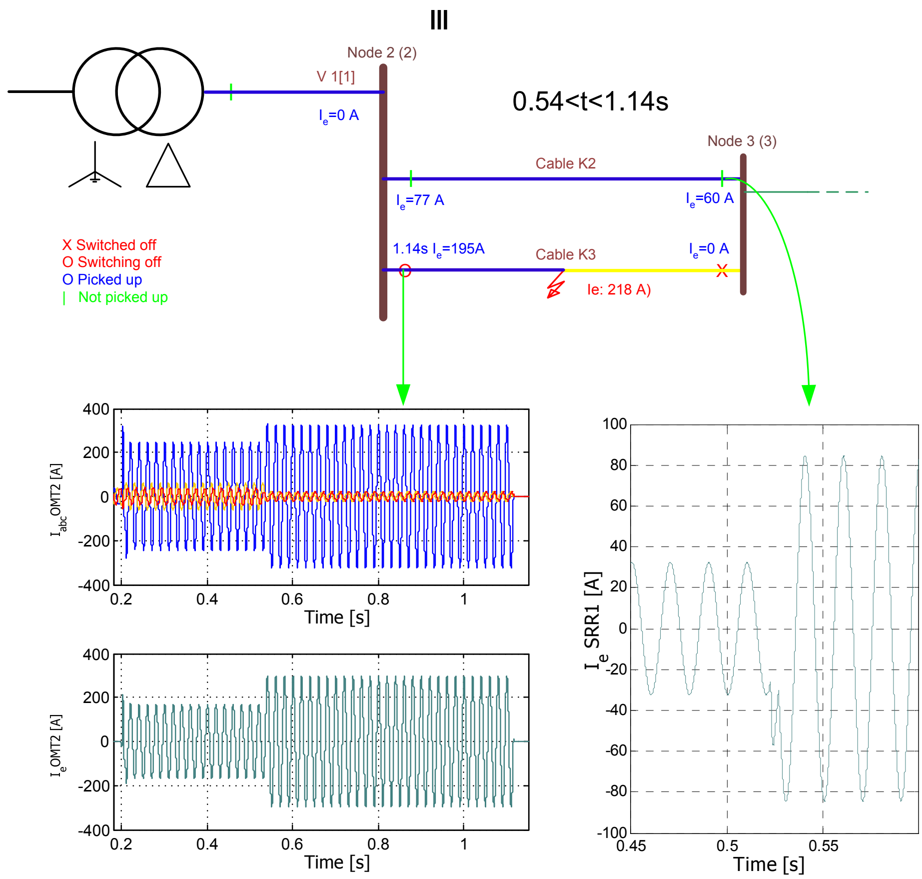

Figure 2-26. Phase 3: OMT2 Current waveforms after fault initiation and SRR2 trip at t=0.52s. Right: earth-fault current direction shift.

At t=1.14, the overcurrent relay has also tripped and the short-circuit has been isolated from the healthy part of the network by opening the circuit breaker at the substation part of the feeder cable. Figure 2-27 illustrates the **post-fault** period in which the system is in balance again. Now, the load current flows through just one feeder cable and the RMS-value is well below the maximum current rating for the post-fault situation as well.

Phase-voltages experience a high DC-component with a large time-constant after fault-clearance. In fact, the system's neutral is defined by the cable's capacitances to ground. The neutral voltage is defined as the centroid of the voltage-triangle caused by the charging currents of the cables[7]. During unbalanced faults, the neutral voltage is being displaced to $\underline{U}_0$. At the fault clearing time instant, the charging current of the cleared phase recovers while the capacitances of the healthy phases are fully charged and thus charge is being trapped inside the cable. This leads to a symmetrical three-phase voltage system with a residual voltage of $\sqrt{2}U_{ph}$ which gradually in- or decreases with a time constant of $\tau \approx 5s$.

In theory, no path between cable conductors and ground exists, thus the residual charge will continue to stay trapped with the whole system left at the discussed dangerously high residual voltage. In the simulation however, switches are used which need snubber resistances to let the simulation run smoothly. Charge can 'leak' away through this snubber resistance, and therefore the residual voltage declines with a time constant of approximately

$$\tau \approx 3R_{snubber}C_{0,Network} = 3*\left(1e5\Omega \parallel 1e5\Omega\right)*35.6\mu F = 5.34s. \tag{3.31}$$

In practice the charge will not be trapped forever as well: due to shunt leakage resistance and leakage conductance the charge will flow towards ground and the neutral voltage will decline back to zero. In order to control the time constant and hence the duration of the overvoltage, neutral grounding should be applied[7]. Figure 2-28 gives the result of a single phase-to-ground-fault switched off successfully without any leakage (a) and with a neutral resistance of 1kΩ (b). It should be noted that in stead of a wye-delta transformer (Yd5), a wye-wye transformer (Yy6) has been used to make neutral grounding possible. The primary's neutral was left ungrounded during the simulation. The transformers' winding connection difference have no influence on single phase-to-ground-faults since the source circuit is left out of the zero-sequence network, as can be seen in Figure 2-8.

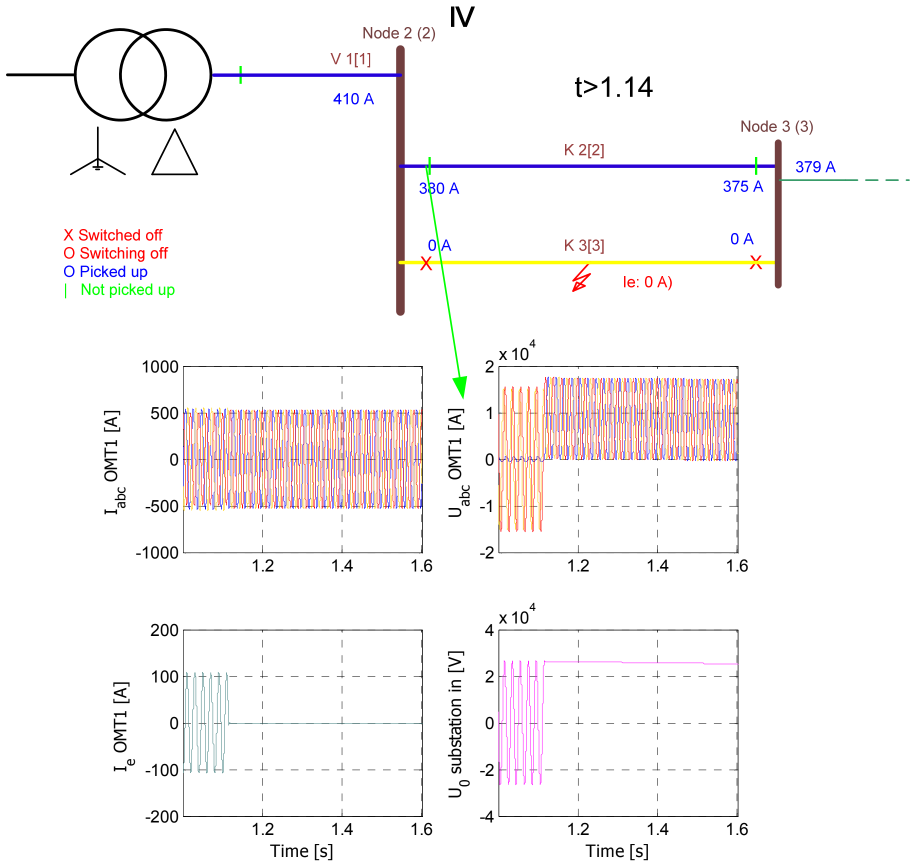

Figure 2-27. Phase 4: Cable K2[2] voltage and current waveforms after fault interruption.

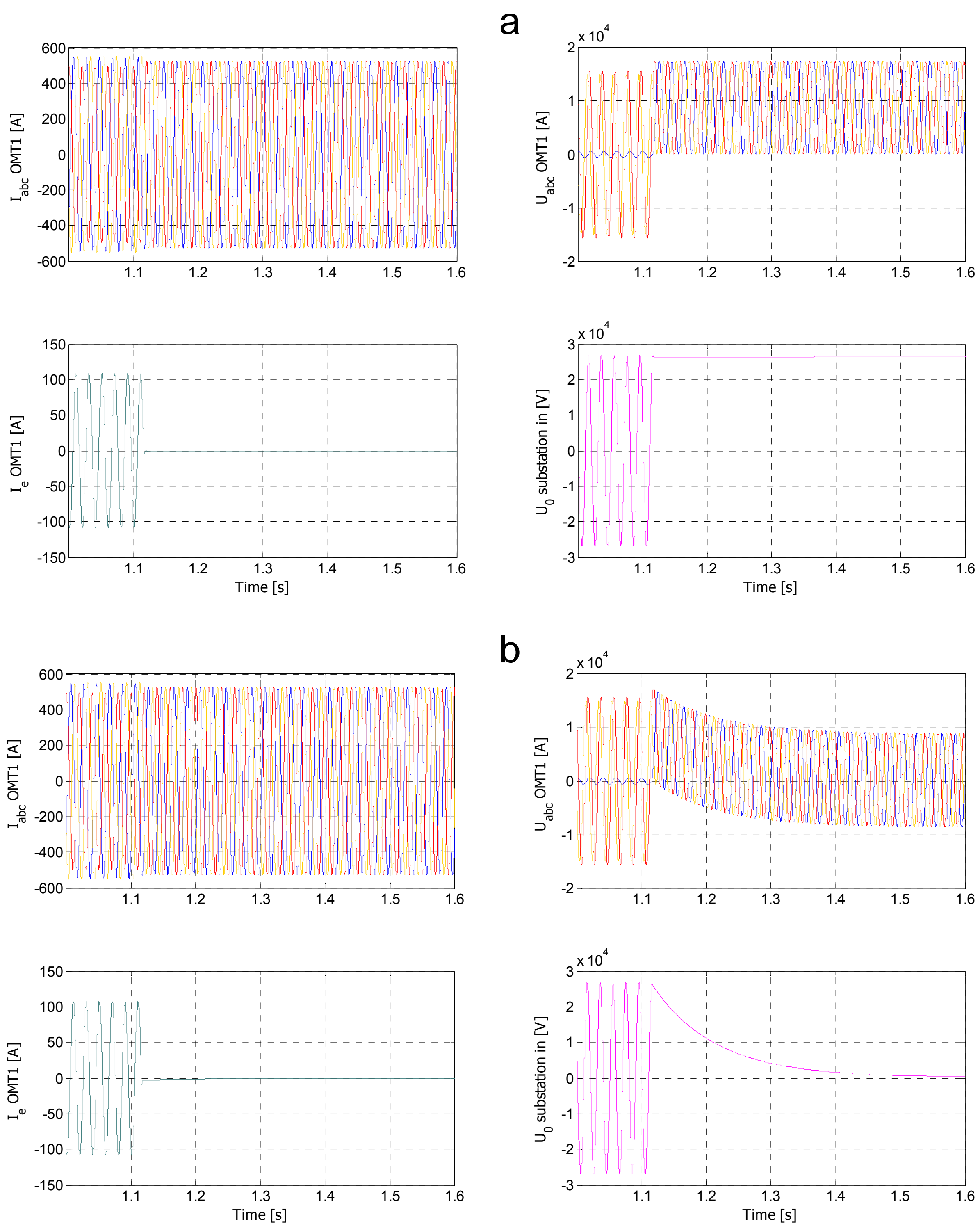

Figure 2-28: OMT1 current and voltage waveforms after fault interruption for a) No shunt resistance and b) Neutral grounding through high resistance.

3 Connecting a directional relay to the RTDS

3.1 Introduction to the RTDS

In the mid 1990's a growing demand for extensive Electro Magnetic Transient Program (EMTP) calculations considering power systems has led to the development of the Real Time Digital Simulator (RTDS)[24]. The operating speed of conventional EMTP software was inadequate especially for large systems. Moreover, expensive equipment such as converters, fuel cell and to a lesser degree protection relays, should be tested before applying them to the power system. Therefore a simulator has been developed which simulates one second for an event which lasts for one second in the real network as well. The RTDS can also simulate in non-real-time implying an even broader field of application.

Principle of operation

A RTDS arrangement consists of several identical *racks* (Figure 3-1) which operate independently by default. Each rack contains 3 standard card types:

Processor card: 18 Tandem Processor Cards(TPC also:3PC) with 2 processors each. TPC's are equipped with analogue as well as digital I/O in order to interface with other cards and external equipment. TPC's perform the actual calculations and are the most essential part of a rack. Each processor can be assigned in the *draft interface*.

Workstation Interference Card(WIC):Regulates the communication between TPC and the workstation on which the *runtime environment* is being located. The WIC also directs data from the workstation to the TPC and sends the compiled network to the assigned processors.

Inter-Rack Communication Card(IRC):For large networks, multiple racks should be used. In order to divide calculations between these racks, communication is necessary. A IRC allows direct communication up to 4 other racks.

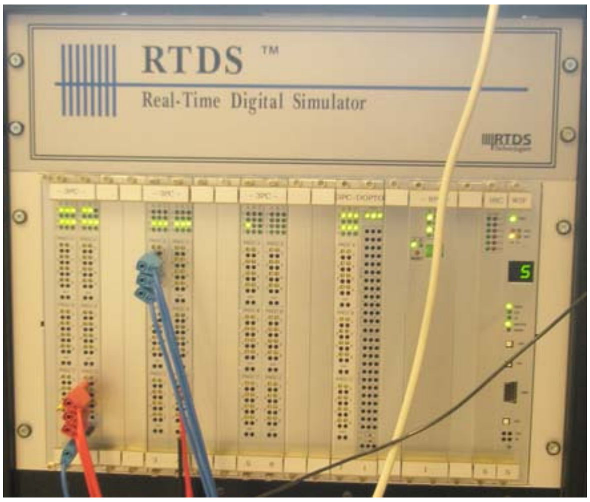

Figure 3-1: RTDS rack 5. Green LED's indicate active processors.

Besides the default rack-configuration, Delft University of Technology has the disposal of a TPC with optical separation for safety reasons (3PC-DOPTO). The feedback of the protection relays is being connected to this card as will be shown later on.

The cards themselves are being programmed using a specific protocol. In order to improve user-friendliness a graphical user-interface has been developed (RSCAD) in which the networks should be drawn (DRAFT). This software highly relies on PSCAD and in some cases PSCAD files can be imported as well. In the DRAFT interface network topology, parameters and control systems should be entered. Moreover, the minimum time-step, the rack-number and the assigned control processors should be set. For more sophisticated systems it is recommended to use the (processor usage) button which gives the structure of the minimum time-step in relation to the assigned control processors. Input and output-operations between the RTDS and the external equipment should also be initialised in the DRAFT file. After building the system that should be simulated, it should be compiled. Now, the RSCAD file is being translated to the RTDS-language in which the hardware communicates. After compiling, the system still has to be sent to the RTDS. This is being done in the runtime-environment of RSCAD. The runtime-environment couples the RTDS to plots, buttons, switches and diagrams at the workstation. At the end, the real-time simulation can be started. An overview of the simulation system is shown in Figure 3-2. For extensive hardware and software specifications of the RTDS is being referred to the RTDS manuals [25].

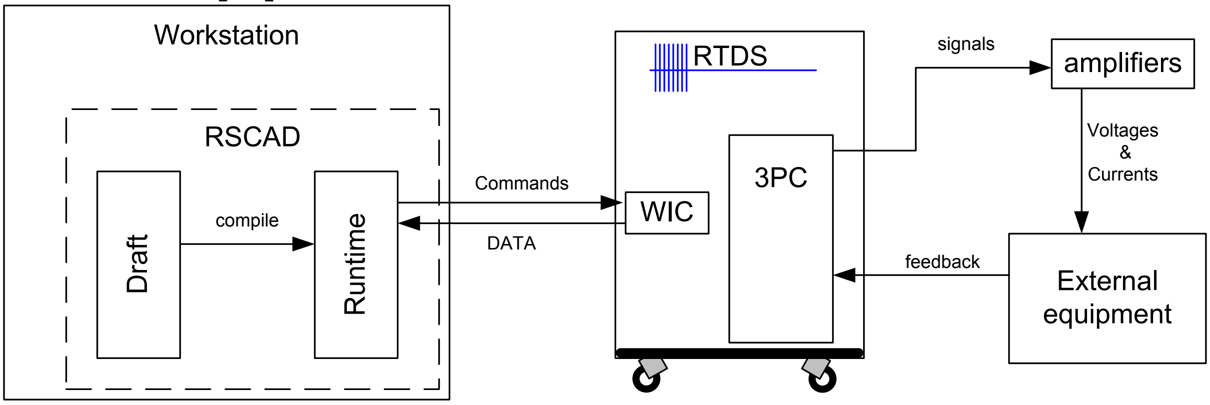

Figure 3-2: Schematic impression of a closed loop system using RTDS.

A time step of 50 μs is being used to simulate the MV network, which means 400 calculation steps per period. For steady-state, fault-current calculations and transitional periods between steady-state situations, this time-step should be convenient. For very fast transients like travelling waves, lightning impulses and switching impulses however, 50 μs is too large and non-real-time operation should be considered. The analogue output channels are being used to interact with external equipment. A specific control block should be added to voltage and current signals in the draft-file which determine the output channel (Card x, Proc y, Channel z), the control processor and the output amplification. Figure 3-3 shows how the simulated voltage is represented with an amplification ratio of 5V/20kV at 3PC card 2, Processor 2, Analogue output channel 1. Note that, in order to specify the output channel, two control blocks are needed to fulfil this. For extensive information about interfacing with external equipment is being referred to[25].

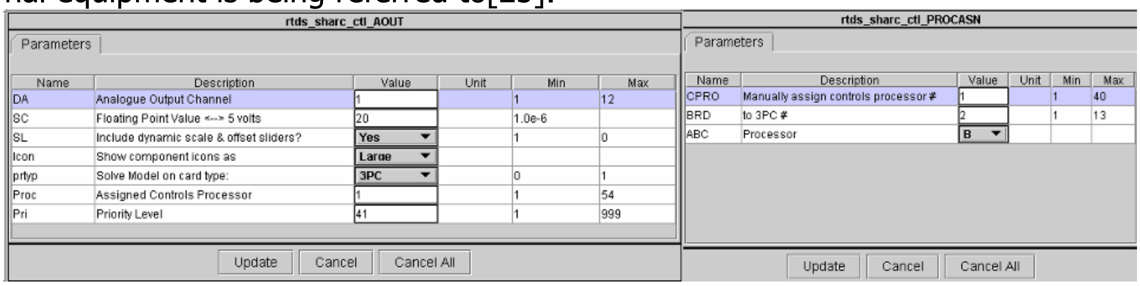

Figure 3-3: Output channel and 3PC assignment block.

Simulated current signals are also represented at the output as voltage signals since the RTDS itself cannot produce any current. External amplifiers should be applied for that purpose. The maximum amplitude of the output signal is -10V/+10V, which means a maximum RMS value of approximately 7 V. An amplification ratio of 5V/20kV is used in order to supply overvoltage and current of at least $2U_{rated}$ and $2I_{rated}$ to the external equipment as well.

3.2 Introduction to the 7SJ62 Directional Relay

As already mentioned, usage of directional relays is necessary for correct relay co-ordination in MV networks with feeder cables. During the authors internship, the operation of protection relays in general and of the Siemens 7SJ62 directional overcurrent relay (Figure 3-4) in particular was studied. As a follow-up study the 7SJ62 relay should be connected to the RTDS by which single phase-to-ground-faults could be studied even more.

Modern electronic directional relays are a cost-effective alternative for mechanical directional relays. Settings can be uploaded by commercially available software such as DIGSI. Faults can be viewed and analysed with SIGRA, which is a COMTRADE viewer and analyser.

The 7SJ62 is positioned at the end of feeder lines (in this case feeder cables) and needs the secondary phase voltages and currents to determine the fault direction correctly. Nominal secondary line voltage is set to 110V (by DIGSI) and nominal secondary current is set to 1A (by jumpers inside the relay). An overview of the most common relay settings are given in Table 3-1. For detailed information about the functions and setting of the 7SJ62 is referred to[13]. Voltage and current transformer ratios have been determined experimentally. The amplifier gain is adjusted in such way that no fading occurs during amplification of a 1 kA current signal. Therefore, the relay's internal current transformer ratio is set to 788/1A.

Figure 3-4: The Siemens 7SJ62 directional overcurrent relay.

Setting	Value
$+I_{e>},+t_{e>}$	$65A, 0.3s$
$I_{e>},t_{e>}$	n/a
$+I>,+t>$	$600A, 0.3s$
U_{rated}	110V
I_{rated}	1A
Voltage Transformer ratio	10.4kV/110V
Current Transformer ratio	788A/1A
Current input Burden	0.05 VA
Voltage input Burden	0.3 VA
$I_{e,7SJ62}$ or $-3I_0$	$I_{e,7SJ62}$
Current transformer grounding	Towards Busbar

Table 3-1: Major 7SJ62 relay settings

3.3 *Interfacing the 7SJ62 with the RTDS*

Interfacing with the RTDS is highly dependent on whether real voltages and currents are needed for the equipment to operate correctly. The 7SJ62 need real secondary voltages and currents. The maximum analogue output of the RTDS is +/- 10V and therefore amplifiers are needed to produce rated secondary voltages of $110V_{rms}$ and rated secondary currents of $1A_{rms}$. The amplifiers should have the following (desired) specifications:

- Bandwidth of approximately 20 kHz (DC→20kHz);
- For voltages as well as currents sufficiently small phase-shift;
- Current output of at least $2.5A_{rms}$ (=2.5 I_{rated});
- Voltage output of at least $110A_{rms}$;
- Adjustable gain;
- 'Low' harmonic distortion;
- Voltage input of +/- 10V;

Above specification imply a proper signal conversion of the RTDS output to the 7SJ62 relay. Commercially available amplifiers with excellent specifications are for instance the OMICRON CMA-156 (Current only) and CMS-156 (Current+Voltage). Acquisition of these amplifiers was not possible however and alternative needed to be found.

The faculty could try to make the amplifiers as well. The reader should notice however that making such an amplifier takes a lot of time and especially current amplification with a sufficiently small phase shift can be very hard. Designing such an amplifier could badly decrease the available time left for activities within the scope of this research. Furthermore, 2 designs should be made: one for voltage amplification and one for current amplification. These considerations have led to the conclusion that it is too risky to design an amplifier.

Real-time simulation without connecting the relay was also a considerable option. Relays can be modelled very well in RSCAD especially the essential operations such as definite overcurrent-time protection. The relay could have been tested with an OMICRON relay testbox in non real-time. However, interfacing the relay with the RTDS was the major challenge during the project.

3.3.1 Quad amplifier

In the past, the faculty had had some experiments with a quality unit amplified domestic (QUAD) 50E single channel audio amplifier. A synchronous motor was being driven by a couple of these amplifiers. Using audio amplifiers in general has some major drawbacks:

- Audio amplifiers cannot produce a DC-component.
- The frequency characteristic in the low frequency range can badly influence results.
- In fact, audio amplifiers are voltage to voltage amplifiers, so amplification of the current could be a challenge.

However, Quad 50E amplifiers (Figure 3-5) are very well documented including electronic schemes[26]. The electronic scheme is for the sake of completeness being added in Appendix D. Major specifications of the Quad 50E are given in Table 3-2.

Setting	Value
Input impedance	14 – 50kΩ depending on gain
Input level	$0.5V_{rms}$,higher level possible through adjustable gain
Output source impedance	0.5Ω in series with 25μH for 5.8Ω as output connection. Other inductances in proportion
Power into load	Max 50W at 5.8,12.5,23,50,200Ω
Total Harmonic Distortion	40 Hz <0.35% 1kHz <0.1% 10kHz <1.0%

Table 3-2: QUAD 50E specifications.

Input voltage is dependent on the preset gain which is $0.5V_{rms}$ by default. In this case, a smaller gain has been used to allow a higher input voltage. Output power is dependent on the externally applied output impedance. In fact, output impedance can be adjusted by applying different types of output connections at the output transformer of the amplifier. Figure 3-6 gives the possible connections with their voltages at nominal load. It should be emphasised that the depicted connection numbers correspond with the connection numbers *inside* the connectors. For voltage operation, 200Ω is used while 5.8Ω is used for current operation. Figure 3-7 gives the relation between load impedance and output power for several types of external output impedances.

Figure 3-5: QUAD 50E amplifier front. Left connection is the power supply; Centre connection the voltage output(102 V); Right connection the RTDS' voltage signal

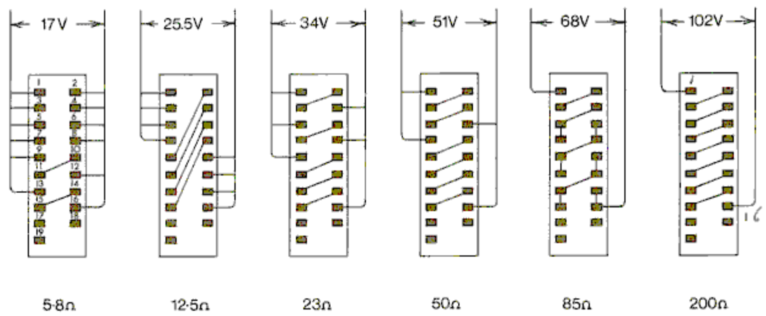

Figure 3-6: Quad 50E output connection possibilities

Since the output of the amplifier is floating, the output of a set of three amplifiers can be connected in wye without facing any grounding difficulties. In this way, a secondary circuit is being simulated which bears strong similarities with the specifications of a real secondary circuit.

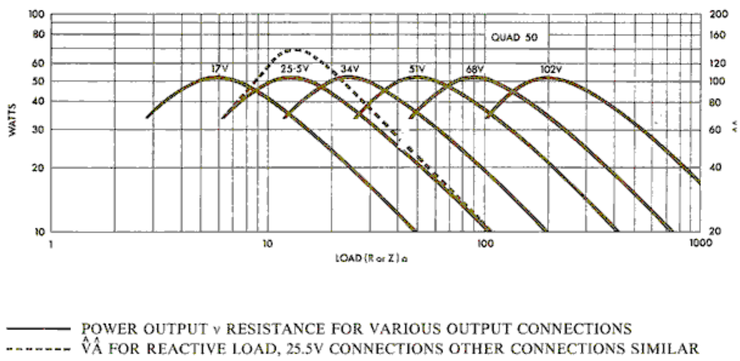

Figure 3-7: Power into load curves for connection types of Figure 3-6. A mainly resistive load is utilised.

Toroïdal transformers

QUAD amplifiers that amplify phase voltages face a high output impedance: The voltage input burden of the 7SJ62 relay is 0.3 VA meaning an input impedance of several kΩ. No seriously high currents will flow in this part of the secondary circuit. The reader should be aware for the dangerously high voltages at the voltage inputs however ($110V_{rms,line}$) and hence the amplifiers should be switched off during the adjustment of the relay's connections.

Quad amplifiers that amplify phase currents face a low output impedance: 5.8Ω for the amplifier output and a very low relay input impedance (~0.05Ω). Tests considering the behaviour using this low output impedance show an instable behaviour of the measured current. In order to increase the external impedance faced by the amplifier, toroïdal transformers (Figure 3-8) have been connected in series with the amplifiers' outputs. The primary sides are connected to the amplifiers' outputs while the secondary sides are connected to the relay. Now, two major benefits have been achieved. First, the amplifiers face higher output impedance, which results in a more stable operation point. Second, since the voltage of the output is higher compared to the situation without extra transformers, a larger current at the secondary side will flow. The secondary circuit current connection diagram is shown in Figure 3-9.

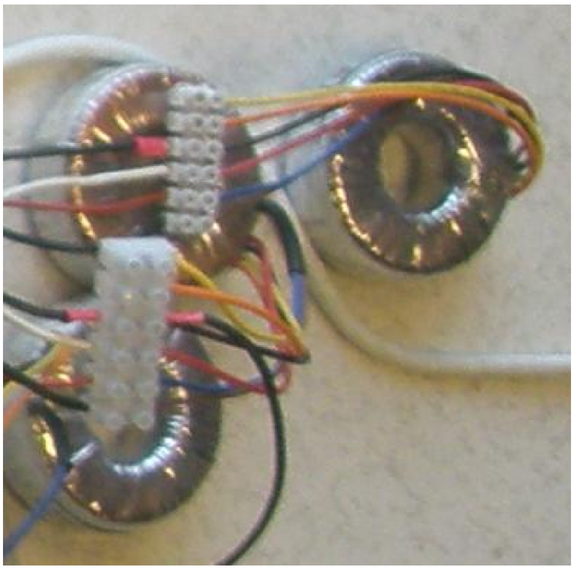

Figure 3-8: 230V/6V 50VA Toroïdal transformers connected in wye as used for current signal amplification.

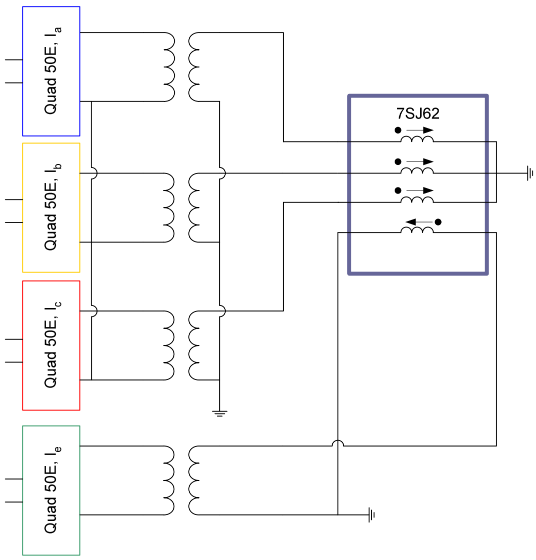

Figure 3-9: Current signal amplification block diagram. $\underline{I}_e$ is connected separately.

3.3.2 Frequency characteristics

To examine the behaviour of the amplifier during operation, the frequency response of the amplifiers should be determined. The frequency response gives information about the amplitude gain and phase shift of a sinusoidal signal at the input for a given frequency. In the Electrical Power Processing (EPP) laboratory of Delft University of Technology, the amplifier setup has been extensively tested. The test setup is shown in Figure 3-10, The amplifier intended for voltage to current amplification is tested. The reader should notice that only one phase at a time is tested. This should not be a problem because one of the two relay input pins (pin 29) is connected to ground, which corresponds to the neutral connection right to the relay in Figure 3-9.

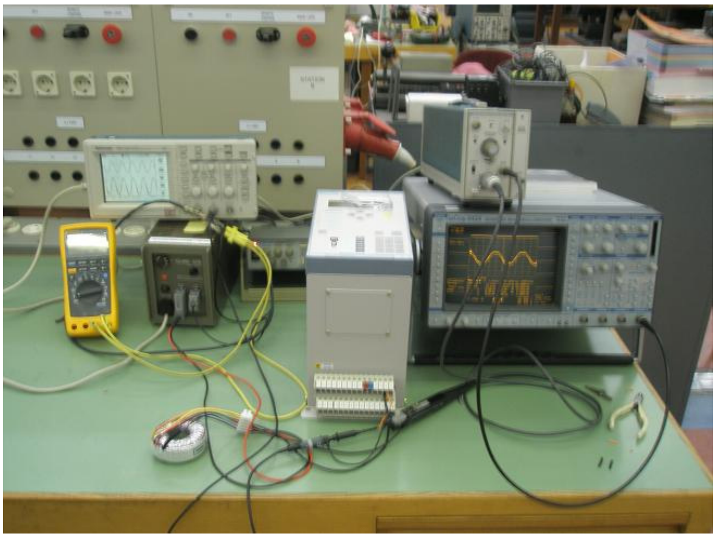

Figure 3-10: Measurement setup for frequency characteristic determination.

Waiting for service for probably more than 10 years, the QUAD amplifiers should be cleaned up in order to prevent flashover and short-circuits caused by dust. The amount of noise can be reduced by choosing a small gain. As input, a signal generator is used which can produce sinusoidal voltages from almost DC to a few MHz. Currents can be measured accurately with a flux-meter (right to the relay in Figure 3-10). The RMS value of both input and output voltage is measured with the Fluke-meter to the left and with the Tektronix oscilloscope. Phase shift is also measured with oscilloscope: for a given frequency the phase shift (in seconds) can be measured accurately by comparing 2 cursors each corresponding to the maximum

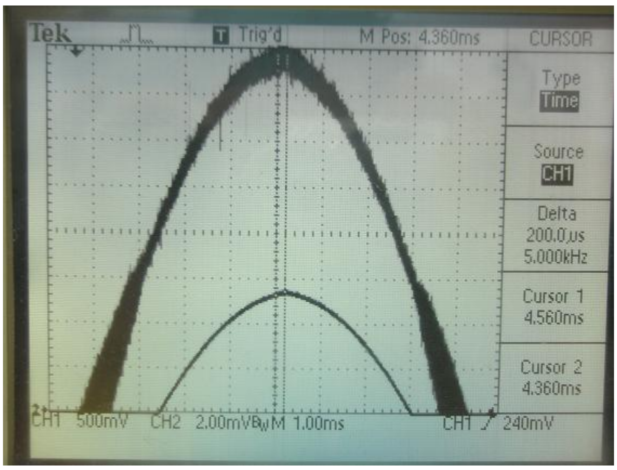

Figure 3-11: Voltage signal phase shift determination at oscilloscope.

value, as can be seen in Figure 3-11. Subsequently, the phase shift *in degrees* should be calculated as frequency is varied and the phase shift is measured as time difference. The used Quad amplifiers are not exactly equal which results in small variations between the tested amplifiers. Therefore, all phase current amplifiers have been tested separately.

Voltage amplifier

The amplifier is operating as a voltage amplifier since the output is connected to the high voltage input winding of the relay. The 102 V connection of Figure 3-6 has been used as amplifier output. Around 50Hz, more measurements have been taken to increase accuracy. Figure 3-12 shows the frequency response of the phase voltage amplifier. It can be concluded that within a bandwidth of 5 kHz, voltages will be amplified by a phase shift smaller than 20°. The -3 dB point is positioned above 20 kHz, which means that the amplitude of the RTDS voltage signals will be amplified correctly over the whole RTDS' frequency range. However, DC signal cannot be amplified since audio amplifiers in general are not designed for DC amplification. 30 Hz is the minimum frequency at which the amplified signal is still sinusoidal.

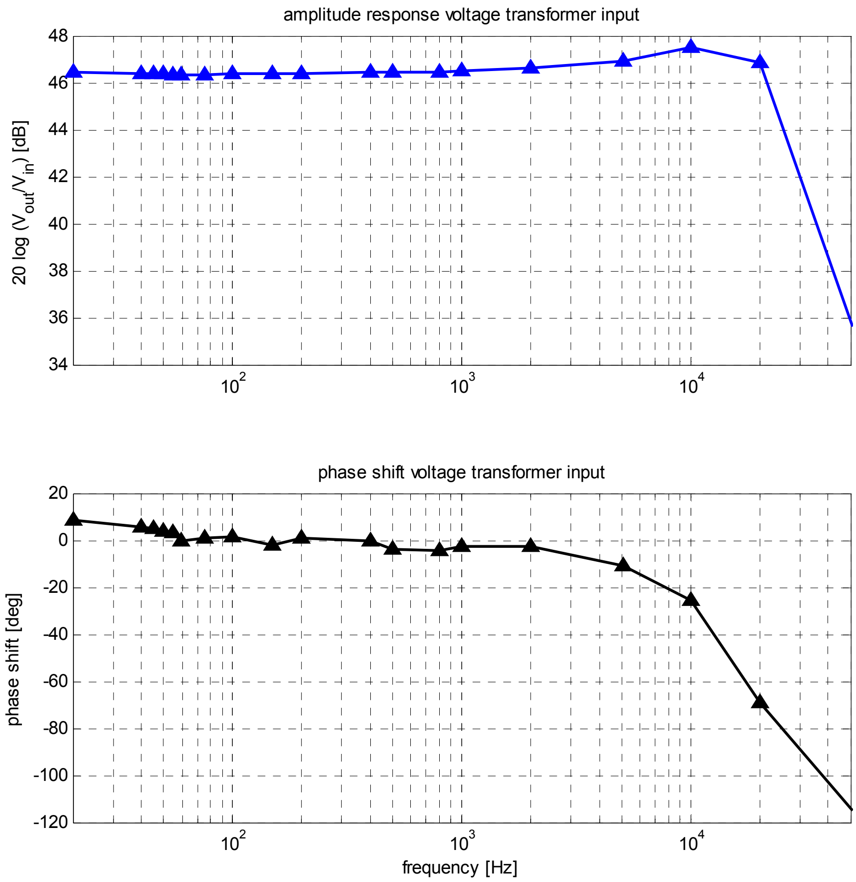

Figure 3-12: Amplitude response (upper trace) and phase shift (lower trace) as a function of frequency for voltage amplification.

Current amplifier

The QUAD amplifier can only amplify voltage and therefore the amplitude and phase of currents measured depend on the burden of the current input of the 7SJ62 Relay. Therefore the current input impedance of the relay has accurately been measured and is equal to 0.05Ω with an angle of 5° lagging. It should also be noted that the amplifier has a maximum power rating and thus a maximum current rating. For a high gain, the current output signal will start to fade at its peaks as shown in Figure 3-13. For every phase current amplifier the frequency response has been determined. Phase shift measurement has been achieved by measuring the voltage across the current input of the relay and dividing it by the measured burden impedance. Figure 3-14 to Figure 3-16 depict the frequency response of the phase current amplifiers. It can be concluded that although the bandwidth is smaller than the phase voltage amplification, the current signal is still well amplified in the steady-state region. Moreover, the phase-shift introduced by the burden impedance is very small over a large bandwidth making the proposed amplifier setup suitable for interfacing between RTDS and the 7SJ62 Relay.

Figure 3-13: A too high gain will cause the amplifier to start fading.

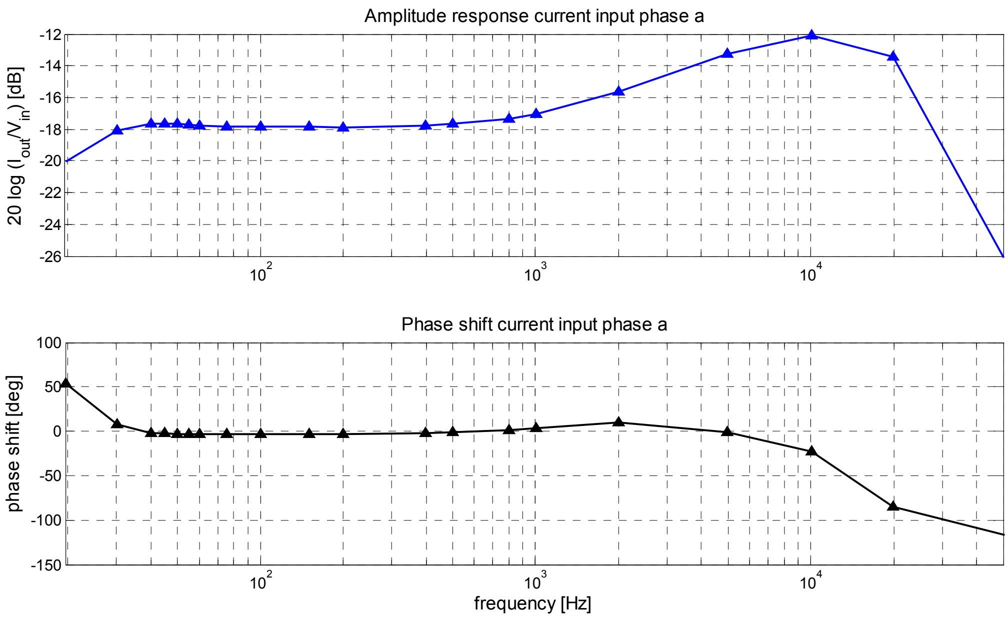

Figure 3-14: Amplitude response and phase shift as a function of frequency for phase a current amplification.

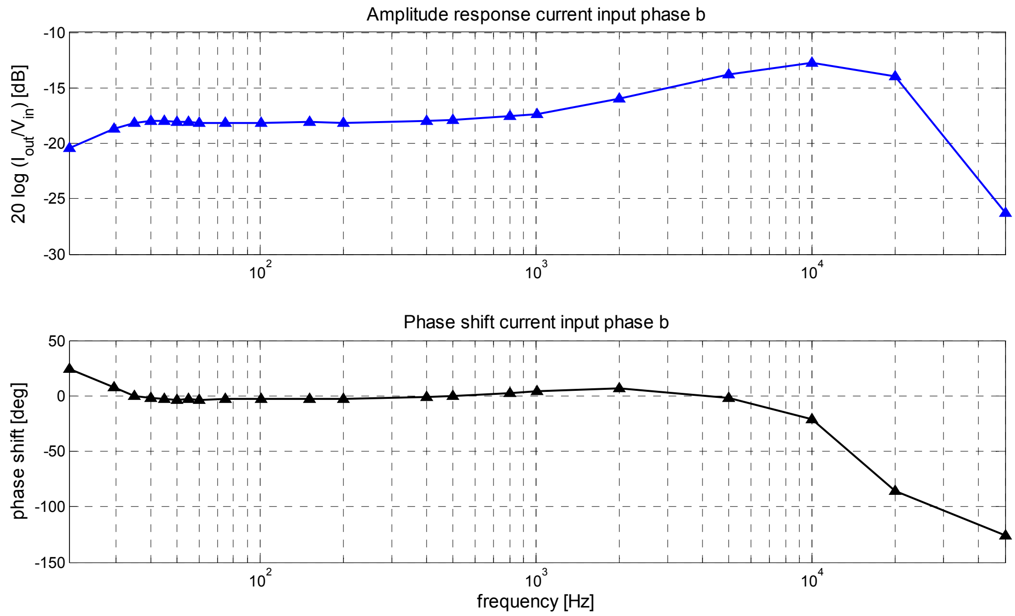

Figure 3-15: Amplitude response and phase shift as a function of frequency for phase b sinusoidal current amplification.

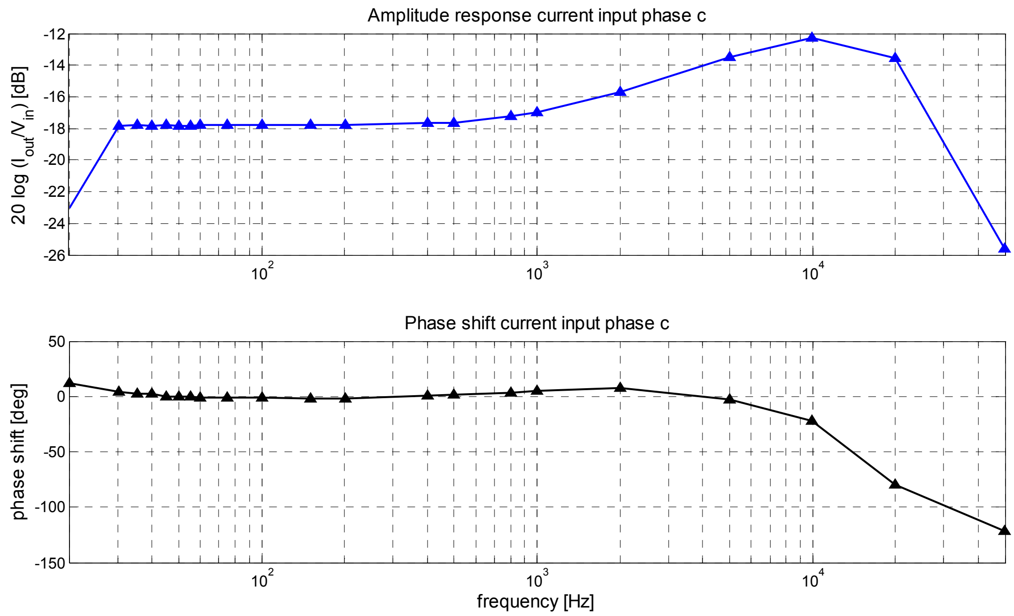

Figure 3-16: Amplitude response and phase shift as a function of frequency for phase c sinusoidal current amplification.

3.4 Connection Diagram RTDS to 7SJ62

The 7SJ62 relay is used as external equipment in Figure 3-2 and thus amplifiers should be connected between RTDS and elay in order to convert signal to secondary voltages and currents. As a result, the amplifiers neutral grounding method should be determined to simulate the real secondary circuit as good as possible. The voltage and current signal connections have been derived from the proposed *Holmgreen* connection in the manual [13] which is for convenience depicted in Figure 3-17. In this connection, the return current is equal to $\underline{I}_{e,7SJ62}=-3\underline{I}_0$ and only 3 current transformers are needed for correct measurement. The calculated value of $\underline{I}_{e,7SJ62}$ should be equal to the measured value of $\underline{I}_{e,7SJ62}$. However, the amplifier setup did not behave as it should, since the current amplifiers did not amplify the currents properly during asymmetrical conditions. Therefore, $\underline{I}_{e,7SJ62}$ is fed separately to the neutral current input. In practice, this measurement setup is being used to measure the cable sheath current. In the modelled network, the sheath currents will not be measured but since the sheath current is equal to $-\underline{I}_e$, this input can be used very well. The primary side of the toroïdal transformers is floating since the primary sides of current transformers are ungrounded in practice as well. The secondary side of the toroïdal transformers is grounded as the neutral point of the current transformers is also grounded in practice. Figure 3-18 depicts the connection diagram of the test setup as it is being applied during the relay co-ordination study.

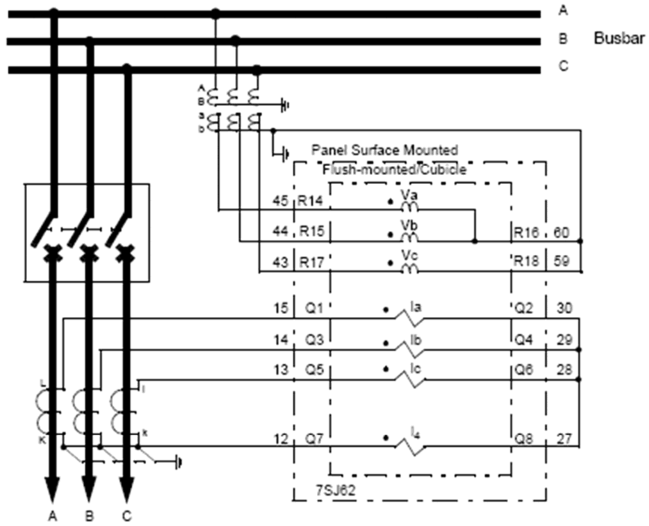

Figure 3-17: Cable-side grounded "Holmgreen" connection. The proposed closed-loop circuit is busbar-grounded.

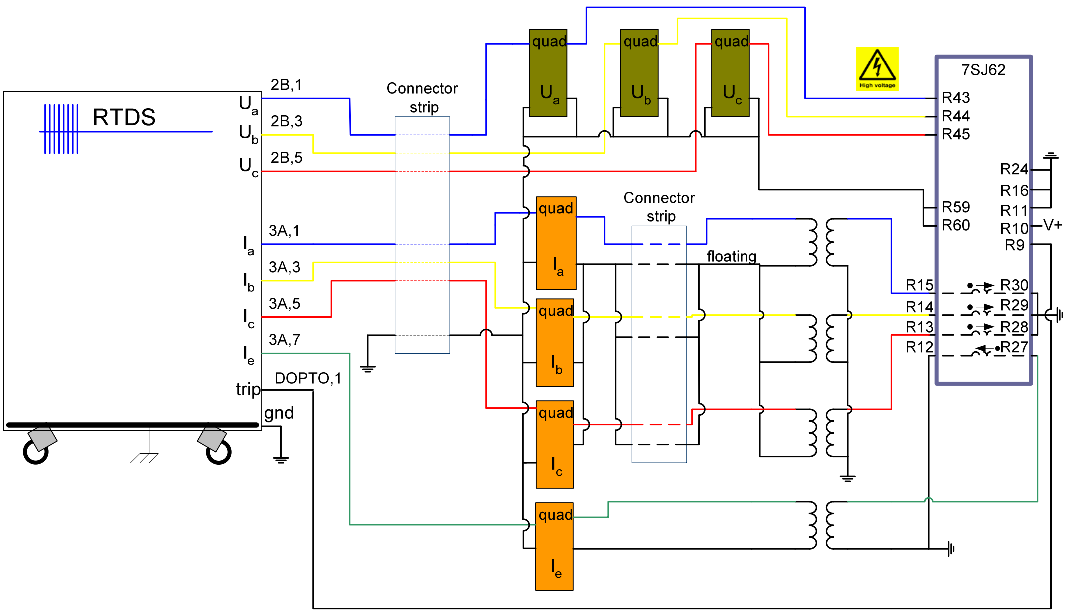

Figure 3-18: RTDS to 7SJ62 connection diagram.

3.5 RSCAD network design

General considerations

The network of Figure 2-2 with parameters given in Appendix C should be modelled in RSCAD in order to be simulated with the RTDS. The design in RSCAD is discussed below while design of a network in general is extensively described in [25]. Before designing, some important issues should be considered:

- What kind of I/O should be used for the test setup to communicate correctly
- Which rack will be used;
- What cable model will be used;

I/O: Phase voltages and currents as well as $\underline{I}_e$ at the 7SJ62 relay location will be amplified. The relay trip signal shall be fed back to the RTDS. Output signals will be assigned to the 3PC analogue output channels. It should be pointed out that it is impossible to use an analogue input for the trip signal and therefore the trip contact will be connected to the 3PC-DOPTO input.

Rack:The choice of racks to be used is limited by the availability of 3PC-DOPTO cards. Therefore, only racks 1, 3, 5 and 7 could be used. Moreover, it turned out to be impossible to even communicate with rack 7. Therefore, rack 5 has been used for the closed loop test setup depicted in Figure 3-19.

Cable model: RSCAD can use several cable models, including sophisticated models for asymmetrical cables. A cable model builder has also been included. Since both Simulink and Matlab use a pi-network model and not enough cable data was available for sophisticated modelling, a pi-network model has been used. For relative short cables and relative large time scales (the minimum time-step of the RTDS is 20μs) this model is satisfactory.

Figure 3-19: Closed loop test circuit. Right: 6 QUAD 50E amplifiers and the 7SJ62 relay.

RSCAD design

By means of the RSCAD overview of the designed network depicted in Figure 3-20, it will be discussed step-by-step what design considerations have been taken.

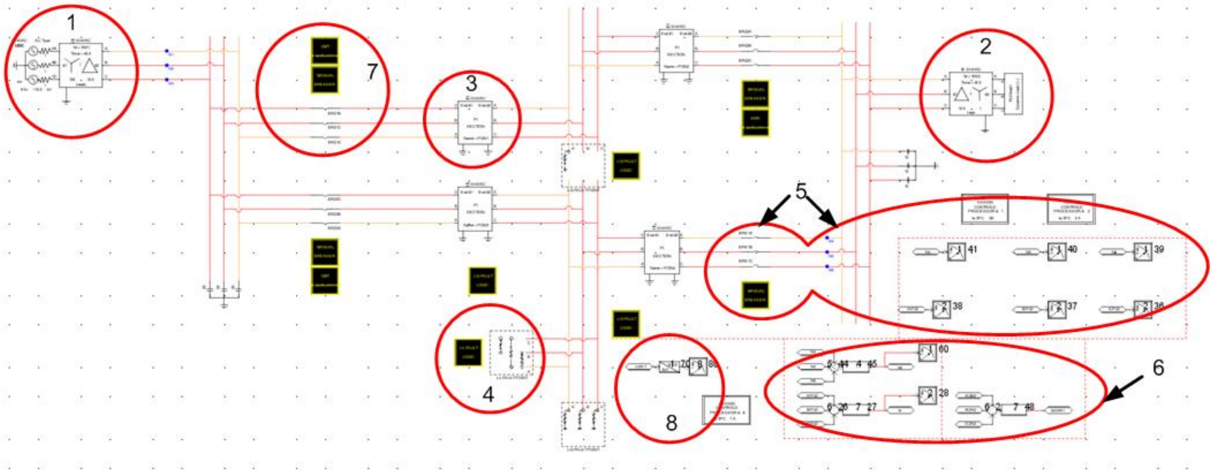

Figure 3-20: Three phase diagram of Figure 2-2's circuit modelled in RSCAD.

1 Source and transformer modelling: The source and distribution transformer have been modelled according to the given network parameters. The transformer is modelled by its per unit short-circuit impedance. The source has been modelled as an infinite grid with a line voltage of 110kV and a short-circuit resistance of 1mΩ. The source parameters are not very critical since only load currents flow through the transformer during a single phase-to-ground-fault. Figure 3-21 shows the concerned part of the network with the block parameters of the HV/MV transformer.

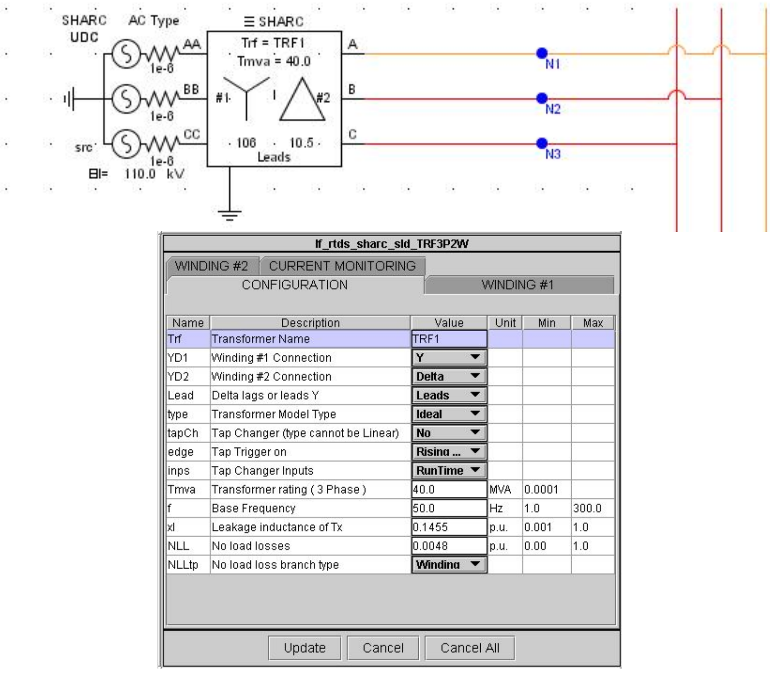

Name	Description	Value	Unit	Min	Max
Trf	Transformer Name	TRF1			
YD1	Winding #1 Connection	Y			
YD2	Winding #2 Connection	Delta			
Lead	Delta lags or leads Y	Leads			
type	Transformer Model Type	Ideal			
tapCh	Tap Changer (type cannot be Linear)	No			
edge	Tap Trigger on	Rising ...			
inps	Tap Changer Inputs	RunTime			
Tmva	Transformer rating (3 Phase)	40.0	MVA	0.0001	
f	Base Frequency	50.0	Hz	1.0	300.0
xl	Leakage inductance of Tx	0.1455	p.u.	0.001	1.0
NLL	No load losses	0.0048	p.u.	0.00	1.0
NLLtp	No load loss branch type	Winding			

Figure 3-21: Source model with (pu) parameters.

2 Load and MV/LV transformer modelling: The MV/LV transformer has been modelled in a similar way as the HV/MV transformer using the given parameters. A serious model limitation arises during load modelling. As can be seen in Figure 3-22, the minimum operating voltage of the load block is 1kV. However, the given network operates at 400 V at the low voltage side. For phase to phase and three-phase faults this is a serious limitation since the short-circuit currents at the *secondary side* of the transformer are smaller during RTDS simulation than in practice. Single phase-to-ground-fault currents are largely caused by the cable's capacitances and thus transformer impedances play a negligible role considering earth-fault currents in the MV network. In the Runtime Environment, active and reactive power absorbed by the load can be adjusted by a slider.

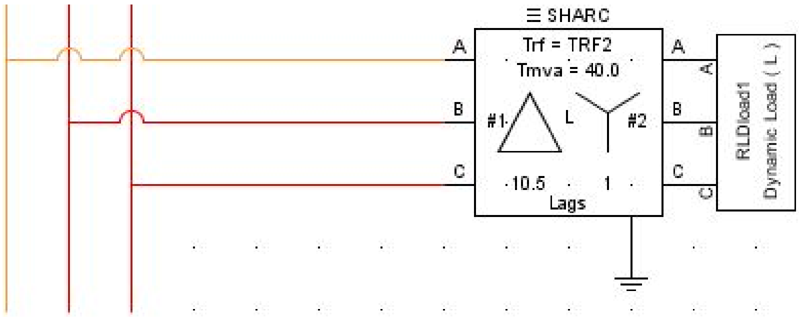

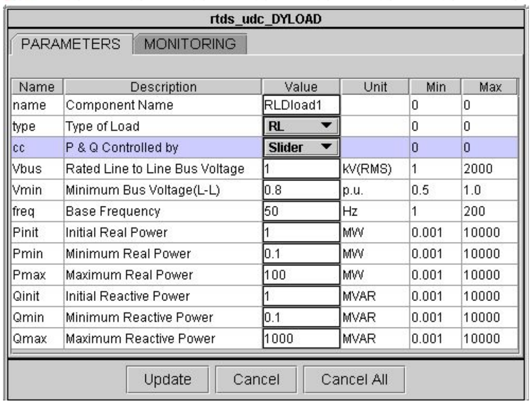
rtds_udc_DYLOAD

PARAMETERS | MONITORING

Name	Description	Value	Unit	Min	Max
name	Component Name	RLDload1		0	0
type	Type of Load	RL		0	0
cc	P & Q Controlled by	Slider		0	0
Vbus	Rated Line to Line Bus Voltage	1	kV(RMS)	1	2000
Vmin	Minimum Bus Voltage(L-L)	0.8	p.u.	0.5	1.0
freq	Base Frequency	50	Hz	1	200
Pinit	Initial Real Power	1	MW	0.001	10000
Pmin	Minimum Real Power	0.1	MW	0.001	10000
Pmax	Maximum Real Power	100	MW	0.001	10000
Qinit	Initial Reactive Power	1	MVAR	0.001	10000
Qmin	Minimum Reactive Power	0.1	MVAR	0.001	10000
Qmax	Maximum Reactive Power	1000	MVAR	0.001	10000

Update | Cancel | Cancel All

Figure 3-22: MV/LV transformer and load model. Load is voltage dependent.

3 PI-section: The used pi-section model is comparable to the model used in Simulink and Matlab. For a pi-section of 5 km, the parameter-window is shown in Figure 3-23. It is important to notice that the monitored current is flowing *into* the pi-section. This holds for both sides of the pi-section. Note that capacitive reactance *of the whole section* has to be given in MΩ.

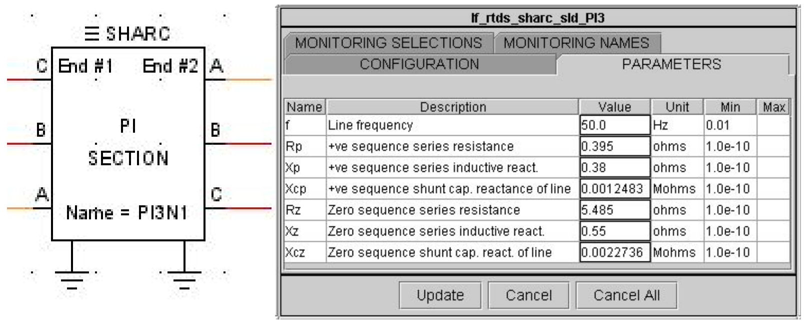

Name	Description	Value	Unit	Min	Max
f	Line frequency	50.0	Hz	0.01	
Rp	+ve sequence series resistance	0.395	ohms	1.0e-10	
Xp	+ve sequence series inductive react.	0.38	ohms	1.0e-10	
Xcp	+ve sequence shunt cap. reactance of line	0.0012483	Mohms	1.0e-10	
Rz	Zero sequence series resistance	5.485	ohms	1.0e-10	
Xz	Zero sequence series inductive react.	0.55	ohms	1.0e-10	
Xcz	Zero sequence shunt cap. react. of line	0.0022736	Mohms	1.0e-10	

Figure 3-23: Pi-section model (left) with cable parameters (right)

4 Ground-fault model: The short-circuit model consists of a short-circuit block and a subsystem with logical operators. The short-circuit block can be set as line-to-line fault or line-to-ground fault. In the runtime environment, the type of ground-fault can be adjusted by a dial. The logical operator block is shown in Figure 3-24 and consists of a lifetime slider and a fault activating push-button. Both are included in the runtime environment. The lifetime slider can be adjusted to the number of cycles the fault lasts. The upper button is always equal to 1, the lower push button is only equal to one when pushing. LLFLT will stay 'true' for the number of cycles multiplied by the time per period (20 ms).

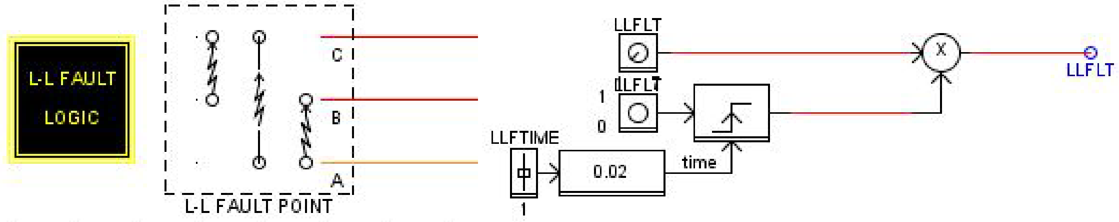

Figure 3-24: Line-fault model utilised in ground-fault mode. Right: Fault duration logic

5 Current and voltages output: Voltages and currents at the relay's location should be assigned to an output channel. Therefore, voltages at nodes N4, N5 and N6 and phase currents flowing from the relay *into* the pi-section should be 'exported' to the 3PC output channels, as shown in Figure 3-25. First, the signal names have to be extracted from the network with an *import/export block*. Second, an analogue output channel should be assigned. Note that the channel number and the controls processor has to be set in this block. The 3PC card should be assigned in the 'Assign Controls Processor #' block. In this way, the output channel is fixed. Otherwise the output channel is being assigned automatically and can be retrieved in the .map file pushing the 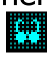 (view) button. Note that the scaling factor should be given in KV and kA, as show in Figure 3-26

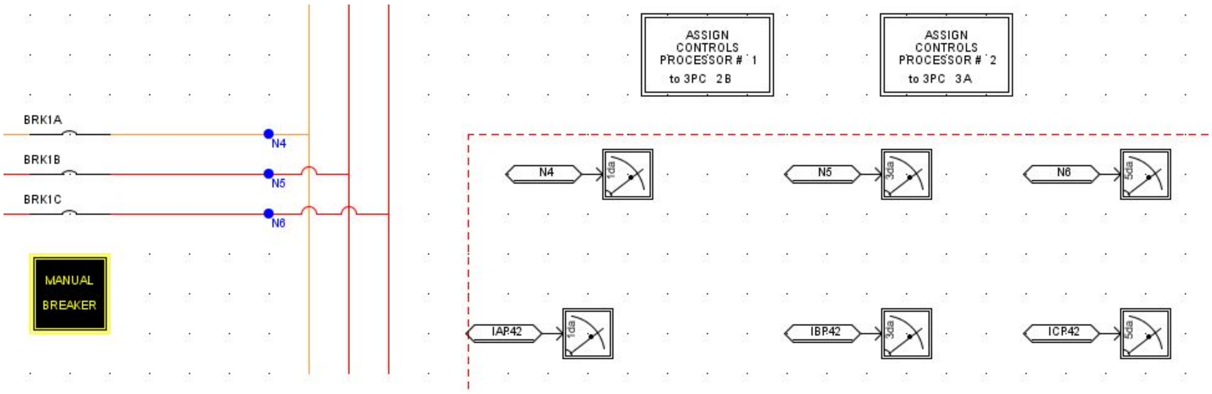

Figure 3-25: Circuit breaker subsystem (left), Voltage and current signals output blocks (right) and Assign Controls Processor # blocks (upper-right).

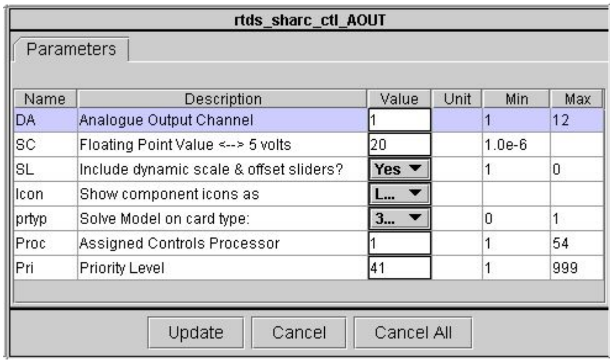

rtds_sharc_ctl_AOUT

Parameters

Name	Description	Value	Unit	Min	Max
DA	Analogue Output Channel	1		1	12
SC	Floating Point Value <--> 5 volts	20		1.0e-6	
SL	Include dynamic scale & offset sliders?	Yes		1	0
Icon	Show component icons as	L...			
prtyp	Solve Model on card type:	3...		0	1
Proc	Assigned Controls Processor	1		1	54
Pri	Priority Level	41		1	999

Update Cancel Cancel All

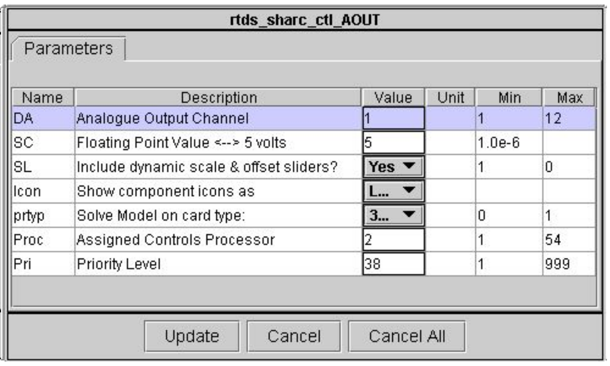

rtds_sharc_ctl_AOUT

Parameters

Name	Description	Value	Unit	Min	Max
DA	Analogue Output Channel	1		1	12
SC	Floating Point Value <--> 5 volts	5		1.0e-6	
SL	Include dynamic scale & offset sliders?	Yes		1	0
Icon	Show component icons as	L...			
prtyp	Solve Model on card type:	3...		0	1
Proc	Assigned Controls Processor	2		1	54
Pri	Priority Level	38		1	999

Update Cancel Cancel All

Figure 3-26: Interfacing output blocks' parameters for voltage signals (left) and current signals (right).

Now, phase voltages and currents will be sent to the output correctly and the relay should react on short-circuits properly. The trip-signal is fed back to the RTDS and therefore an input should be defined. Since some difficulties arose while defining analogue inputs, a digital input is being used now. In fact, the trip output of the relay is being connected to ground as the relay trips: a logical '0'. The 3PC-DOPTO input experiences a bit mask of 'ffffff' meaning a logical '0' at input channel 1 only when the relay trips.

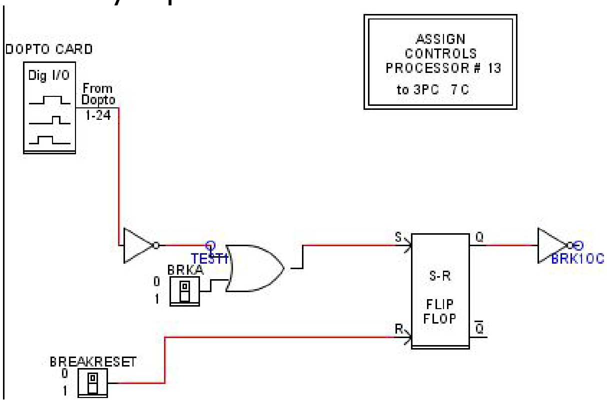

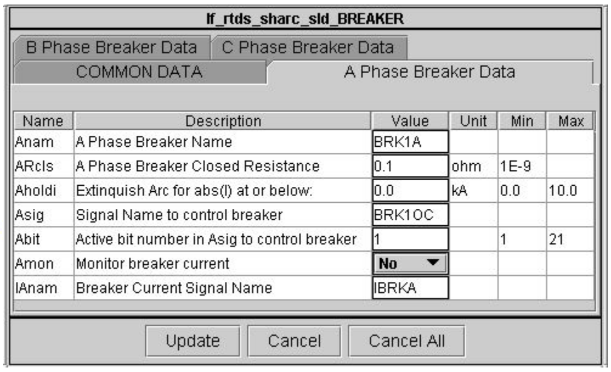

lf_rtds_sharc_sld_BREAKER

B Phase Breaker Data | C Phase Breaker Data | COMMON DATA | A Phase Breaker Data

Name	Description	Value	Unit	Min	Max
Anam	A Phase Breaker Name	BRK1A			
ARcls	A Phase Breaker Closed Resistance	0.1	ohm	1E-9	
Aholdi	Extinquish Arc for abs(I) at or below:	0.0	kA	0.0	10.0
Asig	Signal Name to control breaker	BRK1OC			
Abit	Active bit number in Asig to control breaker	1		1	21
Amon	Monitor breaker current	No			
IAnam	Breaker Current Signal Name	IBRKA			

Update Cancel Cancel All

Figure 3-27: Manual circuit breaker's logic (left) and circuit breaker control block (right).

Figure 3-27 depicts the circuit breaker's logical circuit and the breaker parameters. The operation of the CB relies on the *S-R flip-flop*. When the set input (S) becomes '1', Q becomes '1' as well and holds this value until a reset signal (R) is given even when set input drops to '0'. The signal (BRK10C) operates the breaker. A logical '1' closed the breaker while a logical '0' opens the breaker. A logical '0' at the input of the DOPTO card (Relay trips) should yield a logical '0' for BRK10C and hence open the circuit breaker. To achieve this, two inverters have been placed before and after the S-R flip-flop. The circuit is interrupted at current zero-crossing like in practice.

6 Zero-sequence component calculation: As depicted in Figure 3-28, zero-sequence components will be calculated. Notice that the output blocks are labelled as 'I0' and 'U0', but in fact, since signal names may not start with a number, $3\underline{U}_0$ and $\underline{I}_e(=-3\underline{I}_0)$ have been calculated. Both $3\underline{U}_0$ and $\underline{I}_e$ are assigned to an analogue output but only $\underline{I}_e$ will be amplified.

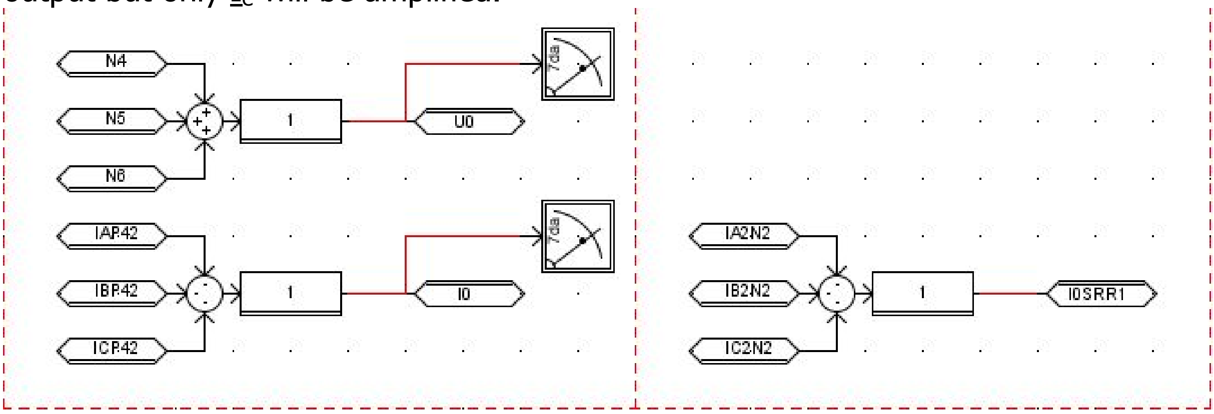

Figure 3-28: $3\underline{I}_0$ and $3\underline{U}_0$ analogue output blocks.

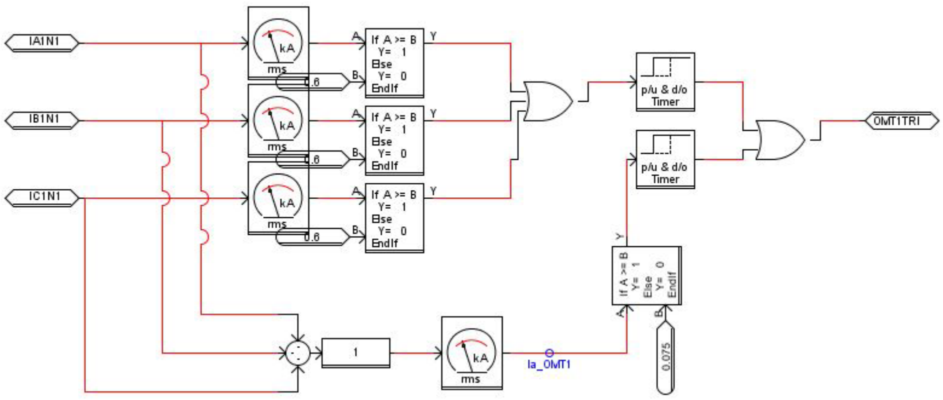

Figure 3-29: Overcurrent relay logical model.

7 Overcurrent relay model: Only one relay can be connected to the RTDS since only 7 suitable amplifiers are available. Therefore, both overcurrent relays and directional overcurrent relays have been modelled in RSCAD. Although both types of relays have an apparently inexhaustible amount of functions, some fundamental functions needed for overcurrent operation have been modelled. Figure 3-29 gives the control scheme for the overcurrent relay subsystem as it appears in RSCAD. In fact, the overcurrent relay model consists of two functions: Overcurrent measurement and earth-fault overcurrent measurement. The RMS-value of each phase current is being measured and compared to the pick up value (0.6 kA in this case). A logical '1' results in pick-up/drop-off timer to be triggered. After a given pick up time (0.9s, not shown), this block creates a logical '1' that will trigger the Circuit Breaker. Note that the RMS value of the earth-fault current is calculated by first subtracting the phase currents and then by calculating the RMS value of the summated signal. The relay model will trip by either an earth-fault trip signal or a phase current trip signal.

8 Directional overcurrent relay model: As one directional overcurrent relay is connected to the RTDS, the other one should be modelled in RSCAD. The most fundamental function, direction determination, is being described using Figure 3-30, in which the used model of the directional relay is shown. In order to save calculation time, only zero-sequence quantities have been taken into account. Therefore, only the fault-current direction of phase-to-ground faults can be determined correctly.

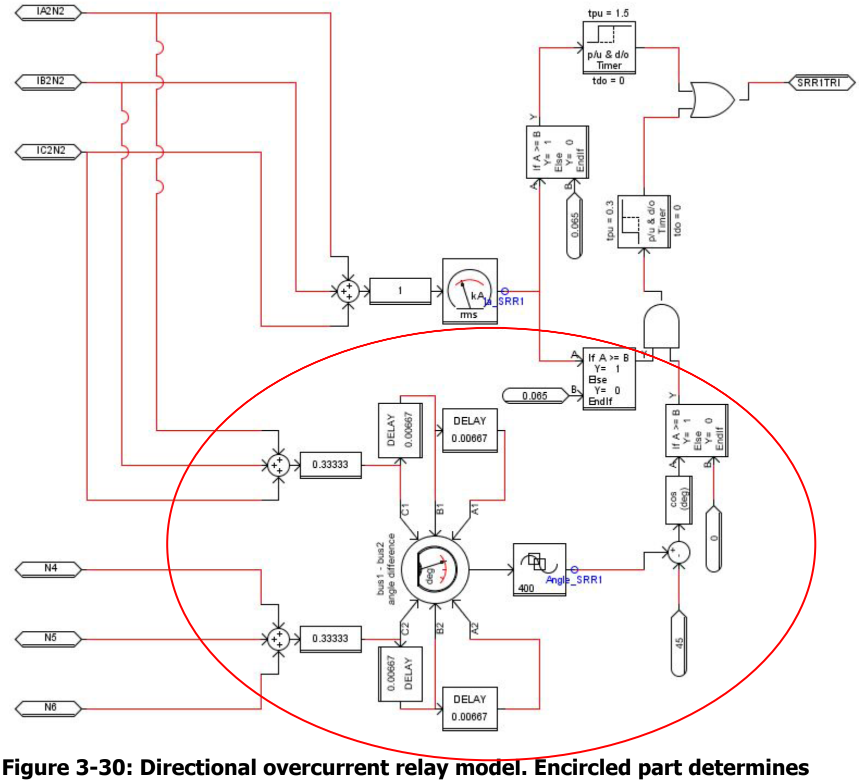

Figure 3-30: Directional overcurrent relay model. Encircled part determines direction.

The encircled part is a block model representation of Eq. 2.7 with a RCA of 45°. Note that two conditions should be fulfilled for a 'forward' pick up. First, the RMS-value of I_e should be above its pick up value (65 A) and second, the direction is being determined by calculating the phase difference between $\underline{U}_0$ and $\underline{I}_0$. *Delay* blocks ensure the angle-difference block to work correctly since it needs 3 phases. The phase angle difference signal is averaged over 400 calculation steps to smoothen the phase difference characteristic.

The runtime environment

After successful compilation, a .sib file has been created by RSCAD. This file can be loaded into the runtime environment, which also uploads the compiled data to the RTDS by clicking the (run) button. Figure 3-31 shows the runtime environment before simulation start. Push-buttons have been placed to initiate short circuits while sliders have been implemented to control active load, reactive load and fault duration. The switches can be used to close circuit breakers again after short-circuit isolation. Plots are automatically updated after adjusting sliders, pushing buttons and opening switches. Moreover, plots can be saved as COMTRADE-files[27], which can comprehensively be used for further analysis.

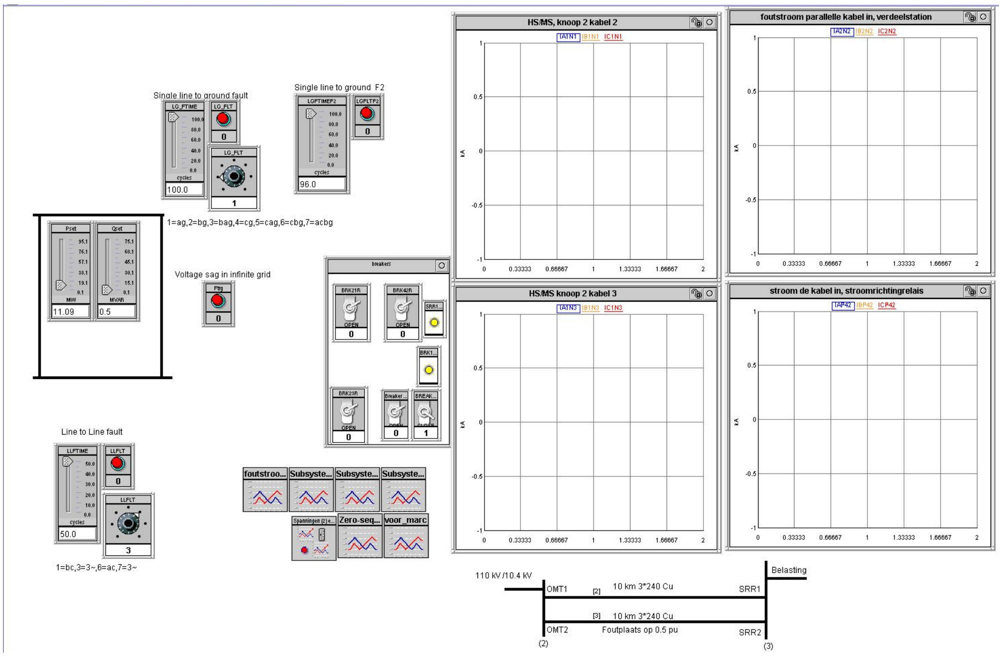

Figure 3-31: Runtime environment impression;simulation is not running

3.6 Measurement results and test results

The stated closed loop test system offers a lot of opportunities regarding the application of electronic relays with the RTDS. The proposed MV network has already extensively been simulated in Simulink and Matlab and discussed in chapter 2. Therefore it will be shown how the relay reacts during real time operation. Three cases are studied:

Single phase-to-ground-fault at k=0.5 per unit: The relay will pick up instantly after fault initiation. Earth-fault current direction should be determined correctly and the relay trips after 0.3s During initiation, measured waveforms are captured in a 1s relay buffer.

Single phase-to-ground-fault at k=0.2 per unit: The relay cannot pick up instantly as the fault location is too close to the feeding substation. Therefore, the opposing overcurrent relay should pick up using its earth-fault element. After overcurrent relay tripping, the 7SJ62 relay picks up and eventually encloses the fault.

Death-zone at k=0.5 per unit: As being predicted in chapter 2.1, a death-zone arises when distribution strings become too long compared to the rest of the MV network. This is being verified for a single phase-to-ground-fault at k=0.5 pu for a distribution capacitance of 20µF.

Moreover, the system connected to the RTDS has been verified at KEMA T&D. Captured waveforms are compared with the original waveforms produced by the RTDS.

3.6.1 Single phase-to-ground-fault; k=0.5 per unit

The fault initiates at k=0.5 per unit at t=0.2s The SRR2 waveforms are captured by the relay since the relay's directional earth-fault element picks up. The OMT2 waveforms have been extracted from the COMTRADE file created by the RTDS. It is emphasised to the reader that the 7SJ62 relay determines the fault direction using $\underline{I}_{e,7sj62}$=-3$\underline{I}_0$.which is *leading* $\underline{U}_0$ during a forward single phase-to-ground-fault. This waveform is also included in the COMTRADE-file labeled "I_e". In order to comply with previous results and to avoid confusion, $\underline{I}_e=3\underline{I}_0=\underline{I}_a+\underline{I}_b+\underline{I}_c$ is chosen to be shown. The waveforms during the initiation period are shown in Figure 3-32.

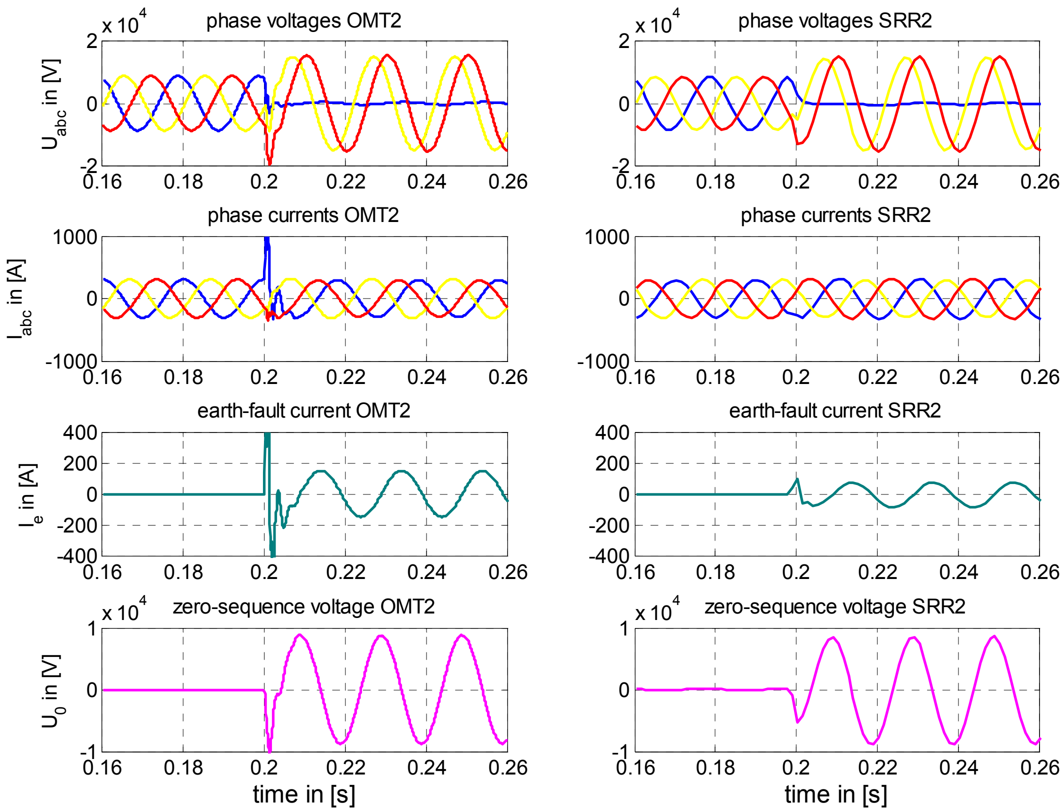

Figure 3-32: OMT2 and SRR2 waveforms during ground-fault initiation. SRR2 waveforms have been captured from the relay.

The most characteristic feature during fault initiation is the relative short transition period between the system's balanced operation and short-circuit operation. It should be noted that the network is modelled as if it is perfectly symmetric. Transient phenomena like travelling waves are not modelled. The fault arc is purely resistive and a simplified circuit breaker model is used. In practice the fault will possibly be intermitting and a single phase-to-ground-fault is very likely to change to a phase-to-phase-fault in bundled cables. Nevertheless, the relay detects faults using steady-state rms-values of measured currents and voltages and operates in definite time. Therefore, sophisticated circuit modelling is beyond the scope of this thesis.

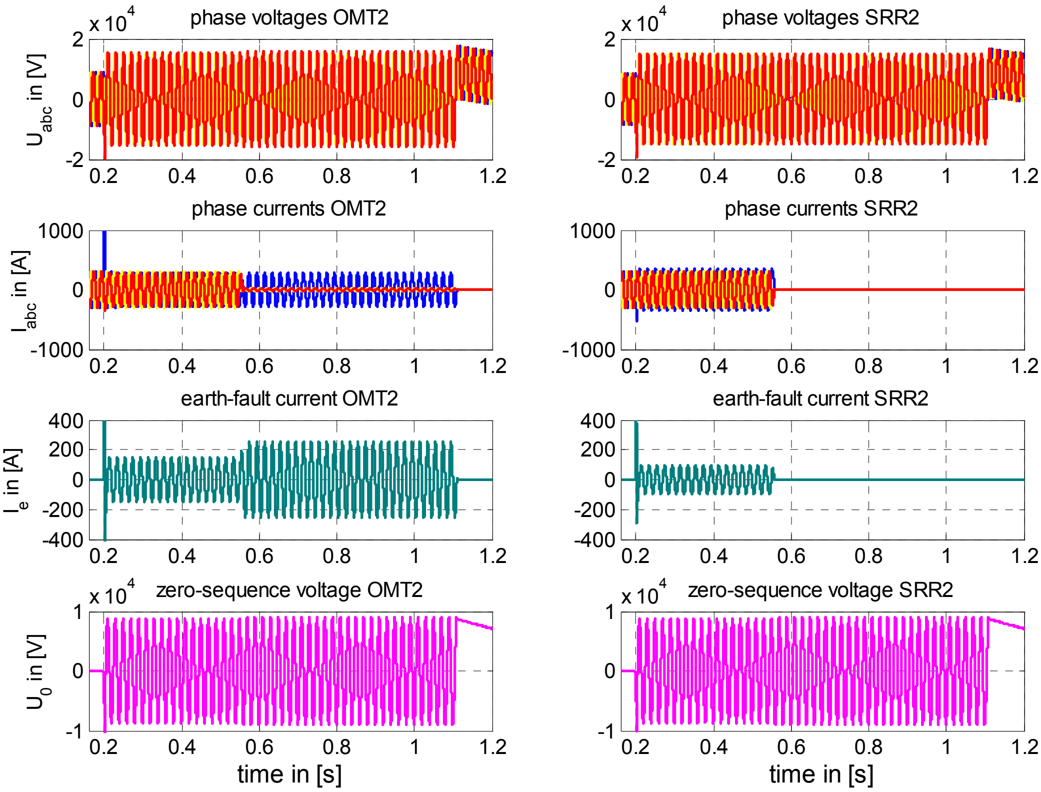

Figure 3-33: OMT2 and SRR2 waveforms during a single phase-to-ground-fault at k=0.5 per unit. SRR2 waveforms have been extracted from the RTDS. Fault clearance at t=1.1s.

Figure 3-33 depicts the waveforms during the period which is needed for the protection system to isolate the fault. After fault initiation (t=0.2 s), both overcurrent relay's earth-fault element and directional overcurrent relay's earth-fault element pick up. Since both relays operate in definite-time, the directional overcurrent relay will trip first at t=0.5 s. Thereafter, the fault current flows from the substation side only and the modelled overcurrent relay will trip at t=1.1 s, 0.9 s after fault initiation.

The earth-fault protection process is depicted in Figure 3-34. Since the relay is enclosed in the circuit, it can be extracted how much time is needed between fault initiation and switching. From the relay's COMTRADE file it turns out that it trips after being picked up for 297 ms. The relay theoretically needs one period (20 ms.) to determine rms-value and direction [13] of the current. It is remarkable that in this case 2 periods (40 ms) are needed for the relay to pick up. The trip signal (a step from 5 V to 0 V) immediately reaches the RTDS since the trip itself is a very fast (~µs) mechanical process. One period delay exists between the relay trip and actual circuit breaker interruption. In practice this delay exists as well, as a result of breaker interrupting time [18].

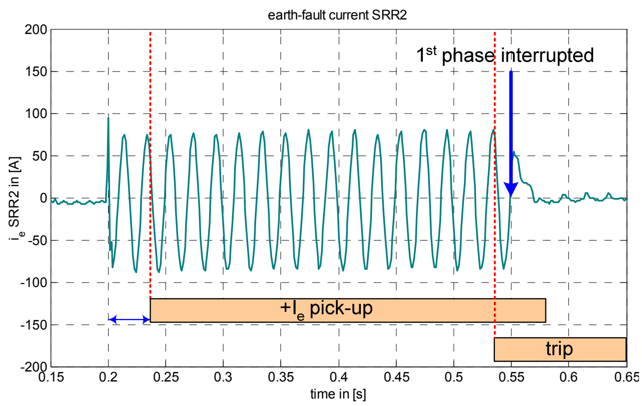

Figure 3-34: SRR2 captured earth-fault current. Relay trip at t=0.54s.

3.6.2 Single phase-to-ground-fault; k=0.20 per unit

The fault initiates at t=0.2 s. and only the overcurrent relay will pick up. The waveforms are shown in Figure 3-35. The ground-fault is too close to the HV/MV substation for the directional overcurrent relay to detect. After 0.9s (t=1.1 s) exactly, the modelled overcurrent relay trips by its earth-fault element and circuit interruption takes place immediately. Now, fault current flows through the parallel feeder cable feeding the fault from only one side. The directional relay's earth-fault element picks up and trips after 0.3s (at t=1.44s) isolating the short-circuit from the healthy part of the system.

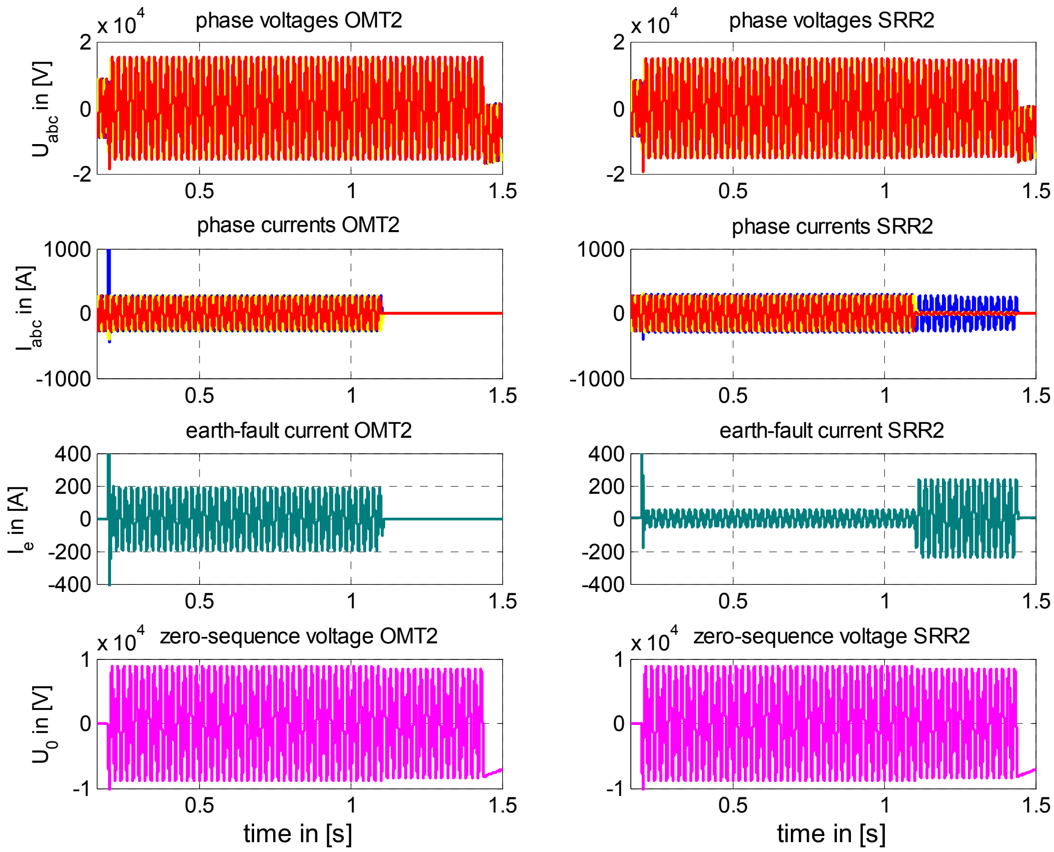

Figure 3-35: OMT2 and SRR2 waveforms during a single phase-to-ground-fault at k=0.2. SRR2 waveforms have been extracted from the RTDS. Fault clearance at t≈1.4s.

The waveforms in Figure 3-35 are extracted from the RTDS COMTRADE-file since the relay only captures voltages and currents during pick up. As can be seen in Figure 3-36, the relay needs less time (20 ms.) to pick up. This could possibly be described to the fact that the direction was already determined correctly before pick up and hence only the rms value must be measured for the relay to pick up.

It can be concluded that the short-circuit is being switched off correctly for both fault locations. Somewhere between k=0.2 per unit and k=0.5 per unit the directional overcurrent relay will fail to pick up on the short-circuit current immediately after fault initiation. In fact, the described situation is a variation on Figure 2-13 using other values of $C_{Grid,0}$ and $C_{dist,0}$.

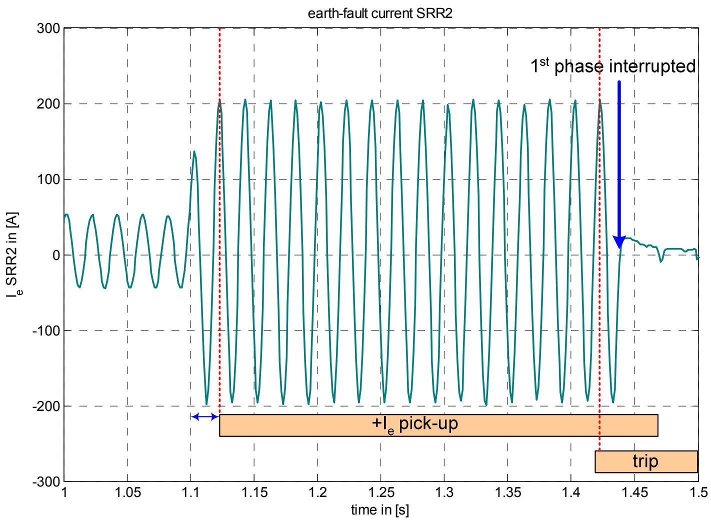

Figure 3-36: SRR2 captured earth-fault current. Relay trip at t=1.42s.

3.6.3 Single phase-to-ground-fault: 'death-zone'

Until now, all single phase-to-ground-faults are interrupted correctly. As described in chapter 2.1, a death-zone will arise when gradually increasing $C_{dist,0}$. This is applied within the RTDS' network, using parameters given in Table 3-3 . These parameters are extracted from Figure 2-19 for α=25 and relay parameters are set according to Table 2-2. Figure 3-37 shows that for the chosen system's parameters, a fault location of k=0.5 per unit lies well inside the death-zone of the protected cable.

Setting	Value
$C_{Grid,0}$	20 µF
$C_{dist,0}$	20 µF
α	25
SRR 1&2:{$+I_e$,$+t_e$}	$143A, 0.3s$
SRR 1&2: {I_e,t_e}	n/a
OMT 1&2: {I_e, t_e}	$163A, 0.9s$
Fault location	k=0.5 pu

Table 3-3: Adjusted network and relay parameters.

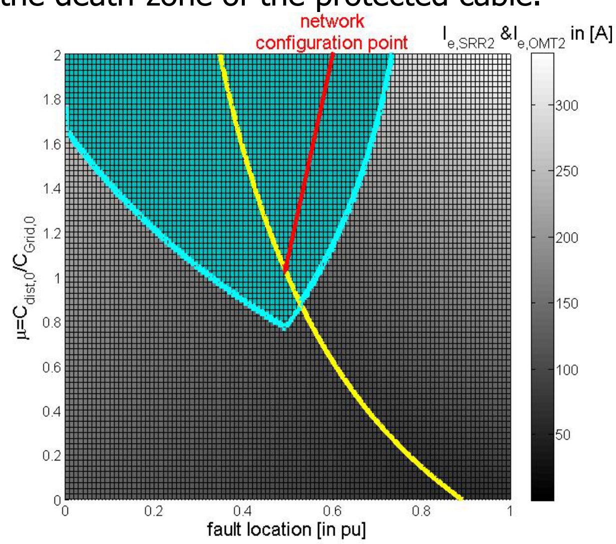

Figure 3-37: X-Y view of a death-zone development for the proposed network parameters.

The I_e,t_e functionality of the directional relay is disabled since it can only be used as a backup for backward faults (inside the distribution string, beyond directional relays) and as a backup for the directional functionality. Note that k=0.5 is not the only fault location inside the death-zone. From k≈0.33 to k≈0.55 both relays fail to pick up. Smaller current settings would result in uncoordinated circuit interruptions.

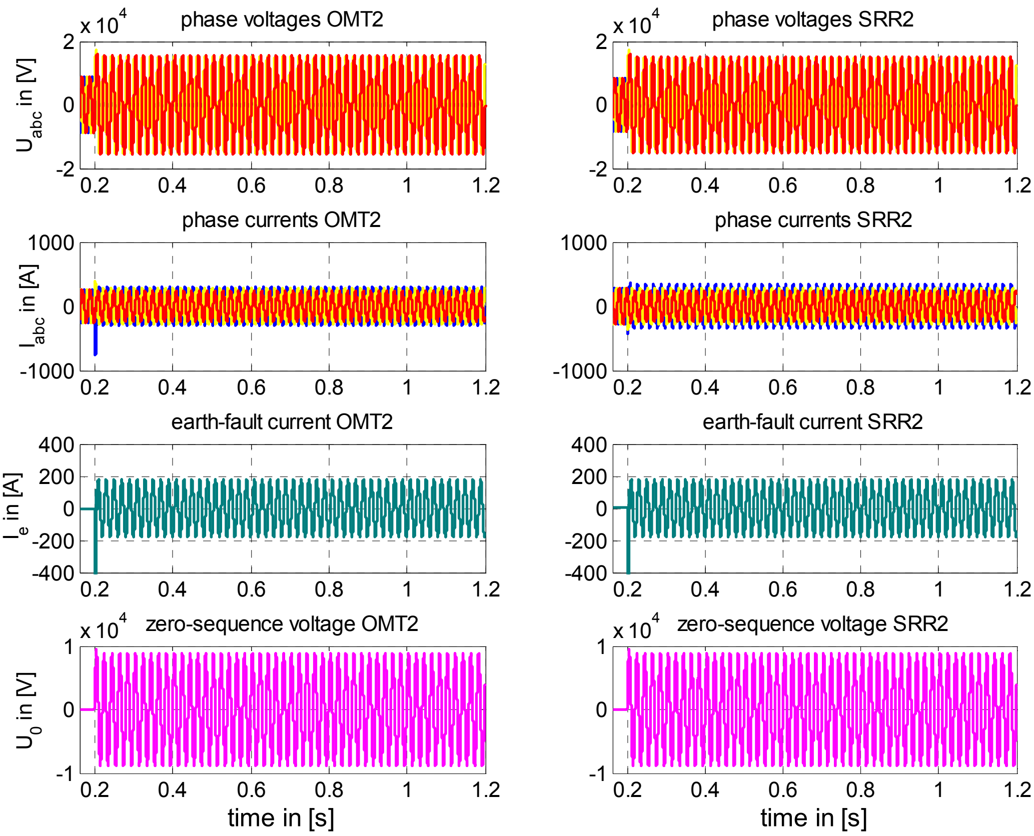

Figure 3-38: OMT2 and SRR2 waveforms during a single phase-to-ground-fault at k=0.5 per unit with adjusted network capacitances. SRR2 waveforms have been extracted from the RTDS. No fault clearance.

Figure 3-38 gives the waveforms as captured from the RTDS COMTRADE-files. It is clear that the protection equipment fail to detect and interrupt the single phase-to-ground-fault. It can be questioned if such a situation would occur in practice: The sum of the distribution string's cables is as long as the sum of the remaining MV network's cables. Moreover, extensive distribution networks are meshed in practice which need a sophisticated protection philosophy since the simple relation of Eq. 3.3 does not hold anymore.

Although not simulated, a remote phase-to-ground-fault in the distribution string will usually cause the overcurrent relays to pick up by the fault current of the rest of the MV-network. Therefore, **all** ground-faults located "beyond" the feeder cables should be interrupted before the feeder cables' overcurrent relays do so. This is a serious extension of the proposed relay co-ordination method. This generally means that, beside the directional overcurrent relays in the feeder cables that need to be installed, every outgoing distribution cable should be protected with an overcurrent relay with earth-fault element. This can seriously push up costs for feeder protection. Moreover, interrupting ground-faults in distribution strings will increase the total down-time for the consumer. A follow-up relay co-ordination study is needed for this challenge.

3.6.4 Measurement setup verification at KEMA T&D

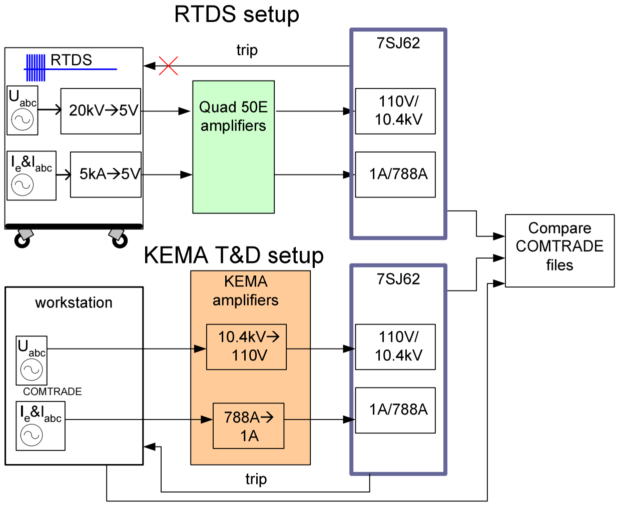

Figure 3-39: RTDS setup and KEMA T&D test setup. Comtrade files are compared.

Although a lot of information about QUAD 50E application was provided by frequency characteristics, complete verification should unquestionably allow amplifier application within the proposed test system. After unsuccessfully applying an OMICRON relay test set, KEMA T&D testing services offered the possibility to verify the test setup. Therefore, RTDS primary voltages and currents were captured in COMTRADE-format and played back at the relay with certified amplifiers. Current transformer ratio (788A/1A) and voltage transformer ratio (10400V/110V) have been taken into consideration. Figure 3-39 shows the KEMA verification setup together with the RTDS amplifier system. Both relay COMTRADE-files are compared to the original COMTRADE-files. The network of Figure 2-2 with the parameters given in Appendix C are used. The fault location is k=0.5 per unit. The COMTRADE-file to be replayed follows from a slightly different method since the relay may not switch open the simulated circuit. Doing so should imply a fault current for only 0.3 s, the pick up time of the relay. Offering this current to the relay would increase the risk of undesired drop-off after exact 0.3 s. Therefore, the relay trip contact was interrupted to let the short-circuit run for a longer time, namely for 0.9s, the earth-fault pick up time of the opposing overcurrent relay. Now, fault currents measured by the relay can be compared accurately. COMTRADE analysis is performed by importing them in Matlab.

First, the phase angle difference ($<\underline{I}_a - <\underline{U}_a$) between the two tests will be examined. Voltages are used as a reference for this purpose. Second, phase-currents and phase-voltages waveforms are analysed. Finally, zero-sequence voltage and current waveforms will be compared for both tests. The relays' COMTRADE-files have a sample rate of 800 and therefore 16 samples a period. Unfortunately, transient phenomena are not measured by the relay which makes verification suitable only for steady-state (short-circuit) voltages and currents.

Phasor angle difference

Phase angles are determined using SIGRA, a commonly used COMTRADE viewer for Siemens relays. Phasor-diagrams of steady-state voltages and load currents just before fault initiation are shown in Figure 3-40 for KEMA amplifiers (left) and Quad amplifiers (right). For system frequency, 50 Hz, phasor angles are not likely to differ from each other. Although angle differences have been shown in a table with 2 decimal places using SIGRA, angles are not determined accurately and differences are likely to occur within the measurement accuracy limit of 16 samples a period. Nevertheless it can be concluded that voltages and especially currents are well amplified. In contrast to the frequency characteristic measurements, a current phase lag was not measured during the KEMA tests. This is possibly caused by the relative long cables between the toroïdal transformers and the relay's current input, which increases the resistance and hence decreases the burden's phase angle. The reader should notice that the phase-angle between measured phase currents and voltages is about 170°. This is due to the current transformer connection which is *busbar-grounded* as shown in Figure 1-10. Load currents will therefore be measured as 'backward' while fault currents will be measured as 'forward'.

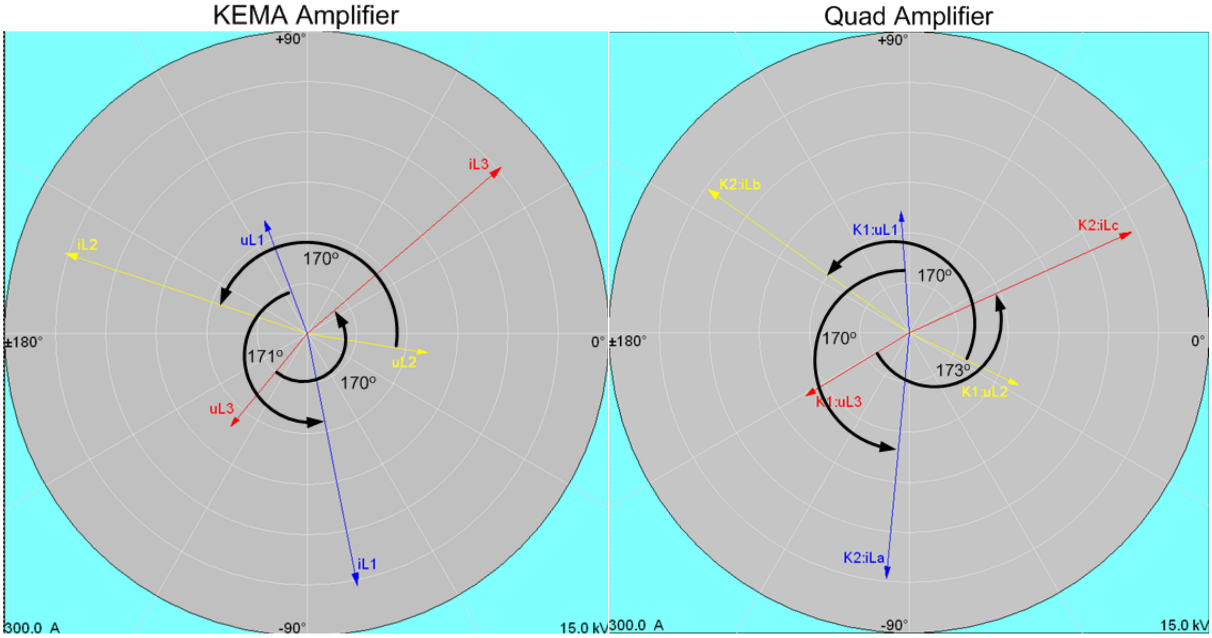

Figure 3-40: Phase-angles for balanced three-phase voltages and currents. Captured by the 7SJ62 relay.

Phase currents and voltages

During fault initiation, a transition between a symmetrical three-phase system and an asymmetrical three-phase system takes place. Therefore, it is important to measure in what way the amplifier reacts on this system change. Stored current and voltage waveforms are plotted in Figure 3-41 and compared to the original RTDS waveforms which are equal to the waveforms produced by the KEMA amplifier.

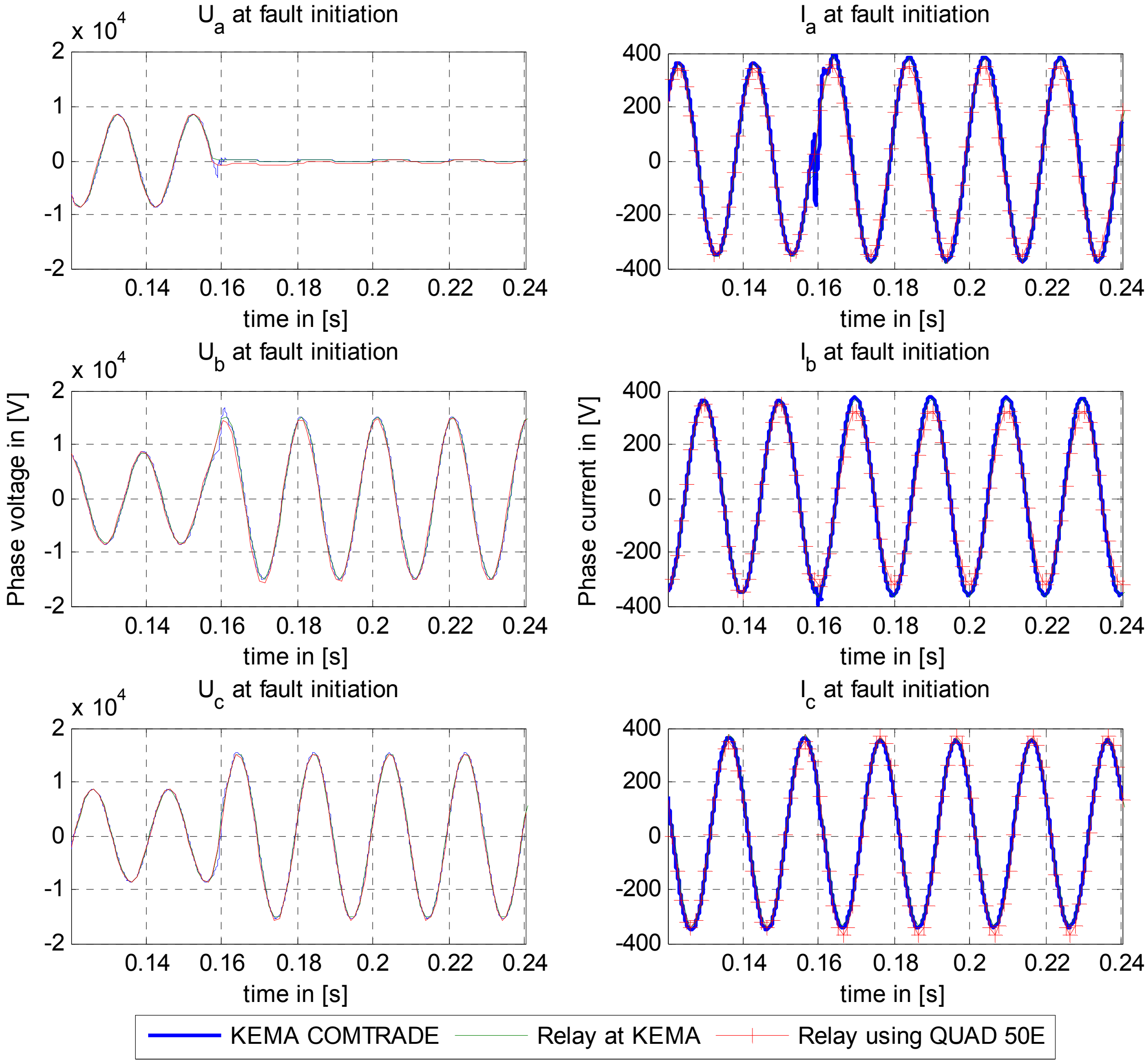

Figure 3-41: Captured voltage and current waveforms compared to the original KEMA (and thus RTDS) waveforms.

It turns out that the amplified voltage signals are almost exactly equal to the original waveforms produced by the KEMA amplifier whereas the captured currents differ a little bit. It should be noted that the KEMA amplifier operates at its very minimum current level for which secondary currents can be produced. This requires a short explanation. Normally, secondary (fault) currents are in the range of a few Amperes ($I_{sec,rated}$=1A) to considerable high values (up to 250 A for thermal tests). In this case, when single phase-to-ground-faults in isolated neutral MV networks are present, the secondary currents range from 0 to 1 A. Even with a very small amplification error (<0.5%), small deviations in the test results can be expected. Moreover, Quad amplifiers are audio amplifiers and are hence not designed for current amplification. Captured waveforms give nevertheless a good representation of the original signal.

Zero-sequence voltages and currents

Since the captured waveforms differ slightly from the original, the secondary current measurement circuit is not connected in *Holmgreen* (Figure 3-17) and hence $\underline{I}_e$

is fed separately to the relay. Since direction determination is done using zero-sequence quantities, these waveforms are compared as well. Figure 3-42 shows U_o and I_e during fault initiation. It can be seen that the relay fails to measure the dynamic current peak correctly. Since the relay operates in definite-time mode, measuring this peak is not of major importance. The steady-state earth-fault current is being amplified correctly and the relay trips after 0.3s (not shown). Zero-sequence voltage is being calculated from the captured phase voltage waveforms. A small pre-fault zero-sequence voltage can be observed. This indicates that voltages are not amplified completely symmetrically. For direction determination this asymmetry should not cause major complications and hence the test results are satisfactory.

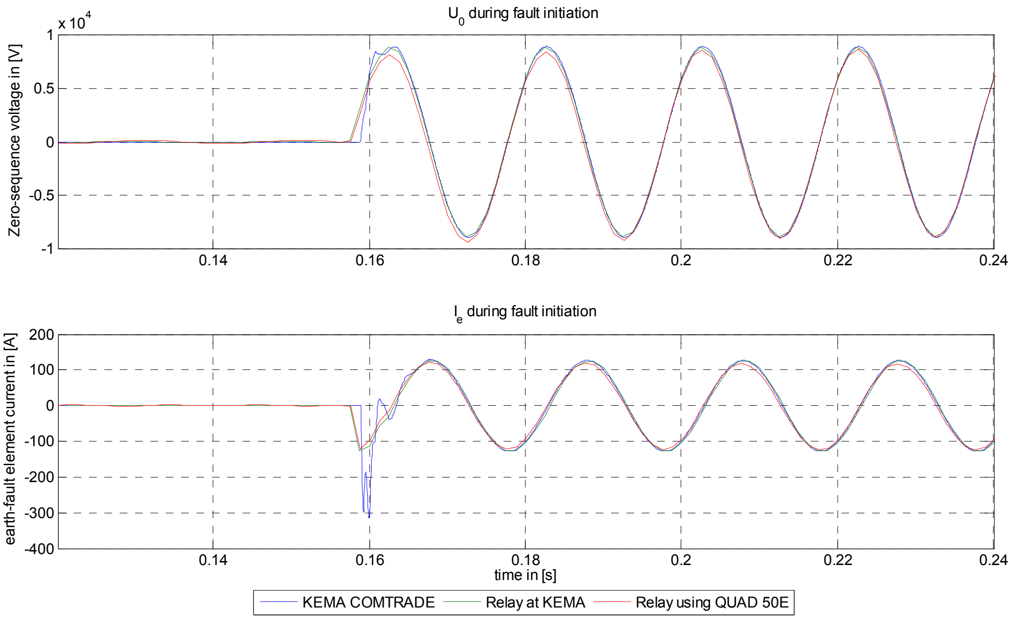

Figure 3-42: Relay-captured Zero-sequence voltage and earth-fault current compared to the original KEMA waveforms.

It can be concluded that, although small differences occur in comparison to the KEMA waveforms, the QUAD 50E amplifiers can be applied within the closed loop test system. It is emphasised to the reader once more that captured waveforms have a sample rate of only 800 Hz, making the model verification only suitable for relative low frequencies.

Conclusions and recommendations

Conclusions

The thesis presents a detailed relay co-ordination study. Several protection methods have been discussed. Single phase-to-ground-faults have extensively been studied and the proposed fault calculation method can be used more generally as well. A protection method for single phase-to-ground faults has been established.

Protection equipment should make use of an earth-fault element to detect magnitude and direction of the fault current. During a single phase-to-ground fault, the RMS value of the zero-sequence current is defined by the total MV network capacitance to ground. Direction is determined by measuring the phase-angle between $\underline{U}_0$ and $\underline{I}_0$. For a fault in 'forward' direction (fault inside feeder cable) $\underline{I}_0$ lags $\underline{U}_0$ by 90°. It is emphasised to the reader that it should be known how current transformers are connected before settings are adjusted.

Overcurrent and directional overcurrent relays should be set using Table 2-2. The current measured by the directional overcurrent relay is mainly dependent on the capacitance to ground of the distribution string's cables and hence determines the minimum pick up value. The minimum current setting of the overcurrent relay is also dependent on the capacitance of the protected feeder cable. A margin factor α was introduced to prevent incorrect relay pick ups.

The proposed method protects feeder cables from single phase-to-ground faults. The following should be noted about the method's application:

- for a 10 km feeder cable α=25 is advised to be chosen;
- μ_{lim} is equal to 0.86 but only for a limited range of network capacitance;
- The method has only been applied for two parallel cables. More parallel cables should lead to less critical protection co-ordination;
- All phase-to-ground faults in the MV network should be switched off selectively;
- For the given network, a maximum $C_{dist,0}$ of 25 μF can be applied for correct relay co-ordination;

The method has been applied for several network sizes. Furthermore, it should be noted that cross-country faults (2 single phase-to-ground faults in 2 different cables) have not been discussed in this work. However, fault current direction is not determined correctly during these faults and therefore, phasor-elements of protection relays should react correctly during these faults.

The RTDS has been used for closed loop application of the 7SJ62 directional relay. An interface between the RTDS and the relay has been established. QUAD 50E audio amplifiers have been used for correct amplification of voltage and current signals. Amplifiers have extensively been tested. Frequency characteristics have been determined during tests in the faculty's EPE lab. Amplified voltage and current waveforms have been compared to waveforms created by certified KEMA equipment and therefore the interface between RTDS and 7SJ62 has been verified. It turned out that great similarities exist between both waveforms, allowing the amplifiers to be applied. The interfacing method has comprehensively been described for further application by the faculty.

Recommendations

Regarding to the current results, single phase-to-ground-faults inside feeder cables can only be interrupted selectively if all ground-faults occurring in the MV network are detected and switched off. This can be avoided by adding another demand to the overcurrent earth-fault current pick up setting: The overcurrent relay should not pick up on single phase-to-ground-faults beyond the feeder cable. Although this will certainly decrease the value of μ_{lim}, it is certainly worthwhile to study this in future work. Differential feeder protection can also be applied in new feeder cable configurations.

Besides this report, which is mainly a technical one, a complementary reliability and financial study is needed in order to develop a feasible protection philosophy. Three protection methods should be studied in that case:

- The discussed method with minimum pick up current setting defined by the distribution string's capacitance;
- The (still to be technically studied) method by which not every ground-fault has to be interrupted, only those in feeder cables;
- Differential feeder protection.

The used amplifiers are verified and work well for this test setup. However, when more sophisticated protection equipment has to be tested, it takes a lot of time to re-establish the interface between RTDS and relay. Furthermore, no high secondary currents (>5A) can be created by the interface. Therefore, if the department considers to focus on protection studies using the RTDS, the author advises to invest in sophisticated, professional amplifiers.

Appendix A: Introduction to sequence components

In this appendix, the theory of symmetrical components is explained briefly. The theory of symmetrical components (also: sequence components) is a powerful tool for short-circuit calculation and it has been used extensively in this work. The method was first proposed in 1918 [28] describing in what way an n phase system of asymmetrical phasors can be composed of a n phase system of symmetrical phasors. In this case, the transformation decomposes a three-phase system of phasors to three balanced three phase systems:

- Positive-sequence system in which the phasor sequence is clockwise;
- Negative-sequence system in which the phasor sequence is counter-clockwise;
- Zero-sequence system in which all three phasors are equal;

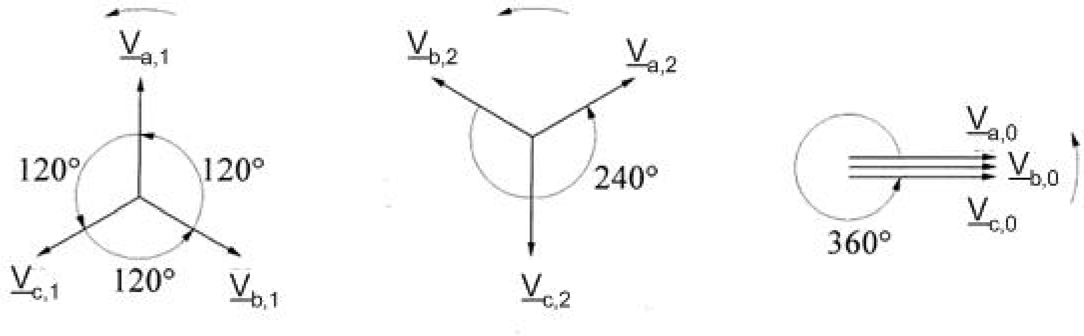

(a) Positive-sequence components (b) Negative-sequence components (c) Zero-sequence components

Figure A-1: Sequence components [32]

Figure A-1 depicts the phasor diagrams of a decomposed unbalanced three-phase system. For a three phase set of sinusoidal voltages holds:

$$\begin{aligned} v_a(t) &= \sqrt{2}V_a\cos(\omega t+\beta) = \sqrt{2}\,\mathrm{Re}\left(\underline{V}_a e^{jwt}\right) \\ v_b(t) &= \sqrt{2}V_b\cos\left(\omega t+\chi\right) = \sqrt{2}\,\mathrm{Re}\left(\underline{V}_b e^{jwt}\right) \\ v_c(t) &= \sqrt{2}V_c\cos(\omega t+\delta) = \sqrt{2}\,\mathrm{Re}\left(\underline{V}_c e^{jwt}\right) \end{aligned} \qquad \text{(A.1)}$$

In which

$$\begin{aligned} \underline{V}_a &= V_a e^{j\beta} \\ \underline{V}_b &= V_b e^{j\chi} \\ \underline{V}_c &= V_c e^{j\delta} \end{aligned} \qquad \text{(A.2)}$$

are the RMS phasor quantities. Since both the pre-fault system and the faulted system are assumed to be in steady-state, phasor quantities will be used further on. The decomposition of the given three phase system in sequence quantities is defined as[30]:

$$\underline{\boldsymbol{V}}_{012} = \boldsymbol{S}^{-1}\underline{\boldsymbol{V}}_{abc} \qquad \text{(A.3)}$$

Where

$$\boldsymbol{S}^{-1} = \frac{1}{3}\begin{bmatrix} 1 & 1 & 1 \\ 1 & a & a^2 \\ 1 & a^2 & a \end{bmatrix};\; a = e^{j\frac{2\pi}{3}} \;\Rightarrow \boldsymbol{S} = \begin{bmatrix} 1 & 1 & 1 \\ 1 & a^2 & a \\ 1 & a & a^2 \end{bmatrix} \qquad \text{(A.4)}$$

And

$$\underline{\boldsymbol{V}}_{012} = \begin{bmatrix} \underline{V}_0 \\ \underline{V}_1 \\ \underline{V}_2 \end{bmatrix}; \underline{\boldsymbol{V}}_{abc} = \begin{bmatrix} \underline{V}_a \\ \underline{V}_b \\ \underline{V}_c \end{bmatrix} \tag{A.5}$$

For a set of balanced three-phase voltages holds

$$\begin{aligned} \underline{V}_a &= V_a e^{j0} \\ \underline{V}_b &= V_a e^{-j\frac{2}{3}\pi} \\ \underline{V}_c &= V_a e^{j\frac{2}{3}\pi} \end{aligned} \tag{A.6}$$

And consequently for the sequence quantities

$$\begin{aligned} \underline{V}_0 &= \frac{1}{3}\left(\underline{V}_a + \underline{V}_b + \underline{V}_c\right) = 0 \\ \underline{V}_1 &= \frac{1}{3}\left(\underline{V}_a + a\underline{V}_b + a^2\underline{V}_c\right) = \underline{V}_a \\ \underline{V}_2 &= \frac{1}{3}\left(\underline{V}_a + a^2\underline{V}_b + a\underline{V}_c\right) = 0 \end{aligned} \tag{A.7}$$

Similar equations should be used for current phasors. The reader should notice that the used transformation is power-variant. Since relays' setting should be non per unit quantities and correct measurement of real power as well as reactive power is of minor importance, the power variant symmetrical component transformation is used. Moreover, $I_e=3I_0$ and $U_{neutral}=U_0$ follow directly from the power variant transformation.

Appendix B: On the sequence-component network parameters.

In this appendix, pi-section's lumped sequence parameters are derived from lumped cable parameters. Results are summarised in Table 1-1. First, sequence parameters of a bundled three phase cable are derived. Then, sequence parameters of three single phase-cables are derived. Zero-sequence parameters can be determined by connecting each phase to the same voltage, $\underline{V}_0$, and measuring the source current which is equal to $3\underline{I}_0$ [29]. Positive-sequence parameters can be determined by measuring phase currents after connection the phases to a balanced three phase source.

Bundled cable

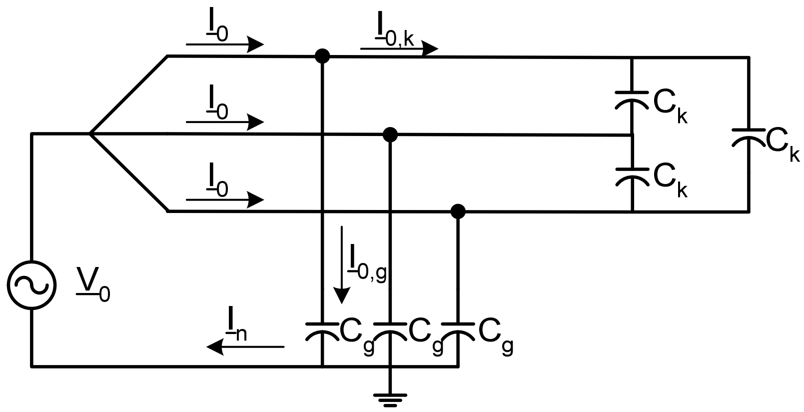

Figure B-1: Zero-sequence capacitance calculation scheme

C_0 will be derived from the physically lumped capacitances using Figure B-1. First, a delta-wye transformation is used to represent the mutual capacitances between conductors (C_k) as capacitances to an imaginary neutral point (C'_k):

$$\frac{1}{j\omega C'_k} = \frac{\frac{1}{j\omega C_k}\frac{1}{j\omega C_k}}{\frac{1}{j\omega C_k}+\frac{1}{j\omega C_k}+\frac{1}{j\omega C_k}} \Rightarrow C'_k = 3C_k \tag{B.1}$$

For the zero-sequence current $\underline{I}_0$ now holds:

$$\underline{I}_0 = \underline{I}_{0,k} + \underline{I}_{0,g} = 0 - j\omega U_0 C_g \tag{B.2}$$

and thus for the measured zero-sequence impedance and capacitance

$$Z_0 = \frac{\underline{V}_0}{\underline{I}_0} = -j\omega\left(C_g\right) \Rightarrow C_0 = C_g \tag{B.3}$$

C_1 will be derived from the physically lumped parameters using Figure B-2. For the phase current holds:

$$\underline{I}_a = \underline{I}_{a,k} + \underline{I}_{a,g} = -j\omega \underline{V}_{an}(C_g + C'_k) \tag{B.4}$$

And, according to Eq. A.7

$$\underline{V}_{an} = \underline{V}_1; \underline{I}_a = \underline{I}_1 \tag{B.5}$$

And for the measured positive sequence impedance and capacitance

$$Z_1 = \frac{\underline{V}_1}{\underline{I}_1} = \frac{\underline{V}_{an}}{\underline{I}_a} = -j\omega\left(C_g + C'_k\right) \Rightarrow C_1 = C_g + C'_k = C_g + 3C_k \tag{B.6}$$

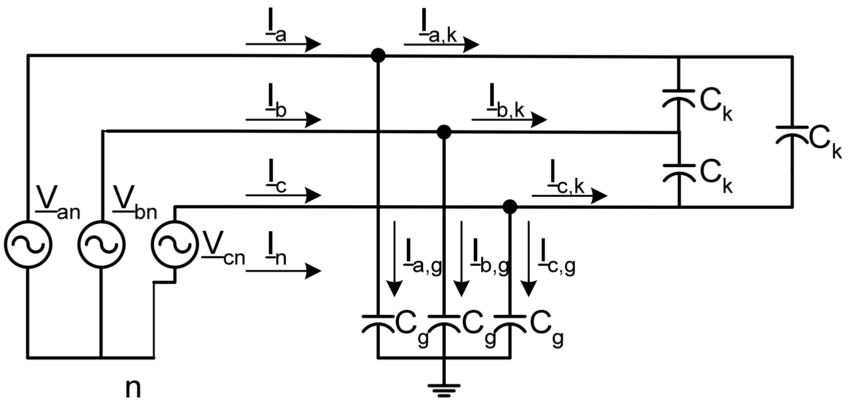

Figure B-2: Positive-sequence capacitance calculation scheme

R_0 and L_0 are derived in a similar way as C_0. Now only inductances, mutual inductances and resistances have been taken into account. A known source voltage $\underline{V}_0$ is connected to the cable's conductors according to Figure B-3. At the cable's end the conductors are connected to the cable's sheath establishing a return path.

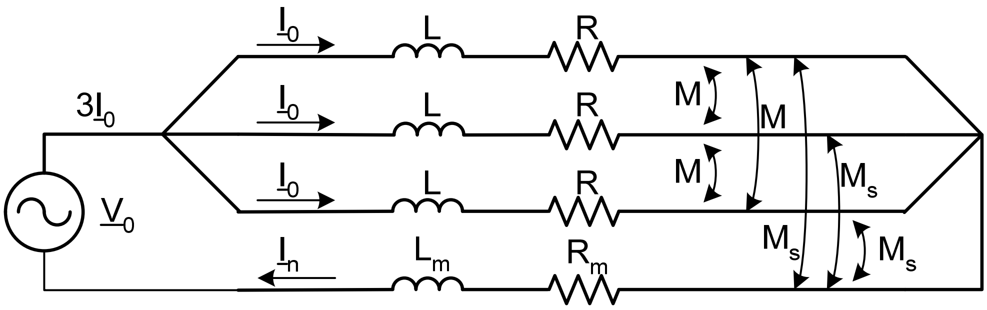

Figure B-3: Zero-sequence impedance calculation scheme

According to Kirchhoff's law holds:

$$\underline{V}_0 - j\omega L I_0 - R\underline{I}_0 - j\omega M\underline{I}_0 - j\omega M\underline{I}_0 + 3\underline{I}_n j\omega M_s + 3\underline{I}_0 j\omega M_s - 3\underline{I}_0 R_m - 3\underline{I}_0 j\omega L_m = 0 \tag{B.7}$$

after rearranging this yields:

$$\underline{V}_0 = \underline{I}_0\left[R + 3R_m + j\omega\left(L + 3L_m + 2M - 6M_s\right)\right] \tag{B.8}$$

And for Z_0:

$$Z_0 = \frac{\underline{V}_0}{\underline{I}_0} = R_0 + j\omega L_0 = \left[R + 3R_m + j\omega\left(L + 3L_m + 2M - 6M_s\right)\right] \tag{B.9}$$

Yielding for R_0 and L_0

$$\begin{aligned} R_0 &= R + 3R_m \\ L_0 &= L + 3L_m + 2M - 6M_s \end{aligned} \tag{B.10}$$

Where R the conductor's series resistance in [Ω/km], R_m the sheath's series resistance in [Ω/km], L the conductor's series inductance in [H/km], L_m the sheath's series inductance in [H/km], M the mutual inductance between conductors in [H/km] and M_s the mutual inductance between conductor and sheath in [H/km].

R_1 , *R_2* , *L_1* and *L_2* are derived using Figure B-4. A balanced three phase source is connected to the cable's conductors. The voltage drop over the depicted piece of cable is calculated assuming a wye connection at the cable's end. Now the calculated currents define *R_1* and *L_1*. Applying Kirchhoff's law to the proposed circuit yields

$$\begin{aligned}
\underline{V}_{an} &= \underline{I}_a R + j\omega \underline{I}_a L + j\omega \underline{I}_b M + j\omega \underline{I}_c M - j\omega \underline{I}_n L_m - \underline{I}_n R_m + \ldots \\
&\quad j\omega \underline{I}_n M_s - j\omega \underline{I}_a M_s - j\omega \underline{I}_b M_s - j\omega \underline{I}_c M_s \\
\underline{V}_{bn} &= \underline{I}_b R + j\omega \underline{I}_b L + j\omega \underline{I}_a M + j\omega \underline{I}_c M - j\omega \underline{I}_n L_m - \underline{I}_n R_m + \ldots \\
&\quad j\omega \underline{I}_n M_s - j\omega \underline{I}_a M_s - j\omega \underline{I}_b M_s - j\omega \underline{I}_c M_s \\
\underline{V}_{cn} &= \underline{I}_c R + j\omega \underline{I}_c L + j\omega \underline{I}_a M + j\omega \underline{I}_b M - j\omega \underline{I}_n L_m - \underline{I}_n R_m + \ldots \\
&\quad j\omega \underline{I}_n M_s - j\omega \underline{I}_a M_s - j\omega \underline{I}_b M_s - j\omega \underline{I}_c M_s
\end{aligned} \tag{B.11}$$

Where

$$\underline{I}_n = -\left(\underline{I}_a + \underline{I}_b + \underline{I}_c\right) \tag{B.12}$$

Rearranging for *I_a*,*I_b* and *I_c* gives

$$\begin{aligned}
\underline{V}_{an} &= \underline{I}_a\left[R + R_m + j\omega\left(L + L_m - 2M_s\right)\right] + \left(\underline{I}_b + \underline{I}_c\right)\left[R_m + j\omega\left(L_m + M - 2M_s\right)\right] \\
\underline{V}_{bn} &= \underline{I}_b\left[R + R_m + j\omega\left(L + L_m - 2M_s\right)\right] + \left(\underline{I}_a + \underline{I}_c\right)\left[R_m + j\omega\left(L_m + M - 2M_s\right)\right] \\
\underline{V}_{an} &= \underline{I}_c\left[R + R_m + j\omega\left(L + L_m - 2M_s\right)\right] + \left(\underline{I}_a + \underline{I}_b\right)\left[R_m + j\omega\left(L_m + M - 2M_s\right)\right]
\end{aligned} \tag{B.13}$$

Or in matrix notation

$$\underline{\boldsymbol{V}}_{abc} = \boldsymbol{Z}_{abc}\underline{\boldsymbol{I}}_{abc} \tag{B.14}$$

With

$$\boldsymbol{Z}_{abc} = \begin{bmatrix} R + R_m + j\omega\left(L + L_m - 2M_s\right) & R_m + j\omega\left(L_m + M - 2M_s\right) & R_m + j\omega\left(L_m + M - 2M_s\right) \\ R_m + j\omega\left(L_m + M - 2M_s\right) & R + R_m + j\omega\left(L + L_m - 2M_s\right) & R_m + j\omega\left(L_m + M - 2M_s\right) \\ R_m + j\omega\left(L_m + M - 2M_s\right) & R_m + j\omega\left(L_m + M - 2M_s\right) & R + R_m + j\omega\left(L + L_m - 2M_s\right) \end{bmatrix} \tag{B.15}$$

Now

$$\begin{aligned}
\underline{\boldsymbol{V}}_{abc} &= \boldsymbol{S}\underline{\boldsymbol{V}}_{012} = \boldsymbol{Z}_{abc}\boldsymbol{S}\underline{\boldsymbol{I}}_{012} \\
\boldsymbol{S}^{-1}\boldsymbol{S}\underline{\boldsymbol{V}}_{012} &= \boldsymbol{S}^{-1}\boldsymbol{Z}_{abc}\boldsymbol{S}\underline{\boldsymbol{I}}_{012} \\
\underline{\boldsymbol{V}}_{012} &= \boldsymbol{Z}_{012}\underline{\boldsymbol{I}}_{012}
\end{aligned} \tag{B.16}$$

The diagonal elements of the obtained matrix, ***Z_{012}***, represent the sequence capacitances of the given network:

$$\begin{aligned}
&\boldsymbol{Z}_{012(1,1)} = Z_0 \;\; ; \boldsymbol{Z}_{012(2,2)} = Z_1 = R_1 + j\omega L_1 = R + j\omega\left(L - M\right); \boldsymbol{Z}_{012(3,3)} = \boldsymbol{Z}_{012(2,2)} = Z_2 \\
&R_1 = R \,;\, L_1 = L - M; \\
&R_2 = R_1 ;\, L_2 = L_1
\end{aligned} \tag{B.17}$$

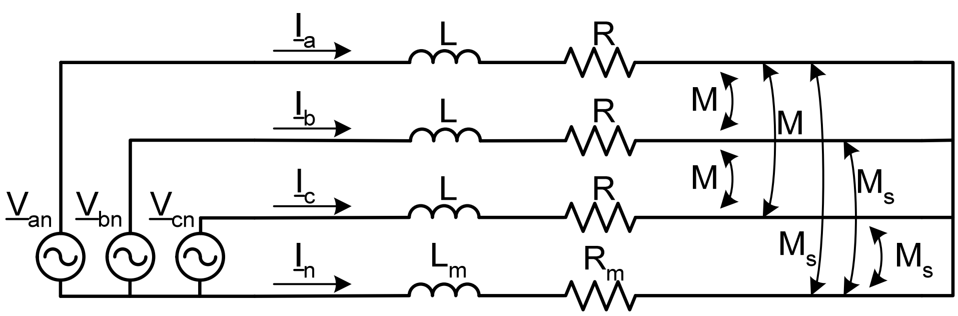

Figure B-4: Positive sequence parameter calculation scheme; bundled cable

Three single-phase cables

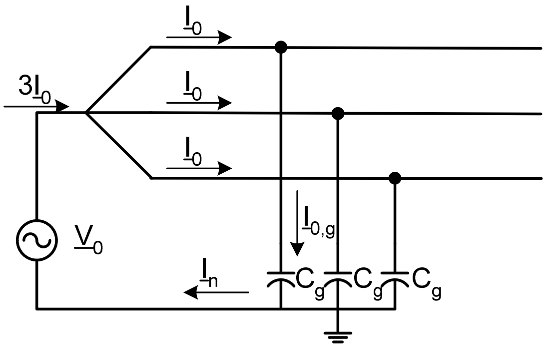

Figure B-5a: Zero-sequence capacitance scheme; 3 single phase cables

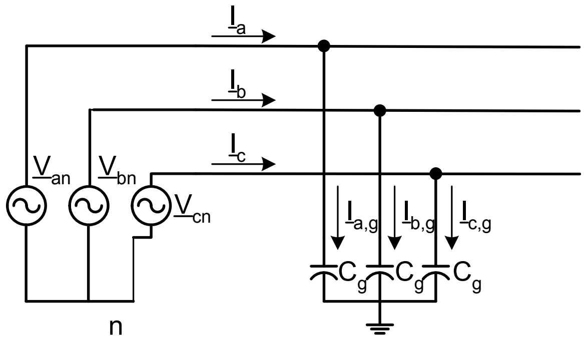

Figure B-5b: Positive-sequence capacitance scheme; 3 single phase cables

Since inside three single-phase cables the conductors are surrounded by the sheaths, no mutual capacitance or inductance exists between phase conductors (Figure B-5a). Therefore, C_0 is determined by the cable's capacitances to ground. For $\underline{I}_0$ holds:

$$\underline{I}_0 = \underline{I}_{0,g} = j\omega \underline{V}_0 C_g \tag{B.18}$$

yielding for Z_0 and C_0:

$$Z_0 = \frac{\underline{V}_0}{\underline{I}_0} = -j\omega C_g \Rightarrow C_0 = C_g \tag{B.19}$$

Analogous to the bundled three phase cable, C_1 is determined by calculating phase currents as a balanced three phase source is being connected to the cables (Figure B-5b). For phase a holds:

$$\underline{I}_a = \underline{I}_{a,g} = -j\omega \underline{V}_{an} C_g \tag{B.20}$$

And since $\underline{V}_1 = \underline{V}_a$ and $\underline{I}_1 = \underline{I}_a$,yields

$$Z_1 = \frac{\underline{V}_1}{\underline{I}_1} = \frac{\underline{V}_{an}}{\underline{I}_a} = -j\omega C_g \Rightarrow C_1 = C_g \tag{B.21}$$

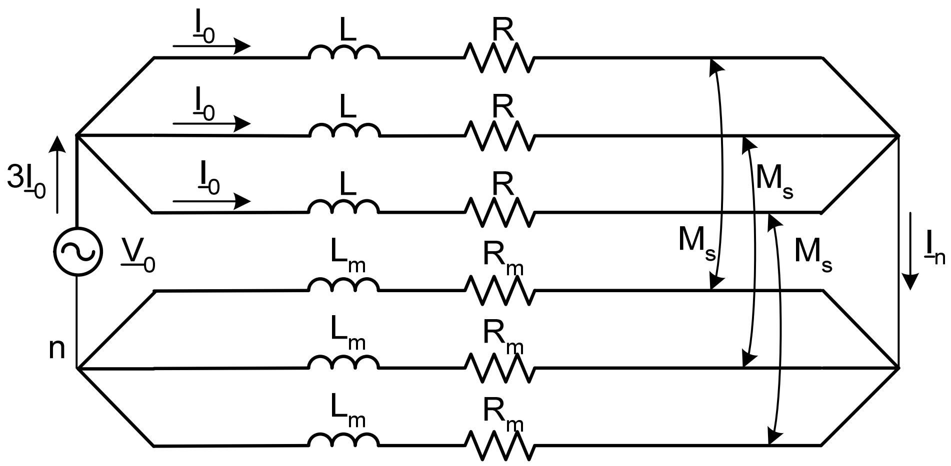

Figure B-6: Zero-sequence impedance calculation scheme; three single phase cables.

R_0 and L_0 are derived according to Figure B-6. Since no mutual inductances between conductors are present, Applying Kirchhoff's law yields for the zero-sequence current $\underline{I}_0$:

$$\underline{V}_0 - j\omega L \underline{I}_0 - R\underline{I}_0 + \underline{I}_0 j\omega M_s + \underline{I}_0 j\omega M_s - \underline{I}_0 R_m - \underline{I}_0 j\omega L_m = 0 \tag{B.22}$$

after rearranging for $\underline{V}_0$ and $\underline{I}_0$

$$\underline{V}_0 = \underline{I}_0 \left[R + R_m + j\omega\left(L + L_m - 2M_s\right)\right] \tag{B.23}$$

And therefore holds for Z_0

$$Z_0 = \frac{\underline{V}_0}{\underline{I}_0} = R_0 + j\omega L_0 = \left[R + R_m + j\omega\left(L + L_m - 2M_s\right)\right] \tag{B.24}$$

And consequently for R_0 and L_0

$$\begin{aligned} R_0 &= R + R_m \\ L_0 &= L + L_m - 2M_s \end{aligned} \tag{B.25}$$

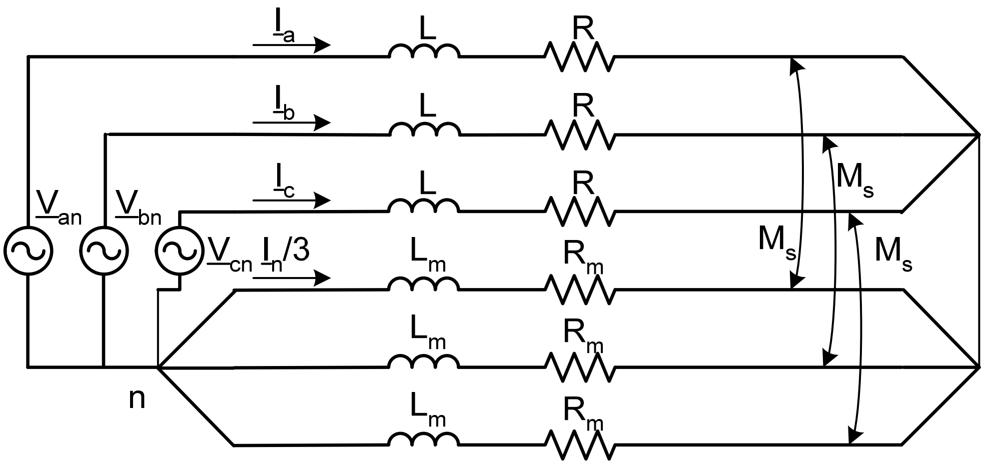

Figure B-7: Positive sequence parameter calculation scheme; three single phase cables

R_1 , R_2 , L_1 and L_2 are derived by the same method as bundled cable's parameters have been calculated. Mutual inductances are not present as depicted in Figure B-7. A three phase source is connected as the sheaths are connected to the neutral point. Kirchhoff's law yields:

$$\begin{aligned} \underline{V}_{an} &= \underline{I}_a R + j\omega \underline{I}_a L - \frac{1}{3} j\omega \underline{I}_n L_m - \frac{1}{3}\underline{I}_n R_m + \frac{1}{3} j\omega \underline{I}_n M_s - j\omega \underline{I}_a M_s \\ \underline{V}_{bn} &= \underline{I}_b R + j\omega \underline{I}_b L - \frac{1}{3} j\omega \underline{I}_n L_m - \frac{1}{3}\underline{I}_n R_m + \frac{1}{3} j\omega \underline{I}_n M_s - j\omega \underline{I}_b M_s \\ \underline{V}_{cn} &= \underline{I}_c R + j\omega \underline{I}_c L - \frac{1}{3} j\omega \underline{I}_n L_m - \frac{1}{3}\underline{I}_n R_m + \frac{1}{3} j\omega \underline{I}_n M_s - j\omega \underline{I}_c M_s \end{aligned} \tag{B.26}$$

Using $\underline{I}_n=-(\underline{I}_a+\underline{I}_b+\underline{I}_c)$ together with the proposed matrix methods it can be concluded that for R_1 , R_2 , L_1 and L_2 holds

$$\begin{aligned} &\boldsymbol{Z}_{012(1,1)} = Z_0 \ ; \boldsymbol{Z}_{012(2,2)} = Z_1 = R_1 + j\omega L_1 = R + j\omega\left(L\right); \boldsymbol{Z}_{012(3,3)} = \boldsymbol{Z}_{012(2,2)} = Z_2 \\ &R_1 = R_2 = R \\ &L_1 = L_2 = L \end{aligned} \tag{B.27}$$

and thereby concluding the parameter derivation of the sequence parameters given in Table 1-1.

Appendix C: MV Network parameters

The aggregated modeled network was already given in Figure 2-2 and is repeated for convenience in Figure C-1. Table C-1 through Table C-3 give the parameters of Figure 2-9 and other parameters used during simulation.

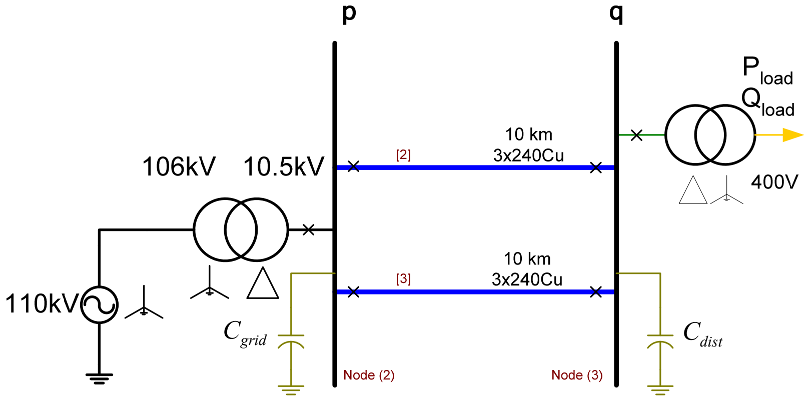

Figure C-1: Aggregated MV network

Source: An infinite grid is used as voltage source. In practice, this is not a correct assumption since double and three phase short-circuit current are partly defined by the X/R ratio of the HV grid. However, single phase-to-ground-fault currents are defined by the cables' capacitances and source impedance is of minor importance.

Transformers: The transformers' parameters are given by the utility company in per unit quantities during no-load and short-circuit. These parameters can directly be applied in RTDS. For MatLab/Simulink actual resistances and inductances should be calculated. It is important to notice that in the MatLab model, 10.5 kV is used as a voltage source and so the transformer parameters must be referred to the MV side.

Load: active and reactive loads are given in MW and Mvar. However, RSCAD as well as MatLab use a voltage dependent load (lumped elements). Therefore, load is modelled as a resistance in series with an inductance.

Source and HV/MV transformer parameters

Symbol	Value	Model
$\underline{V}_{bus,line}$	110kV	RTDS/Simulink
$\underline{E}_{source}$	6.29kV	Matlab
R_{source}/ $Z_{s,0}/Z_{s,1}$	1e-6 Ω	all
S_{base}&$S_{rated,T1}$	40 MVA	all
$V_{T1,prim}/V_{T1,sec}$	106kV/10.5kV	all
V_{base}	106kV	all
$X_{T1,pu}$	0.1455 pu	RTDS
$R_{T1,pu}$	0.0048 pu	RTDS
$Z_{T1,1}$	1.348+j40.87 Ω	Matlab/Simulink
$Z_{T1,0}$	2.7+j33.4 Ω	Matlab[1]

[1] Only applicable during neutral to ground connection

Cable parameters		
Symbol	Value	Model
$C_{grid,0}$[1]	16.8e-6 F	all
$C_{grid,1}$[1]	30.6e-6 F	all
$C_{dist,0}$[1]	7e-6 F	all
$C_{dist,1}$[1]	12.75e-6 F	all
R_{shunt}	1e-5 Ω	Matlab
C_0	0.28e-6 F	all
C_1	0.51e-6 F	all
R_0	1.097 Ω	all
R_1	0.079 Ω	all
L_0	3.5014e-4 H	all
L_1	2.4192e-4 H	all
length 1[1]	10 km	all
length 2[1]	10 km	all
$Z_{cable1,0}$	10.97+j1.1 Ω	all
$Z_{cable2,0}$	10.97+j1.1 Ω	all
$Z_{cable1,1}$	0.79+j0.76 Ω	all
$Z_{cable2,1}$	0.79+j0.76 Ω	all
Z_f	0.1 Ω	all

Table C-1

Load parameters		
Symbol	Value	Model
P_{load}	6.3 MW	all
Q_{load}	3 MW	all
$Z_{load,1}$[2]	5.833+j12.04 Ω	Matlab
$Z_{load,1}$	0.02+j0.0533 Ω	RTDS/Simulink
$Z_{load,0}$	1e-6	all

Table C-2

[1] Has been varied throughout the work presented
[2] Referred to primary side of MV/LV transformer

MV/LV transformer parameters		
Symbol	Value	Model
$S_{rated,T2}$	10 MVA	all
$V_{T2,prim}/V_{T2,sec}$	10.5kV/400V	all
S_{base}	10MVA	all
V_{base}	10.5kV	all
$X_{T2,pu}$	0.18	RTDS
$R_{T2,pu}$	0.02	RTDS
$Z_{T2,1}$[1]	0.2205+j1.9845 Ω	Matlab/Simulink
$Z_{T2,0}$[2]	1e-6 Ω	all

Table C-3

[1] Referred to the primary side of the MV/LV transformer
[2] Value not given by the utility company. Therefore, a very small value has been used.

Appendix D: Quad 50E circuit diagram

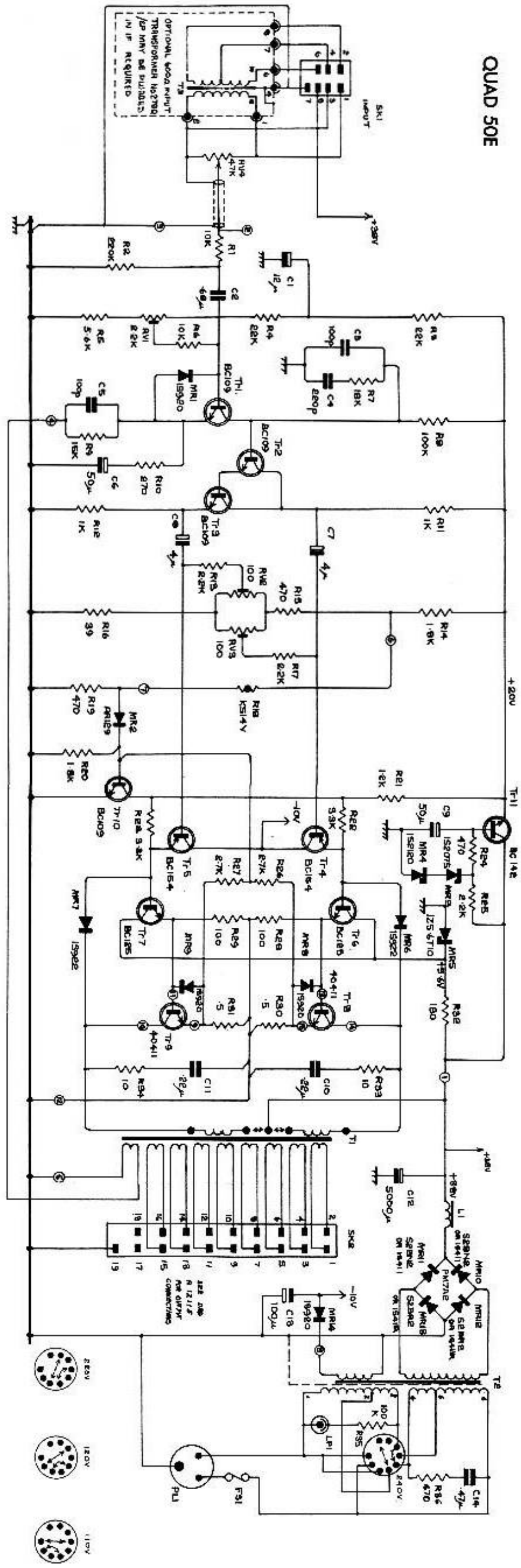

Figure D-1: QUAD 50E electronic scheme

Appendix E: Glossary of symbols

Symbol	Description	Unit
L_n	Grounding inductance	[H]
R_n	Grounding resistance	[Ω]
$C_{0G,n}$	Capacitance to ground of cable n	[F]
$X_{c0,network}$	Cumulative capacitive reactance to ground of the MV network	[Ω]
$C_{0,network}$	Cumulative capacitance to ground of the MV network	[F]
RCA	Relay Characteristic Angle	[°]
MTA	Maximum Torque Angle	[°]
φ_{sc}	Short-circuit angle	[°]
$\underline{I}_0$	Zero-sequence current	[A]
$\underline{I}_e$	$3\underline{I}_0$	[A]
$\underline{I}_{e,dist}$	Distribution string's earth-fault current contribution	[A]
$\underline{I}_{e,grid}$	Substation side MV network earth-fault current contribution	[A]
$C_{dist,0}$	Distribution string zero-sequence capacitance	[F]
$C_{Grid,0}$	MV network side zero-sequence capacitance	[F]
$C_{cable,0}$	Feeder cable's zero-sequence capacitance	[F]
$\underline{I}_{e,OMT}$	Earth-fault current measured by overcurrent relay	[A]
$\underline{I}_{e,SRR}$	Earth-fault current ($3\underline{I}_0$) measured by directional overcurrent relay	[A]
$\underline{I}_{e,7sj62}$	Earth-fault current ($-3\underline{I}_0$) as used by the 7SJ62 relay	[A]
Z_f	Fault impedance	[Ω]
$\underline{I}^{a}_{m\to n,(v)}$	Phase current flowing *from* node m *to* node n in cable v	[A]
α	Fault current setting margin	-
μ_{lim}	Capacitance limit ratio for correct relay co-ordination	-
k	Fault location	[pu]
$\underline{X}$	Complex RMS value(phasor)[33]	-
X	RMS value[33]	-

References

[1] Kling W.L.: "Planning en bedrijfsvoering van elektriciteitsvoorziening systemen", *Delft University of Techology*, 2006.

[2] Kreuger F.H.: "Industrial High Voltage, Electric Fields, Dielectrics and Constructions", Delft University press, 1991.

[3] IEEE Power Engineering Society: "IEEE guide for safety in AC substation grounding", January 2000.

[4] Tang Y., Wang H., Fangtao D., Jiang S.: "Transmission Line Models Used in Travelling Wave Studies", *IEEE Conference Proceeding: Transmission And Distribution Conference*, 1999.

[5] Morren J., "MS Beveiligingsfilosofie 2007", Beveiligingen MS netten Essent Netwerk B.V.,

[6] Popov M.: "Lecture notes Grounding and Protection Ch. 2:Grounding of the network", 2004.

[7] Willheim R., Waters M.: "Neutral grounding in high voltage transmission", *Elsevier publishing company*, 1956.

[8] IEEE Power Engineering Society: "IEEE guide for safety in Electrical Utility Systems", September 2000.

[9] Kreuger F.H.: "Industrial High Voltage, Coordinating, Testing and Measuring", *Delft University press*, 1992.

[10] Christopoulos C., Wright A.: "Electrical Power System Protection", *Springer*, 1999.

[11] Alstöm: "Network protection & Automation Guide", 2002.

[12] Gers J.M., Holmes E.J.: "Protection of Electricity Distribution Networks, 2nd edition", *IEE Power Engineering series*, 2004.

[13] Siemens: "Multi-Functional protective relay with local control 7SJ62/63/64 v4.4 Manual", *Siemens AG*, 2002.

[14] IEEE Power Engineering Society, "IEEE Guide for the protection of Network Transformers", September 2002.

[15] Gafoor S.A., Ramana Rao P.V.: "A New Wavelet Transform Based Busbar Protection", *IEEE region 10 Conference pp. 1-4*, November 2006.

[16] Jingguang H., Xiangyong H., Xianshan L., Hanmei H., Yanping L.: "A Novel Single-Phase Earth Fault Feeder Detection by Traveling Wave and Wavelets", *International Conference on Power System Technology*, 2006.

[17] Zhang N., Kezunovic M.: "Transmission Line Boundary Protection Using Wavelet Transform and Neural Network", *IEEE Transactions on Power Delivery, VOL. 22, NO. 2*, April 2007.

[18] Grainger J.J. Stevenson W.D.: "Power System Analysis", *McGraw-Hill*, 1994.

[19] Smit J.J., Meijer S.: "Asset management college lecture notes", 2007.

[20] Van der Meer, A.A.: "Richtingbepaling 7SJ62 Relais", Essent Netwerk, November 2007.

[21] Funk von Oldenbourg G.: "Der Kurzschluss im Drehstromnetz", 1962.

[22] Paap G.C.: "Collegedictaat Electriciteitsvoorzieningen 1", Delft University of Technology, 1992.

[23] Elgerd O.I.: "Electric Energy Systems Theory: an introduction", *McGraw-Hill series in electrical engineering*, January 1982.

[24] Kuffel R., Giesbrecht J., Maguire T., Wierckx R.P., McLaren P.G., "A fully digital power system simulator operating in real time", IEEE *Conference proceeding vol. 2 pp. 733-736*", 26-29 May 1996.

[25] "RTDS manual set", *RTDS Technologies Inc*, 2002.

[26] Acoustical manufacturing Co. Ltd., "Quad 50E operating instructions", *Hambleden Press*, 1966.

[27] Power Systems Relay Committee of the IEEE Power Engineering Society: "IEEE Standard Common Format for Transient Data Exchange (COMTRADE) for Power Systems", March 1999.

[28] Fortescue C. L.: "Method of Symmetrical Coordinates Applied to the Solution of Polyphase Networks", *Trans. AIEE, pt. II, vol. 37, pp. 1027–1140*, 1918.

[29] Phase to Phase: "Afleiding kabelparameters normaalbedrijf", june 2001.

[30] van der Sluis L.: "Transients in Power Systems", *John Wiley & sons, Ltd.*, 2001.

[31] Paap G.C.: "Symmetrical Components in the Time Domain and Their Application to Power Network Calculations", *IEEE transactions on power systems vol. 15 nr. 2*, May 2000

[32] Kundur P.: "Power System Stability and Control", *New York: EPRI Power System Engineering Series, McGraw-Hill, Inc.*, 1994.

[33] Hoeijmakers M.J.: "Elektrische Omzettingen", *Delft University* Press, 2003.

Acknowledgements

Although a thesis project mainly relies on individual effort, I owe much gratitude to the persons who were participating in my thesis project.

First, I would like to thank my daily supervisor, dr. ir. Marjan Popov for providing me a Thesis project at the Electrical Power Systems department of Delft University of technology. He certainly played a great contribution to the completion of my Thesis project. Many thanks to the other thesis committee members, prof. ir. Lou van der Sluis and dr. ir. Pavel Bauer for taking the effort to evaluate my thesis report. Numerous thanks to Rob Schoevaars for supporting me during frequency characteristics determination in the EPE-lab.

Many thanks go to my former colleagues of Essent Netwerk. Johan Morren has given me a comprehensive introduction to the thesis subject and he certainly changed my way of approaching technical challenges. Bas Rombouts has given me the opportunity to apply the relay co-ordination software "Instelplan" during my thesis. Special thanks to Ron Visser as well for giving me practical secondary circuit knowledge, hardly needed for interfacing with RTDS.

Furthermore, I wish to thank Frank Koers and Marc Achterkamp from KEMA Consulting and KEMA T&D for advising and making amplifier setup verification possible at the KEMA secondary circuit laboratory.

At last, I would like to thank my family in general and Marte Broos in particular for supporting me so well during my thesis project.